NERC Scientific Facilities and Technology
Ion Microprobe Facility

University of Edinburgh
NERC Ion Microprobe Facility

2018 Annual Science Report

Ion Microprobe Facility
School of Geosciences
Kings Buildings
James Hutton Road
Edinburgh
EH9 3FE

http://www.ed.ac.uk/geosciences/facilities/ionprobe

Contents

Ion Microprobe Projects

Understanding the effects of ocean acidification and temperature on coral calcification: insights from the dissolved inorganic carbon chemistry of the coral calcification fluid

N. Allison[1], C. Cole[1], C. Hintz[2] & A.A. Finch[1]

[1]School of Earth and Environmental Sciences, University of St. Andrews, St. Andrews KY16 9AL, UK.
[2] Faculty of Marine Sciences, Savannah State University, Savannah, Georgia, USA

.

Coral reefs are among the world's most biologically diverse ecosystems and are of substantial economic importance in terms of fisheries, tourism and coastal protection. Rising atmospheric CO_2 is causing ocean warming and has fundamentally affected seawater carbonate chemistry, lowering seawater pH. Understanding the effects of these changes is essential for predicting the future of coral reef ecosystems. However, attempts to assess increasing pCO_2 and temperature effects, either separately or in combination, have generated many contradictory observations with reports of both increased and decreased coral calcification [1]. Unravelling the source of the discrepancies between studies is key to accurately predicting the effects of increasing seawater pCO_2 and temperature in different coral species and reef environments. Coral calcification rates are positively correlated with the saturation states of the calcification fluid [2] suggesting that calcification fluid DIC chemistry is a prime driver of calcification. Understanding how coral calcification fluid DIC responds to changes in seawater pCO_2 and temperature is key to predicting the impact of future seawater temperature increases and ocean acidification on reef development.

The boron geochemistry of coral skeletons offers a method to reconstruct the dissolved inorganic carbon (DIC) chemistry of the coral calcification fluid [2]. In this study we cultured several genotypes of massive Porites spp. coral in a large-volume purpose built aquarium system at the University of St. Andrews, UK designed to maintain temperature, salinity and DIC system parameters within narrow limits [3]. *Porites* spp. are major components of coral reefs in the Indo-Pacific. Understanding the impact of rising seawater pCO_2 and temperature on the accretion ability of these reef building species is key to predicting the future of coral reefs. Imported corals were maintained at ambient seawater pCO_2 conditions for 2 months, adjusted to pCO_2 750 µatm over 1 month and then acclimated at this pCO_2 for 4 months at 28°C. The skeleton deposited over the subsequent 5 week period was identified by alizarin red stain for geochemical analysis. Seawater temperatures were then reduced to 25°C over a period of 4 weeks, corals were acclimated at this temperature for another month and then skeleton for analysis was again identified by alizarin red staining (Figure 1). At the end of this period corals were sacrificed and immersed in 3-4% sodium hypochlorite for ≥24 h with intermittent agitation to remove organic contamination, then rinsed and dried. Skeletal strips from the outermost surface of the colonies were sawn along the maximum growth axes and fixed in 25 mm epoxy resin blocks (Epofix, Struers Ltd.). Blocks were polished using silicon carbide papers (up to 4000 grade, lubricated with water) and polishing alumina (0.05 µm, suspended in water). We determined the skeletal $\delta^{11}B$ and B/Ca using the Cameca 1270 and spacing multiple SIMS analyses evenly spaced across sections bounded by the alizarin stain. The high spatial resolution of SIMS allows the analysis of primary coral material.

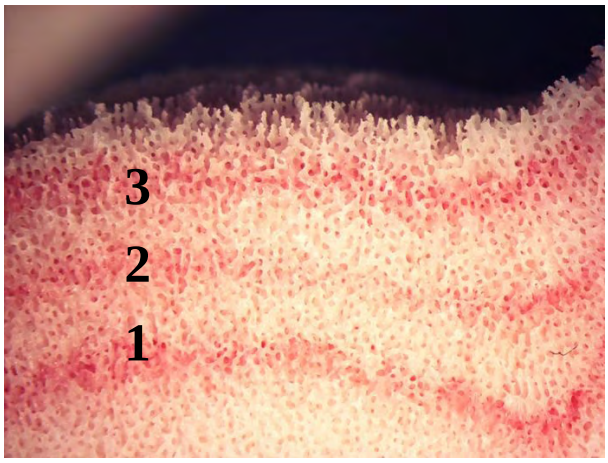

Figure 1. Cross-section though a cultured coral indicating the alizarin stain lines (numbered 1, 2 and 3. Aragonite between stain lines 1 and 2 was deposited at 28°C while aragonite deposited between stain line 3 and the outermost surface of the coral was deposited at 25°C. Aragonite deposited between stain lines 2 and 3 was deposited whilst the culture seawater temperature was changed. Image is 7 mm wide. The alizarin stain appears diffuse but actually occurs as a very fine line which is deposited across a 3 dimensional structure. Note this coral was cultured at low seawater pCO_2.

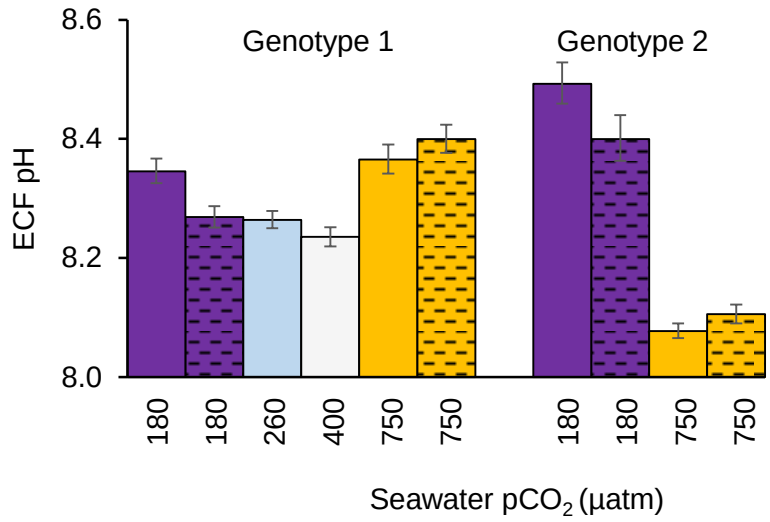

Figure 2. Extracellular calcification fluid (ECF) pH reconstructed from skeletal $\delta^{11}B$ in 2 massive Porites spp. coral genotypes cultured at a range of seawater pCO_2 and at 25°C (plain bars) and 28°C (hatched bars). Error bars are 95% confidence limits of multiple SIMS analyses.

Results and Discussion

The pH of the calcification fluid used to precipitate the skeleton was estimated from skeletal $\delta^{11}B$ using the mean of 2 empirically-determined αB [4,5] and assuming that the $\delta^{11}B$ ECF is the same as culture seawater. Increasing seawater pH from 25°C to 28°C decreased calcification fluid pH in the corals cultured at low seawater pCO_2 (180 µatm) but increased calcification fluid pH in the corals cultured at high seawater pCO_2 (750 µatm). The calcification fluid pH is influenced by the pH of local seawater [6] and by enzyme activities e.g. Ca-ATPase extrudes protons from the calcification fluid [7] while carbonic anhydrases catalyse the interconversion of CO_2 and HCO_3^- [8], thereby increasing fluid pH. Enzyme activities may be both temperature and seawater pCO_2 dependent e.g. ocean acidification suppresses the gene expression and enzyme activities of carbonic anhydrases localised to the coral calcifying cells but increasing temperatures enhance these enzyme activities and may counteract the effect of seawater pCO_2 [8]. Our data indicate that temperature increases (below the coral bleaching threshold) can mitigate against the effect of ocean acidification on calcification site pH in massive *Porites* spp. corals. It is possible that future seawater temperature increases may offset the effects of ocean acidification in this coral genus at reef locations where corals live below their upper thermal stress thresholds. However, in practice, seawater temperature increases are unlikely to enhance calcification at most tropical reef locations where corals already exist close to their upper thermal tolerance limits. Future minor increases in seawater temperature at these sites are likely to induce widespread coral bleaching and thereby suppress coral calcification.

Reference

[1] J. Erez et al. (2011). Coral Reefs: An Ecosystem in Transition. Springer Science, New York. 151-176
[2] N. Allison et al. (2014) Nature Communications 5; 5741 doi: 10.1038/ncomms6741
[3] C. Cole et al., (2018) Coral Reefs, doi.org/10.1007/s00338-018-1672-3
[4] K. Klochko et al. (2006) Earth Planet. Sci. Lett. 248, 276-285
[5] O. Nir et al. (2015) Earth Planet. Sci. Lett. 414, 1-5
[6] A. Venn et al. (2012) PNAS 110, doi: 10.1073/pnas.1216153110
[7] F. Al Horani et al. (2003) Marine Biology 142, 419-426
[8] D. Zoccola et al (2016) Marine Drugs 14, doi:10.3390/md14060109

Towards accurate determinations of magma chamber depths: insights from both olivine- and plagioclase-hosted melt inclusions

E.N. Bennett[1], C.J. Lissenberg[1] & K.V. Cashman[2]

[1] School of Earth and Ocean Sciences, Cardiff University, Park Place, Cardiff CF10 3AT, UK
[2] School of Earth Sciences, University of Bristol, Wills Memorial Building, Bristol BS8 1RJ, UK

Background and rationale

Understanding of sub-volcanic magmatic plumbing systems is important for constraining the timescales of magma storage and transport and understanding eruption dynamics. One critical parameter in reconstructing magma plumbing systems is the depth at which magma chambers occur. One way to constrain this is by using melt inclusions, small volumes of melt that become trapped within growing crystals. Because they become isolated from the surrounding magmatic environment at different depths, they provide a means of studying the evolution of the magmatic system at a fine-scale. In particular, their volatile contents (e.g., CO_2 and H_2O) can be used to determine the pressures at which crystallisation occurs at due to the pressure dependence of CO_2 - H_2O relationships [1]; CO_2 solubility increases with pressure.

In mafic systems, olivine-hosted melt inclusions are often used (e.g., [2,3]) for several reasons; (1) olivine is seen as a tight vessel; and (2) it is a primitive, early-formed mineral so should track the early stages of magmatic evolution. However, melt inclusions form in a variety of different minerals, including plagioclase, which is often more abundant than olivine in mafic systems such as mid-ocean ridges. In addition, recent textural characterisation of olivine and plagioclase crystal cargo from the Gakkel mid-ocean ridge has revealed that plagioclase displays textural complexity unparalleled by that observed in olivine (**Figure 1**). This attests to plagioclase having experienced complex, protracted magmatic histories within the plumbing system. Because plagioclase, in contrast to olivine, often records complex, protracted crystallisation histories, we hypothesised that it records an extended part of the crystallisation history compared to olivine. If our hypothesis is correct, a significant portion of the crystallisation record may be neglected by focussing on olivine-hosted melt inclusions, biasing the record towards pressures recorded in olivine. To test our hypothesis we analysed the volatile contents (e.g., CO_2 and H_2O) of both olivine- and plagioclase-hosted melt inclusions from the Gakkel Ridge.

Results and discussion

Melt inclusion CO_2 and H_2O contents are variable (**Figure 2**). In the dataset as a whole H_2O and CO_2 range from 0.13-0.56 wt.% and 94-2857 ppm respectively. Whilst the range of H_2O concentrations in olivine- and plagioclase-hosted melt inclusions is similar (0.13-0.48 and 0.12-0.56 wt.%), the CO_2 record of these inclusions are markedly different.

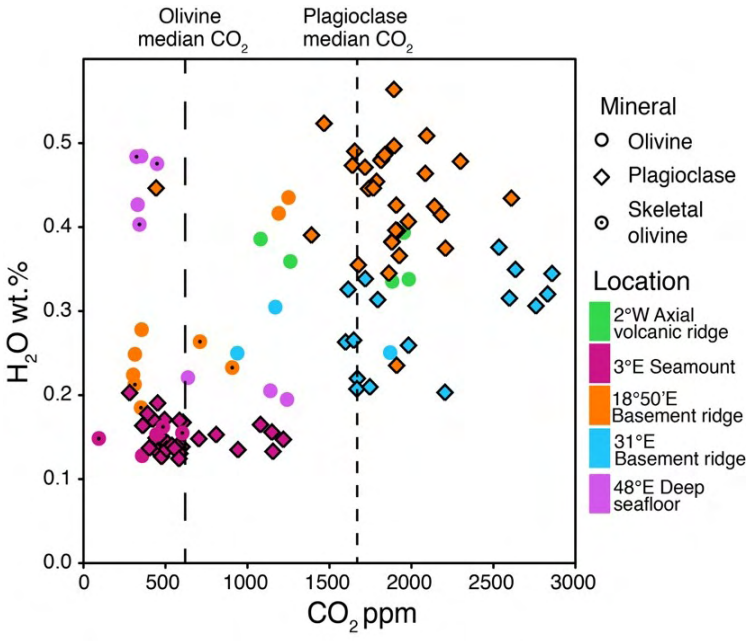

Figure 2. Post-entrapment crystallisation corrected volatile contents of olivine- and plagioclase-hosted melt inclusions from five locations along the Gakkel mid-ocean ridge (Arctic Ocean). The two different inclusions types have similar H_2O contents, but different CO_2 contents as illustrated by their median values (dashed lines). Melt inclusions in skeletal olivines all contain relatively low CO_2.

Plagioclase-hosted melt inclusions record a greater range in CO_2 contents from 282-2857 ppm (median = 1670 ppm) compared to 94-1984 ppm (median = 620 ppm) in olivine-hosted melt inclusions. In addition, the CO_2 content of melt inclusions in skeletal olivine is lower (94-907 ppm) compared to that in non-skeletal olivine (303-1984 ppm).

Based on these results it is clear that olivine- and plagioclase-hosted melt inclusions record different volatile element records, which, in combination with textural observations, is consistent with plagioclase and olivine experiencing different crystallisation histories within the Gakkel Ridge plumbing system, as hypothesised.

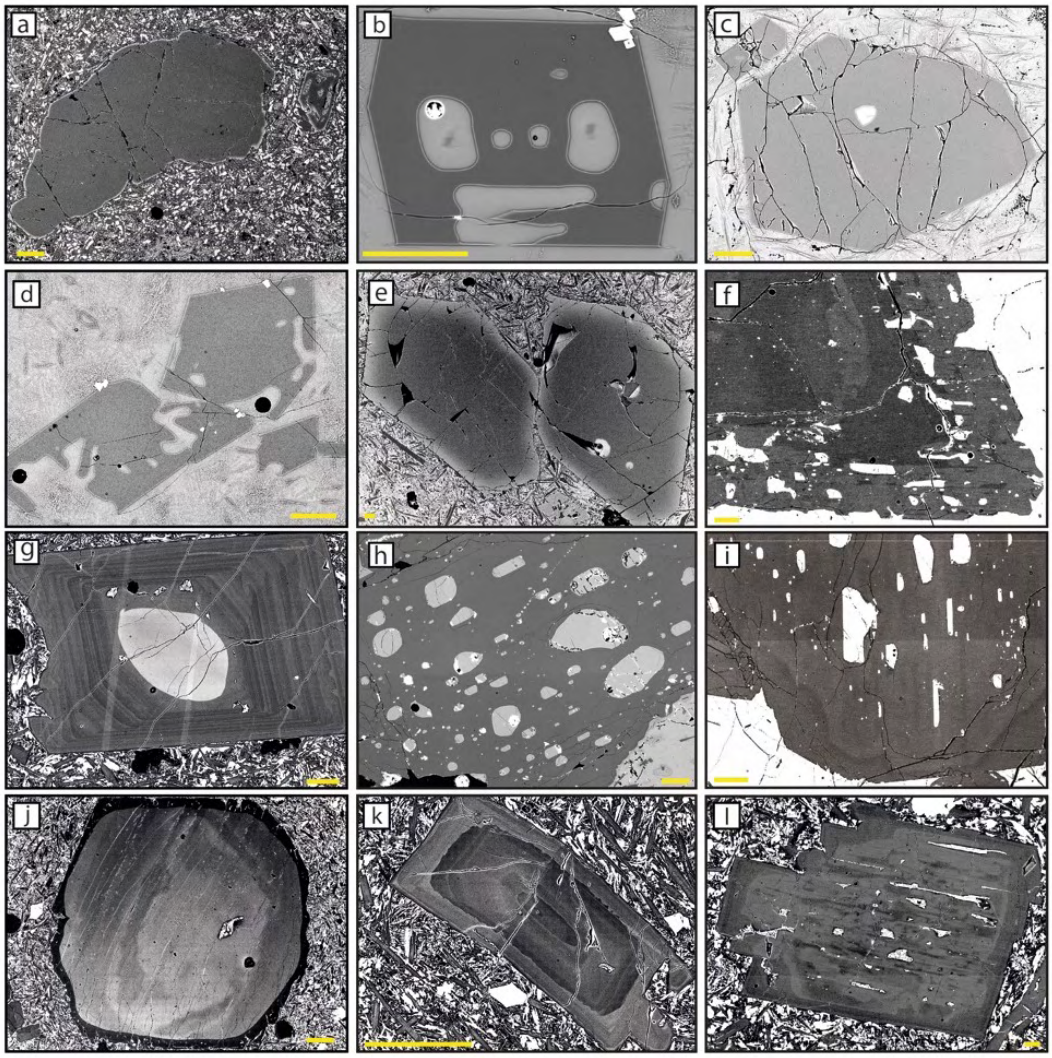

Figure 1. Back-scattered electron images (BSE) of olivine (**a**-**e**) and plagioclase (**f**-**l**) crystals from the Gakkel Ridge. Olivine is rarely resorbed (**a**) and more commonly exhibits skeletal (**b**,**d**) or euhedral crystal forms (**c**,**e**). Olivine is most often unzoned (**b**-**d**), but can exhibit simple zoning such as the normal zoning in panels **a** and **e**. Melt inclusions are found in both euhedral (**c**,**e**) and skeletal olivine (**b**,**d**). In contrast, plagioclase shows a range of habits from resorbed (**f,h**, **j**) to tabular (**g**,**k**,**l**) and zoning is rarely simple (e.g., **h**). Types of zoning include: oscillatory (**g**,**k**); reverse (**f**,**k**); normal (**d**,**g**,**i**,**j**,**l**); and patchy (**f**,**j**,**l**). Plagioclase also shows abundant evidence of resorption (**f**,**g**,**i**-**l**). Melt inclusion are often randomly distributed within the host plagioclase (**h**,**i,l**). All yellow scale bars are 100 μm.

References

[1] J.E. Dixon and E. M. Stolper (1995) Journal of Petrology **36**, 1633-1646
[2] V. D. Wanless and A. M. Shaw (2012) Nature Geoscience **5**, 651-655
[3] V. D. Wanless et al. (2014) Geochemistry, Geophysics, Geosystems **16**, 126-147

What is the temperature of rare earth element (REE) mineralisation in carbonatites?

S. Broom-Fendley[1], B.W.D Yardley[2], D. Cangelosi[2], R.J. Newton[2] & M.P. Smith[3]

[1] Camborne School of Mines, University of Exeter, Penryn Campus, Cornwall
[2] School of Earth and Environment, University of Leeds
[3] School of Environment and Technology, University of Brighton

Project background

Carbonatites are a major source of REE ore minerals but, despite the strong association between the REE and carbonatite magmas, field and mineralogical evidence strongly indicates that hydrothermal reworking is required to form an ore deposit. Despite the importance of hydrothermal fluids, there is a dearth of information on the temperature of REE mineral precipitation, as well as fluid pressure and composition. In this project we have carried out SIMS oxygen isotope analyses of gangue minerals associated with REE mineralisation from carbonatite-hosted REE deposits in order to establish the temperature of the hydrothermal stage. Previous work has been hampered by calcite recrystallization, which renders calcite-dolomite solvus thermometry ineffective in carbonatites [1], while fluid-inclusion microthermometry is often unsuccessful as inclusions, if present, are too small or decrepitate upon heating.

Hydrothermal gangue minerals associated with REE mineralisation include calcite, barite, strontianite and quartz. Oxygen isotope fractionation between calcite, or strontianite, and barite, over the range of temperatures of interest (175–450°C) equates to approximately -1 to -5 ‰ (**Figure 1**). This range in O isotopes is readily resolvable using SIMS and, as such, represents a new, sensitive, geothermometer.

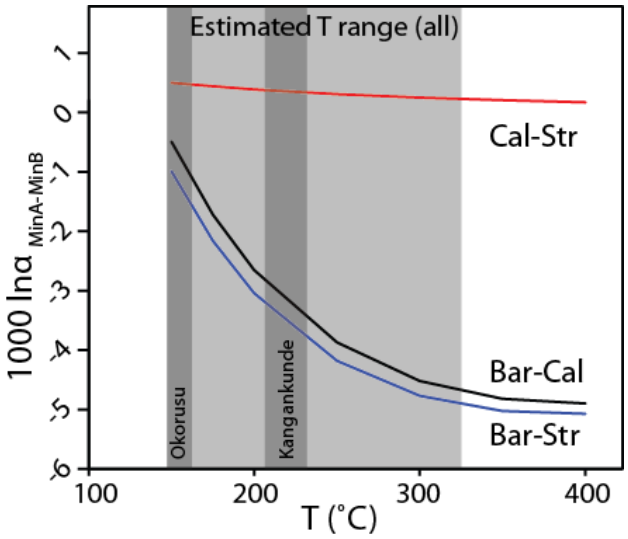

Figure 1. Equilibrium fractionation factors between minerals analysed, and the range of calculated crystallisation temperatures. Fractionation factors from: barite-CO_2, [2]; strontianite-CO_2, calcite-CO_2 & strontianite-calcite, [3].

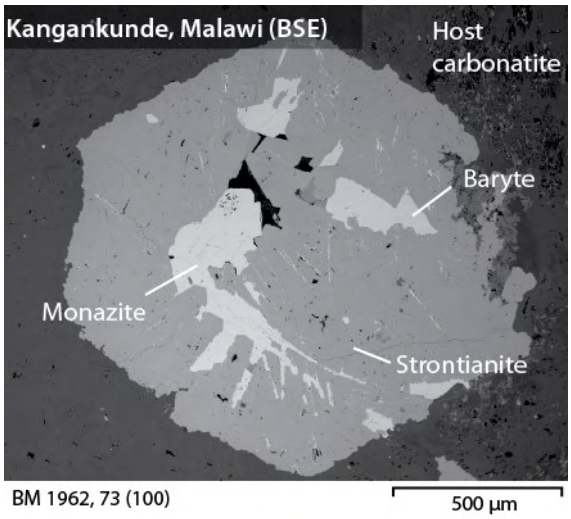

Figure 2. Monazite, strontianite and barite pseudomorphing hexagonal burbankite.

Method Development

To our knowledge, strontianite had not previously been analysed for its O isotope ratios using SIMS and standard material was not available. A barite standard was available, but samples of both minerals were mounted in 3 perpendicular orientations to check for effects of orientation on SIMS analyses. No orientation effects were observed. Oberdorf strontianite (NMNH R10065; [4]), a microprobe standard, was found to be homogeneous for $\delta^{18}O$, and was run as the standard with our unknowns. At present we are awaiting conventional $\delta^{18}O$ results so that our data can be corrected accordingly.

Samples and preliminary results

Secondary REE minerals form either in pseudomorphs of magmatic carbonatite phases (e.g. **Figure 2**) or in recrystallized material, such as vugs and veins, where it is interpreted to form from a hydrothermal fluid which redistributes REE and other elements from magmatic minerals. Barite and strontianite are commonly associated with secondary REE minerals in hydrothermal calcite and were the main target of this study. Mineralisation after hexagonal pseudomorphs was analysed from the Kangankunde (Malawi) and Khibiny (Russia) carbonatites, while vug and vein type samples were analysed from the Okorusu carbonatite (Namibia). We also analysed secondary quartz and calcite from Huanglongpu (China).

Summary O isotope values, relative to VSMOW, of minerals from each study site are presented in Appendix, **Table 1**. Considering the entire barite-strontianite dataset, there is quite a large spread in $\delta^{18}O$ values, the lowest being barite (2.46 ‰) and the highest in strontianite (nominal 25.86 ‰, both Kangankunde). However, the majority of data points from most study sites are within error of 2–4 ‰ for barite, and nominal 5–7 ‰ for strontianite and calcite. Taking the maximum and minimum values for these equates to a temperature range of approximately 175–350°C (Fig 1). We expect to be able to calculate a well-defined temperature estimate for the hexagonal pseudomorphs from Kangankunde because of the narrow compositional range. Strontianite and calcite from Khibiny appear to be out of equilibrium with barite. Calcite from Okorusu is reasonably homogeneous, but individual barite crystals, some only a few hundred microns apart, show very large variations in composition, despite being individually homogeneous. Temperatures for local barite-calcite pairs range from near 200°C to less than 100°C. Quartz and calcite from Huanglongpu mostly give $\delta^{18}O$ values close to 10 ‰; the very small fractionation is indicative of near-magmatic temperatures. Thin crack-fills of secondary quartz, identified by CL imaging, are of very similar composition to the primary quartz, but a secondary crack-fill calcite is around 3 ‰ heavier, indicative of a temperature below 200°C if both crack-fills equilibrated.

Preliminary discussion and implications

Our preliminary data shows that SIMS is a useful technique for determining the temperature of formation of fine-grained hydrothermal assemblages, using barite-calcite and barite-strontianite pairs. Quartz-calcite pairs are also useable, but it is often much harder to constrain the timing of specific parts of these common phases, and so identify equilibrium pairs for geothermometry. We have found that secondary REE mineralisation probably forms below c. 250°C, and may develop to substantially lower temperatures. Hydrothermal redistribution of REE can therefore be linked to geothermal system conditions rather than simple magmatic ones. Variations in mineral $\delta^{18}O$ are also a source of information about hydrothermal activity when the secondary minerals developed. The relatively uniform compositions of calcite from Okorusu, despite large variations in barite, suggest that mineral growth spanned a range of temperatures but fluid composition was predominantly rock-buffered. In contrast, large variations in strontianite from Kangankunde are may indicate ingress of an external fluid.

References

[1] Gittins J (1979) Contributions to Mineralogy and Petrology 69, 1-4
[2] Zheng Y-F (1999) Geochemical Journal 33, 109-126
[3] Chacko T & Deines P (2008) Geochimica et cosmochimica Acta 72, 3642-3660
[4] Jarosewich E & White JS (1987) 57, Journal of Sedimentary Research 57, 762-763

Appendix

The main results are summarised below. Technical issues have delayed calibration of the strontianite standard and so ***results for strontianite are nominal at present.***

Table 1. Oxygen isotope data from nominally coexisting barite, strontianite and calcite, per mil relative to VSMOW, from the different study sites.

Barite	**Kangankunde**						**Khibiny**		**Okorusu**		
Sample Name	123A	123A	162	162	162	162	P2-3	P2-3	P1B	P3	P3
Average	3.99	2.46	2.84	3.38	3.48	3.54	5.96	6.23	3.08	12.73	15.92
1 sigma	0.41	1.00	0.21	1.01	0.19	0.22	0.34	0.26	0.85	1.60	1.26
n=	16	4	10	13	5	10	10	5	10	8	5

Strontianite	**Kangankunde**								**Khibiny**		
Sample Name	123A	123A	123A	123A	162	162	162	100	P3-2	P2-3	P2-3
Average	7.09	11.19	9.44	7.37	6.37	6.36	25.86	12.44	14.11	14.16	14.82
1 sigma	0.38	0.63	1.25	2.00	0.25	0.25	0.45	0.23	0.61	0.43	0.73
n=	10	9	5	5	10	10	5	5	8	4	5

Calcite	**Khibiny**	**Okorusu**		
Sample Name	P2-3	P1B	P3	P3
Average	12.24	4.35	6.59	6.27
1 sigma	0.71	0.82	1.28	1.25
n=	10	9	7	6

Table 2: Oxygen isotope data from quartz and calcite, per mil relative to VSMOW. Huanglongpu sample site.

Quartz			
Sample Name	DSG437 (1ry)	DSG 437 (2ry)	DSG002
Average	9.82	9.87	10.08
1 sigma	0.36	0.34	0.34
n=	25	5	20

Calcite			
Sample Name	DSG437 (1ry)	DSG 437 (2ry)	DSG002
Average	10.23	13.67	10.34
1 sigma	0.64	0.32	0.23
n=	20	5	20

Assessing the volatile contents of zircon-hosted melt inclusions in highly altered porphyry systems

D.A. Butters, J.D. Blundy, B.C. Tattitch & C.J. Hawkesworth

School of Earth Sciences, University of Bristol

Background

Porphyry Copper Deposits (PCD) are magma-derived geochemical anomalies that concentrate economic quantities of metals (i.e. Cu, Mo, Au) in the upper continental crust. Although individual processes behind PCD genesis remain controversial, an overarching model of PCD formation requires highly fractionated hydrous arc magmas, oxidised conditions and the exsolution of magmatic volatile phases (MVP) from the parental porphyry magmas; these exsolved MVP extract Cl, S and metals from the magma, leading to ore precipitation [1]. The corrosive magmatic-hydrothermal fluids associated with porphyry intrusions frequently destroy any petrogenetic evidence preserved in whole-rock samples; this pervasive alteration prohibits determination of parental melt compositions, a key parameter in understanding ore-forming systems.

Aims and Objectives

The aim of this project is to use melt inclusions in the common accessory mineral zircon to see through any whole rock alteration and track the magmatic evolution of porphyry systems. We propose that melt inclusions within zircon represent unaltered vestiges of the original melt prior to significant MVP exsolution, and may therefore be analysed to establish the initial magmatic volatile contents, geochemistry and therein intensive parameters (P, T, fO_2) of the parent magmas. This preliminary investigation aims to address the fidelity of zircon-hosted melt inclusions as recorders of melt composition (major and trace elements and volatiles) and compare compositional results from a porphyry system and associated volcanics, with values of typical arc magmas. The melt inclusions used in this investigation are from the Chiquito Peak Tuff, Alamosa Porphyry and an Intermediate Porphyry Dyke from the San Juan Volcanic District, Colorado.

Sample Preparation

Zircons were separated from whole rock samples using typical crushing and heavy liquid separation techniques (Fig 1). The crystalline melt inclusions were heated at 1000°C for 2 hours in a 1 atm box furnace before quenching to produce a homogeneous glass suitable for SIMS analysis. Zircons were then mounted in epoxy before grinding and polishing to expose the melt inclusions at the surface.

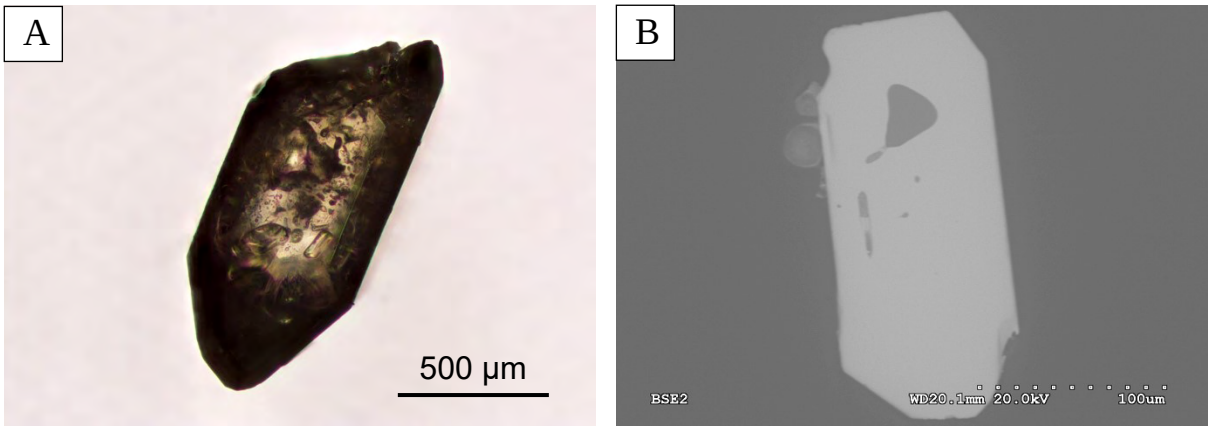

Figure 1. A) Photomicrograph of a zircon from the Chiquito Peak Tuff, exhibiting numerous melt inclusions of varying crystallinity and morphology. B) SEM image of a large (>30 micron) irregular glassy melt inclusion in a zircon.

Results

To our knowledge, these are the first SIMS results of the volatile budgets of zircon-hosted melt inclusions from a porphyry system. The Cl and F values for the three samples (Fig. 2) from SIMS measurements collected in April 2018, range between 0.04 – 0.21wt% and 0 – 0.07 wt% respectively.

These results fall within the expected range for arc magmas: F = 0.001 – 8wt% and Cl = 0.02 – 1wt% [3]. These SIMS data have subsequently been corroborated with EPMA analyses (Fig. 2) obtained at the University of Bristol. All melt inclusions were found to be rhyolitic in composition and followed a liquid line of descent consistent with the composition of regional intrusive rocks [2]. All of the melt inclusions analysed by SIMS had extremely low water contents of ~ 0.1 wt%; these values are much lower than the 4 – 6 wt% H_2O expected for these arc magmas [3]. This prompted further investigation into the capacity for crystalline zircon-hosted melt inclusions to retain their water during homogenisation and thus any implications for slow cooling in the natural environment.

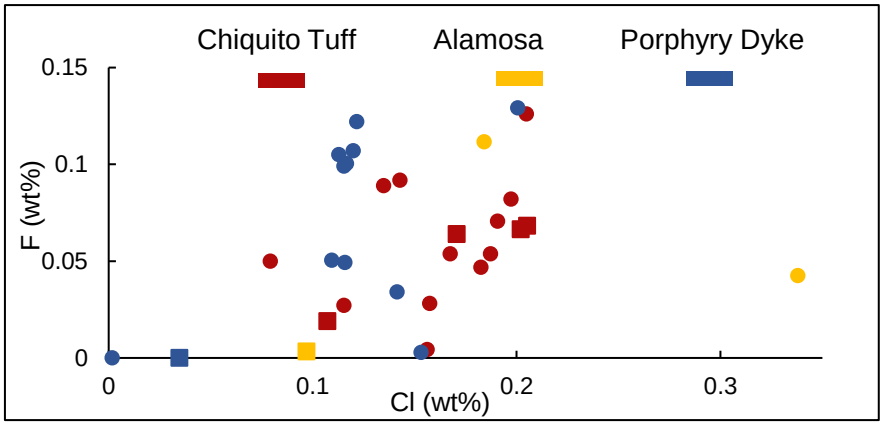

Figure 2. Concentrations of fluorine and chlorine in zircon-hosted melt inclusions from the San Juan Volcanic District, Colorado. Squares and circles correspond to SIMS and EPMA analyses respectively.

Hydration Experiments

Hydration experiments were conducted using zircons from the well constrained Bishop Tuff (BT) to assess whether water diffusion out of ZHMIs can be reversed. At the University of Bristol, a subset of BT zircons was inserted into a cold seal pressure vessel at 850ºC and 300 MPa for 21 days, before quenching. The H_2O content of several experimentally rehydrated melt inclusions was analysed by SIMS in November 2018 (Fig. 3). Unheated and heated melt inclusions (1 atm) both show low water contents implying water may be lost both naturally during slow cooling in the deposit and possibly by experimental reheating. Early results suggest that up to 8.8 wt% H_2O may diffuse back into these melt inclusions in our experiments – a value higher than was ever dissolved in the BT magma [4]. Further SIMS analyses will assess the degree of water diffusion through zircon and thus the fidelity of zircon-hosted melt inclusions as recorders of water content. Preliminary SIMS results indicate that other volatile components (F, Cl, SO_2) are unaffected by diffusion. A subset of these may be included in future analyses depending on the required analytical conditions.

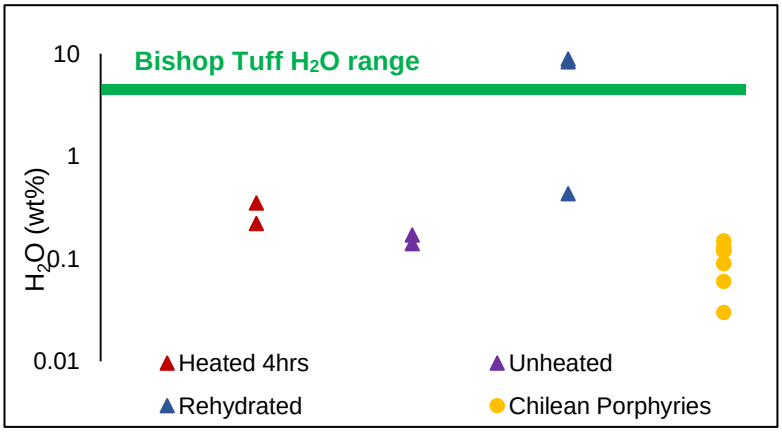

Figure 3. Water contents (SIMS) for Bishop Tuff melt inclusions (triangles) treated under different conditions and a suite of Chilean porphyry melt inclusions (circles) homogenised at 900ºC/1 atm for 2 hours. Green line indicates expected range of water contents for the Bishop Tuff [4]

References

[1] R. H. Sillitoe (2010) Economic Geology, 105, 3–41
[2] D.A. Butters et al. (2018) Goldschmidt Abstracts, 2018, 317
[3] J.D. Webster et al. (2018) Springer Cham, 307–430
[4] A.T. Anderson et al. (2000) Journal of Petrology, 41, 449–473

Tracking magma temperature changes using gas chemistry

M. Cassidy

Department of Earth Sciences, University of Oxford

Motivation

I am attempting to understand how some halogens volatiles (Cl, F, Br) behave during temperature fluctuations within the shallow magma body, by measuring these elements in experimental glasses. The hypothesis being that these species partition between the melt and fluid phase as a function of temperature, and water saturation and thus may provide a means of detecting magma temperature fluctuations by measuring volcanic gas at the surface.

Volcanic gas monitoring of active volcanoes mostly measures SO_2 and CO_2, because previous experimental work has shown that the content of H_2O, CO_2 and SO_2 in the melt is predominantly controlled by pressure, therefore SO_2 and CO_2 are often used as proxies for deep magma ascent due to their different solubility depths [1,2]. However, many volcanic eruptions are directly sourced from magmas that reside from shallow reservoirs and not supplied by deeper mafic inputs to the system prior to eruption (e.g. Kelud volcano [3]). These eruptions are thought to be triggered instead by overpressures in the magma chamber due to cooling and crystallisation. In these instances, gas monitoring of traditional volatile species will be unable to detect changes relating to magma temperature and water saturation.

Recent studies suggest that the temperature of a residing magma reservoir may dictate the explosivity of an impending eruption [3, 4, 5]. This is because temperature has a fundamental role in controlling the magma's rheology, which determines the magma's ability to retain magmatic volatiles. However, there is a very poor understanding of how these and other gases, such as halogens, partition from the melt and fluid phases at varying temperatures. Studies on Cl, suggest that it has its partitioning does not vary with pressure [6], offering promise for Cl and the other halogens, that temperature may be the principle factor controlling it fluid/melt partitioning.

In my current work I have conducted petrological experiments at various pressures, temperatures and XH_2O (degree of water saturation in the fluid phase) on Kelud volcanics (Indonesia). I have constrained the magmatic storage conditions before both explosive and effusive eruptions. This work has unveiled shallow a magma storage body at ~50 MPa, but with variable temperatures and XH_2O ratios between explosive & effusive eruptions. I used my pilot day on the SIMS (9th November 2017) and several days in November 2018, to measure the Br, Cl and F contents of my five of my experimental glass products from Kelud and five experiments from Quizapu volcano, Chile. The samples chosen were isobaric (50 MPa) and ranged in temperature from 1000, 1050, to 1100°C and XH_2O (0.55 – 1). An average of 7 analyses per sample were conducted, averages were calculated along with standard deviation. The precision was good for water-saturated experiments, but there was more heterogeneity in the water under saturated experiments. Along with my unknown samples, secondary standards (MPI Ding reference materials, T1G, ML3bG, and StHs6180), were also measured to check for reproducibility and accuracy. We found that the halogen concentrations for the secondary standards varied between different mounts, supporting the notion that calibration should be conducted on the same mounts as the sample analysis if possible.

Outcomes

The data show some promising results (**Figure 1**). For the dacitic sample, the halogen concentrations of the glass in the water-saturated experiments were mostly higher in the colder experiments and lower than at hotter temperatures. The same trend also occurs for basaltic andesite sample in the water saturated and water undersaturated experiments. However, in the dacitic samples this is not a clear trend, with the experiment at 850° C comprising the lowest dissolved halogen concentrations. This depletion in halogens may be caused by enhanced apatite crystallisation, which could incorporate these halogens.

Another interesting observation in the dacitic experiments is that the water undersaturated experiments display the opposite trend as the water saturated experiments. In these experiments, dissolved Cl, F and Br measured in the glass are highest at the lower temperatures and lowest at the highest temperatures.

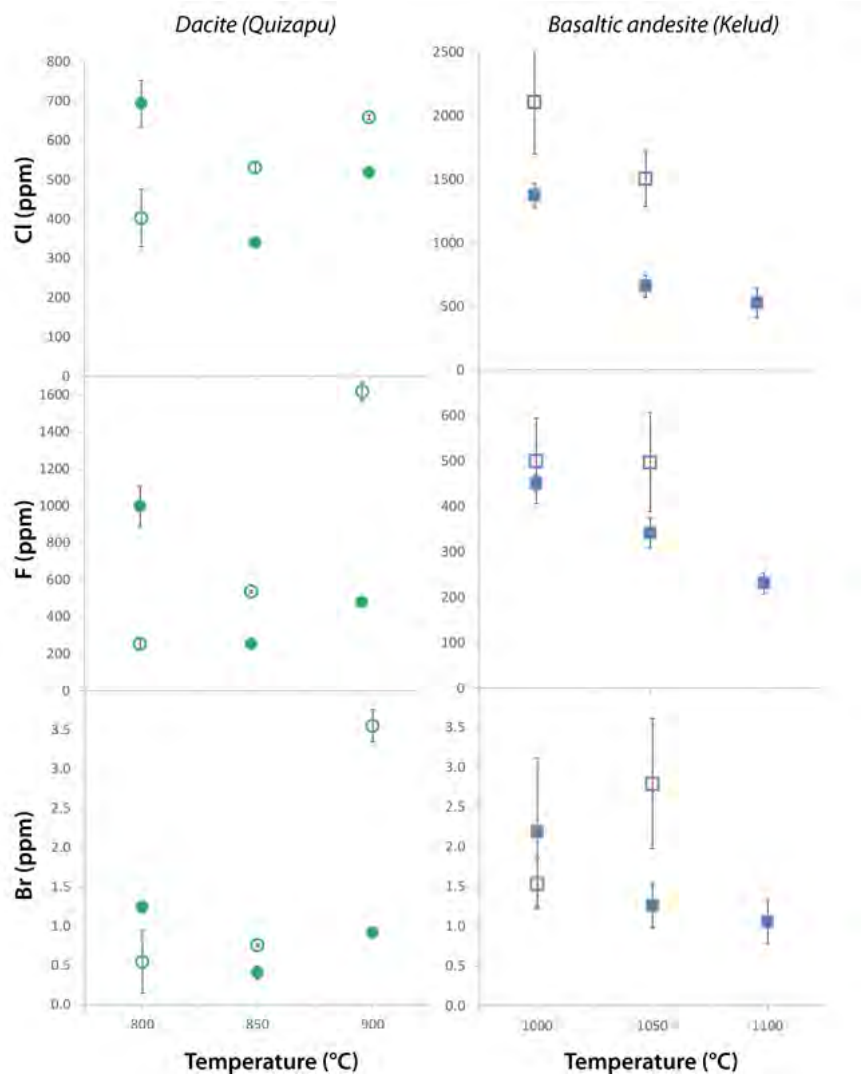

Figure 1. SIMS halogen concentrations of matrix glass from experiments conducted at differing temperatures and degrees of water saturation. Open symbols refer the water undersaturated conditions.

The results thus far show that the halogens do indeed partition from the melt to the fluid phase during temperature and water saturation changes within the magmatic body at shallow depths. Water-saturation is often cited as a trigger for explosive eruptions and therefore these results may prove to be useful if these translate to gas changes monitored at the surface of volcanoes. For instance, a reduction of halogen gas species relative to other gases may suggest that the magma is cooling and crystallising at shallow pressures.

Future work

With the time I have remaining from my proposal, I aim to investigate the role that apatite plays in taking up halogens; to discover if these changes occur at different pressures; and measure the halogen concentrations of the natural glass to develop melt/fluid/apatite partition coefficients.

References

[1] Surono et al. (2012) J. Volcanol. Geotherm. Res. 241–242, 121–135.
[2] Moor, J. M. et al. (2016) J. Geophys. Res. Solid Earth 1–15.
[3] Cassidy, M. et al. (2016) Geology 44.
[4] Ruprecht, P. & Bachmann, O. (2010). Geology 38, 919–922.
[5] Koleszar, A. M. et al.,(2012). J. Volcanol. Geotherm. Res. 219–220, 1–14.

Serpentinite dehydration in a contact aureole Valmalenco, Italy

E. Clarke[1], J.C.M. De Hoog[1], R. Lafay[2]

[1]School of GeoSciences, University of Edinburgh, UK
[2] Institute of Earth Sciences, University of Lausanne, Géopolis, Switzerland

Introduction

Deserpentinization has recently become implicated in the delivery of volatiles to the mantle wedge [1,2]. However, the details of this process are still enigmatic, especially in terms of the volatile composition of deserpentinization fluids. The contact aureole serpentinites of Valmalenco represent a unique opportunity to study deserpentinization away from subduction zone inputs and contamination, as many subducted ophiolite terrains show evidence of infiltration with external fluids [3].

The serpentinites and meta-peridotites of Valmalenco have a long history of metamorphism and deformation. They are thought to represent a section of Permian continental crust-mantle transition, with the lower crustal metapelites welded to the underlying upper ultramafic mantle by a Permian gabbro. The unit underwent granulite facies metamorphism while at depth, then it was exhumed and metasomatized, and the subcontinental peridotitic mantle was serpentinized. Oxygen isotope data confirmed that serpentinization processes occurred due to infiltrating seawater [4].

After exhumation, the Malenco unit experienced lower greenschist facies metamorphism as a result of Alpine orogenic deformation. The regional metamorphism and deformation produced a schistose rock with a greenschist facies mineral assemblage: antigorite + olivine + diopside + chlorite + magnetite; with minor titano-clinohumite and brucite [5]. At 32 Ma and 30 Ma the Malenco unit was intruded by the Bergell intrusives; a suite of calc-alkaline igneous rocks. Contact metamorphism from these instrusives triggered deserpentinization of the Malenco unit, which is reflected in the oxygen and hydrogen isotopes. The Bergell aureole comprises 4 zones in order of increasing metamorphic grade [5]: (A) atg-ol-diopside, (B) atg-ol-trem, (C) tlc-ol-trem and (D) anthophyllite-ol-trem (sometimes enst). The vast majority of the Malenco serpentinite was originally harzburgite, with the exception of parts with greater proportions of tremolite and less talc most likely of lherzolite origin [5]. Two generations of olivine have been identified in the Malenco serpentinites [6] and it is the metamorphic olivine that form the subject of this study.

Boron isotopes are increasingly used to track fluids in serpentinite systems due to their large [B] and positive $\delta^{11}B$. SIMS is one of the few techniques able to measure in situ $\delta^{11}B$, hence why it has been employed in this study.

Analytical details

Instrumental boron isotope fractionation during analysis of different minerals (olivine, serpentine) was evaluated using anhydrous glass standards, and olivine and serpentine minerals analysed independently by TIMS [7, this study]. Significant instrumental mass fractionation of ~8‰ in the serpentine standards was recorded and applied to the presented data. Samples are from Lafay et al. [8].

Results and discussion

There are two isotopically distinct groups of metamorphic olivines (**Figure 1**). Preda Rossa (PR) olivines have positive $\delta^{11}B$ and are 10 to 15 ‰ higher than the serpentine. Alpe Zocca (AZO) olivines all have negative $\delta^{11}B$ and are 10 to 20 ‰ lower than the serpentine. PR olivines have much more B than the serpentine. This indicates that the olivines grew in the presence of externally sourced excess B, most likely an ^{11}B-rich fluid. The PR olivines are closer to the intrusion, but perhaps more importantly closer to the Preda Rossa shear zone. This shear zone developed along the contact between the Bergell intrusion and the country rock (Malenco Unit). A shear zone may provide pathways for such a fluid to gain access to the serpentinite and may explain why the PR olivines have excess B and AZO olivines do not.

Most AZO olivines show little to no excess B, so the reason for their negative $\delta^{11}B$ is probably not excess B from external fluids. AZO samples were situated close to carbonate and gneiss lithologies in the Malenco unit whereas PR samples are from a thick ultramafic unit. Fluids from carbonate rocks are often CO_2-rich and acidic. Boron isotopes have slightly different coordination preferences: ^{11}B preferentially resides in trigonal coordination (III) and ^{10}B in tetragonal coordination (IV) [9]. In acidic

fluids B is boric acid $B(OH)_3$ as III B. Therefore, these fluids would prefer heavy B. If these fluids were B-poor, they would likely strip metamorphic olivine of heavy B leaving a lighter residue. This is potentially what has happened in the AZO samples.

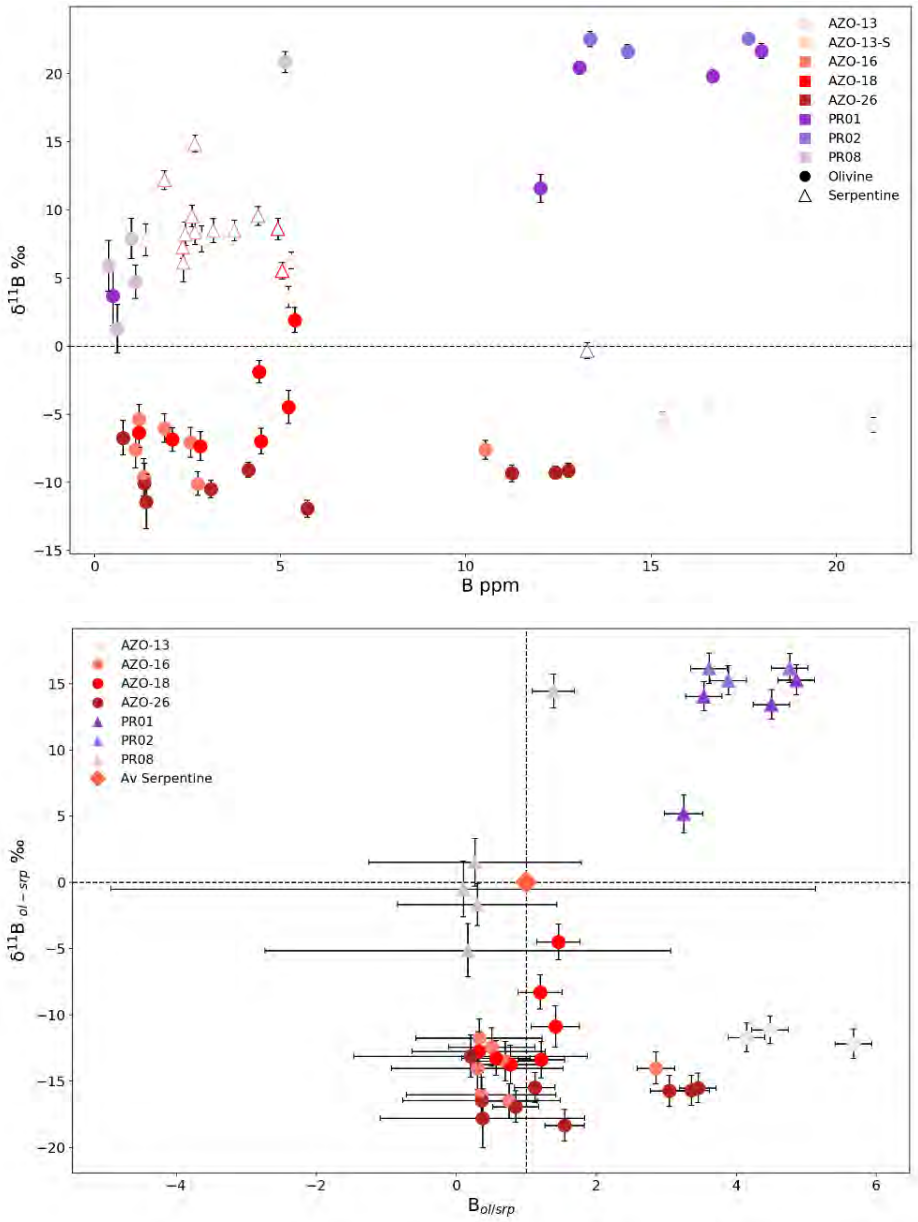

Figure 1.
(A) absolute [B] and $\delta^{11}B$ of olivine and serpentine.
(B) Boron and $\delta^{11}B$ values of olivine compared to that of antigorite in the original serpentinite outside of the Bergell aureole.
PR samples are from Preda Rossa (purple) and AZO samples are from Alpe Zocca (red).

Conclusions

Boron isotopes are particularly sensitive to fluid movements in contact aureole settings. Using B isotopes, we have identified localised fluid networks connecting parts of the Bergell aureole and not others. There must be two different sources of fluids moving through the Bergell aureole: one with excess ^{11}B, able to impart heavy B upon the country rock. Another more acidic fluid, possibly from the carbonate lithologies, that is B-poor and able to strip the country rock of its heavy B.

References

[1] Hyndman and Peacock. (2003) EPSL 212: 417-432 ; [2] Hattori and Guillot. (2003) Geol. 31(6): 525-528; [3] Clarke et al. (in prep); [4] Burkhard and O'Neil. (1988) Contrib Mineral Petrol 99:498-506; [5] Trommsdorff and Evans. (1972) AJS 272 423-437; [6] Peretti et al. (1992) Contrib Mineral Petrol 112:329-340; [7] De Hoog et al. (2017) Goldschmidt Abstracts #872; [8] Lafay et al. (2019) Terra Nova, 1-8 ; [9] Kowalski P.M. and B. Wunder (2018) In Marschall and Foster (Eds) Boron Isotopes, Advances in Isotope Geochemistry, Springer, pp. 33-69

Boron isotopes reflect variations in the supply of fluids in subduction zones

G. F. Cooper[1], J. D. Blundy[1] & C. G. Macpherson[2]

[1]School of Earth Sciences, Wills Memorial Building, University of Bristol
[2]Department of Earth Sciences, Durham University

Introduction

The Lesser Antilles is a global subduction end member with a very slow convergence rate (~2cm/yr). The subducting slow-spread South American Plate contains fracture zones and oceanic core complexes which are significant locations for serpentinisation. Serpentinite therefore has the potential to be a key source of fluids to the Lesser Antilles. Fluids released from serpentine carry a distinctive trace element [1] and boron isotope signature [2] that can be picked up in subduction zone magmas (**Figure 1**), allowing the relative contributions of slab components to be estimated. The Lesser Antilles displays large variations in geochemistry, seismicity and volcanic activity [3,4] and therefore we can test if fluids and/or the relative contribution of slab components is a driver for the along arc variability. In this study, we measured boron isotopic signatures of melt inclusions along the whole length of the Lesser Antilles in order to trace the sources of fluids along the arc.

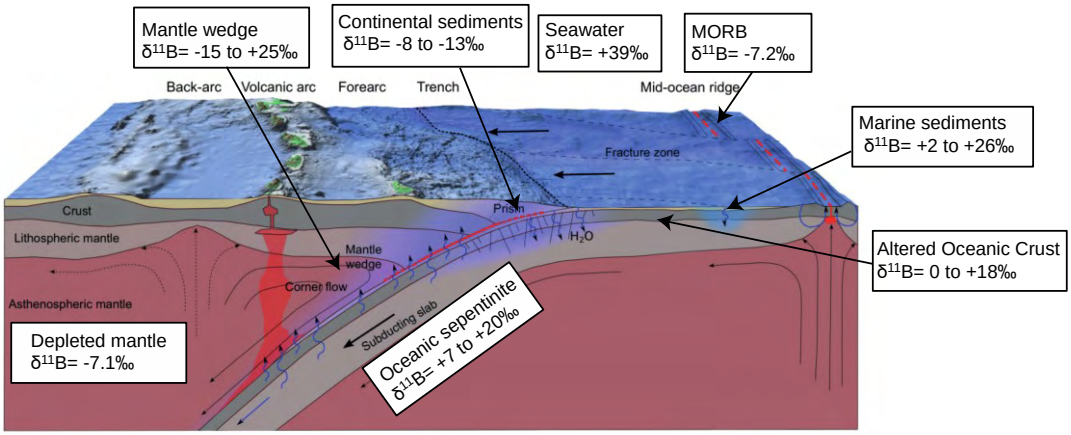

Figure 1. Schematic of the Lesser Antilles subduction zone with boron isotopic compositions of the key subduction components. Range of isotopic values from [2].

Results

Ninety-two melt inclusions, that were previously measured for H_2O, CO_2 Li, B, F, Cl, Rb, Sr, Y, Zr, Nb, Cs, Ba, La, Ce, Sm) were analysed for boron isotopes (^{11}B and ^{10}B) on the Cameca ims-1270 in December 2018. The $\delta^{11}B$ of measured Lesser Antilles melt inclusions showed a large variation from -2.8‰ to +11.2 ‰ (Fig. 2) which coveres much of the global arc range [2].

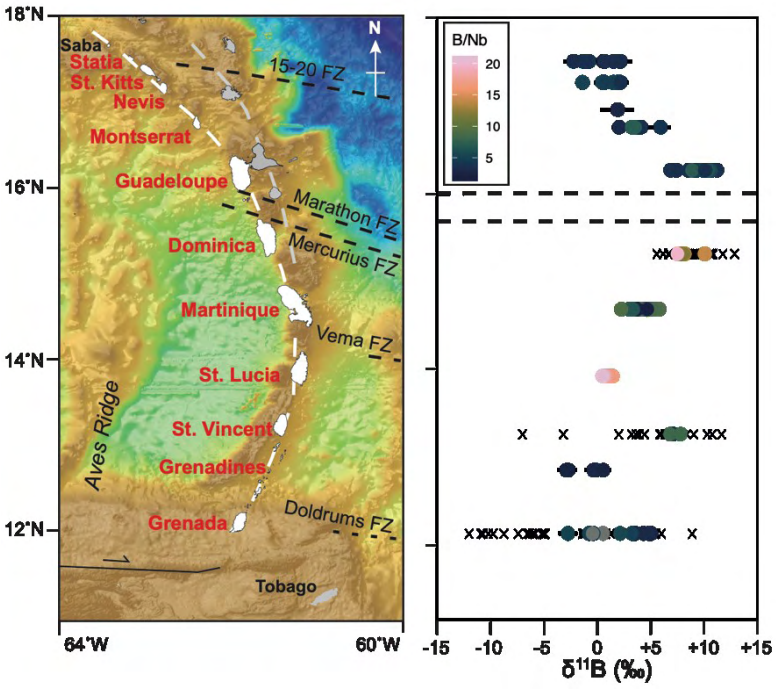

Figure 2. Map of the Lesser Antilles subduction zone with boron isotopic compositions of analysed melt inclusions for each of the islands in red. Circles (coloured by B/Nb ratios of MI's) are data from this study. Crosses represent previously published data.

Melt inclusions have the heaviest $\delta^{11}B$ in the central arc compared to the north and south (**Figure 2**). $\delta^{11}B$ displays variations within each volcanic center, and suggest $\delta^{11}B$ can be modifeid by 2-3‰ during differentiation in the crust. However there are no clear correlations between islands with either indicatiors of differentiation (e.g. Rb/Sr and Ba/Sr) or indicators of fluid addition (e.g. B and B/Nb). This suggests that there are multiple sources of fluids present with disstinct $\delta^{11}B$ signatures.

Key Findings

- There is a large along-arc variation in melt inclusion boron isotopic signatures which suggest there is a variation in the sources of fluids supplied to the arc.
- The central arc (islands of Guadeloupe, Dominica and Martinique) have the heaviest boron, suggesting that fluids in the central arc are sourced from the breakdown of serpentinite (**Figure 3**). In contrast, the southernmost and northernmost islands can be explained from breakdown of altered oceanic crust and sediment (Fig. 3)
- The heaviest boron coincides closely with the location of both the Marathon and Mercurius Fracture Zones suggesting these are likely locations of serpentinisation on the subducting plate.
- The central arc contains the largest islands, with the highest eruption volumes [5] as well as geophysical signals of fluid (e.g. elevated B values [6]). Therefore, the supply of serpentinite derived fluids is a key driver of both magmatism and seismicity in the Lesser Antilles arc.

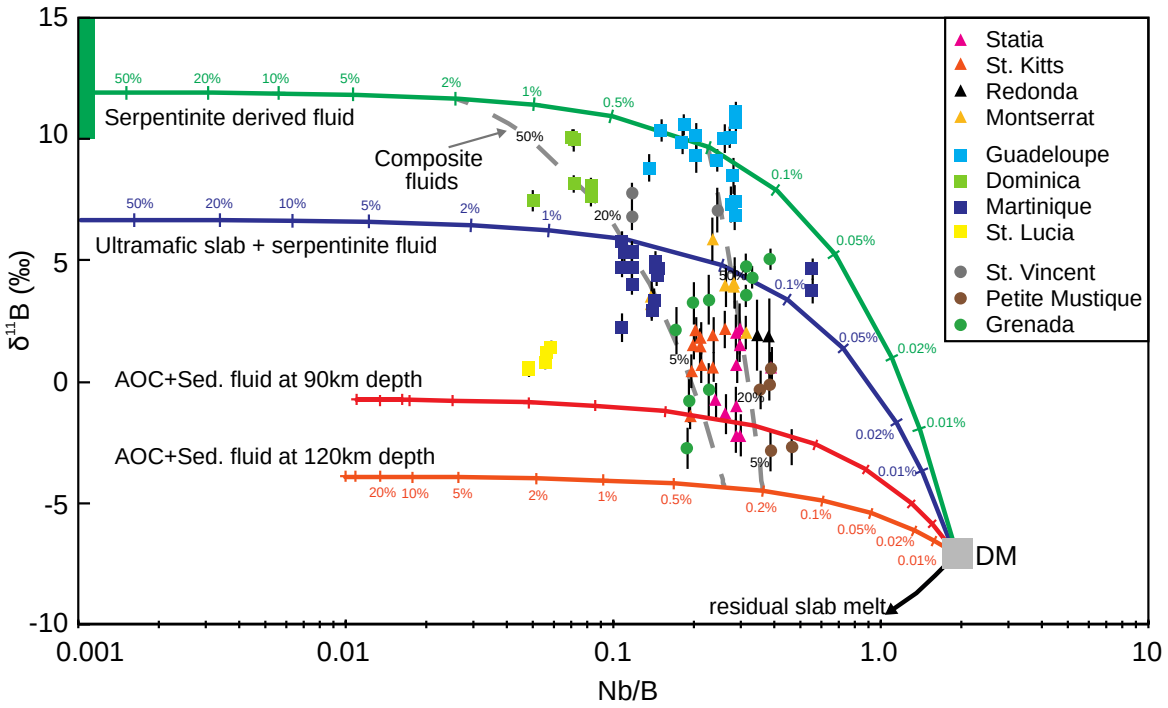

Figure 3. Plot of Nb/B versus $\delta^{11}B$ for Lesser Antilles melt inclusions analysed in this study. Mixing lines are shown for the addition of fluids derived from dehydrating serpentinite to the mantle (DM) and fluids derived from AOC + sediments at different depths to the top of the slab (90 and 120 km). The mixing model illustrates that islands in the central arc (square symbols) must have a contribution from serpentinite fluids.

References

[1] Scambelluri et al., 2004. Int. Geol. Rev. **46**: 595
[2] De Hoog & Savov 2018. In Boron Isotopes, Advances in Isotope Geochemistry 217-247
[3] Boynton et al., 1979. Geophys. J.R.A.S. **58**: 371
[4] Macdonald et al., 2000. Earth-Sci. Rev. **49**: 1
[5] Wadge (1984) Geology **12**, 555-558
[6] Schlaphorst et al. (2016) Geophysical Journal International **204**, 1405

A new record of Eoarchaean to Hadean (?) crustal evolution in the Superior Province

J. Darling[1], C. Storey[1] & D. Moser[2]

[1]School of Earth and Environmental Sciences, University of Portsmouth, UK
[2]Department of Earth Sciences, University of Western Ontario, London ON, Canada

Scientific background

The composition and evolution of Earth's earliest crust remain major unknowns in the geological understanding of our planet, due to the very limited rock record of the first 1 billion years (Ga) of Earth's evolution. Whether the crust during this period was predominantly mafic [1–3] or included large amounts of continental crust [4–7] remains hotly debated, but has major implications for the evolution of the crust-mantle system and early atmosphere, as well as boundary conditions for the origin of life.

Opportunities to test models of early lithospheric processes rely on extremely rare exposures of ancient (>3.5 Ga) rocks. The known examples are highly deformed and metamorphosed, making petrological data and geochemical records difficult to interpret. The accessory mineral zircon is commonly found in crustal rocks and is resilient to metamorphic disturbance, providing unique opportunities to interrogate early crustal evolution. A powerful approach involves the *in-situ* measurement of U-Pb, Hf and O isotopes in zircon, which are used to characterize the nature and origin of the magma source from which the zircon crystallized, and the time since this source separated from the upper mantle. Together, these systems provide patterns of crustal growth that reflect regional geodynamics, and powerful tools for resolving the timing and proportion of juvenile crust formation versus crustal reworking [2,3,7,8].

The recent discovery of Eoarchaean (3.6 to 4.0 Ga), to possibly Hadean (>4.0 Ga), meta-igneous and meta-sedimentary rocks in the Nuvvuagittuq Supracrustal Belt (NSB) offers a new opportunity to investigate the processes of early crustal growth using these techniques. Amphibolites in the belt record very early differentiation of the lithosphere during the active lifespan of the ^{146}Sm-^{142}Nd system ($T_{1/2}$ ≅0.07 Ga [9]), and have reported ages as old as 4.406 ± 0.015 Ga [10,11]. Further evidence for a Hadean origin comes from a 4.1 ± 0.1 Ga ^{147}Sm-^{143}Nd isochron age for intrusive gabbroic sills [11]. However, interpretation of both of these whole-rock Nd ages has been fiercely debated, due to the highly metamorphosed nature of the belt [12], and the geological significance of ^{142}Nd anomalies [13,14]. A range of Eoarchaean granitoids intrude the belt, providing a minimum age of 3.8 Ga [15] and insights into early crustal differentiation.

We have identified new zircon records in the NSB [15], including targets that will provide new U-Pb age constraints on the intrusion of (Hadean?) gabbros and detrital grains that uniquely offer broad sampling of this ancient part of the Superior Province, including units that may not be exposed. These zircon suites have tremendous potential to resolve whether these are Earth's oldest rocks, and provide new insights into the mechanisms of growth, maturation and recycling of Earth's early crust.

Samples and methods

Following on from ion-microprobe (IMS 1270) oxygen isotope ratio measurements of zircon domains at EIMF in November 2017, U-Pb isotope ratio measurements were undertaken on the same samples using the IMS 1270 in 2018. Hf isotope measurements on selected sub-grain domains are underway at the University of Portsmouth. Two sets of newly discovered zircon targets are being analysed:

1. Detrital zircons from semi-pelitic schist N09-23A in the NSB [15]. These zircons have ages up to 3.8 Ga, demonstrating that these grains offer a broad sampling of local Eoarchaean (and older?) crust.
2. Irregular cores in zircons from two metagabbros with a controversial whole-rock Sm-Nd age of 4.1 ± 0.1 Ga. These zircon cores are interpreted to be preserved magmatic zircon domains that are variably replaced by 2.7 Ga metamorphic zircon growth.

Results

New scanning electron microscope imaging has revealed that detrital zircons in semi-pelitic schist N09-23A have a diverse range of internal growth and alteration structures, including many grains with rounded cores that are overgrown by later zircon growth with oscillatory-zonation that is typical of magmatic zircon (Figure 1). This demonstrates that the population records a broad sampling of >3.0 Ga magmatism. The metagabbro zircon grains are predominantly sector zoned, suggestive of a metamorphic origin, but around one-quarter of grains contain cores that are dark in CL that may reflect original magmatic zircon.

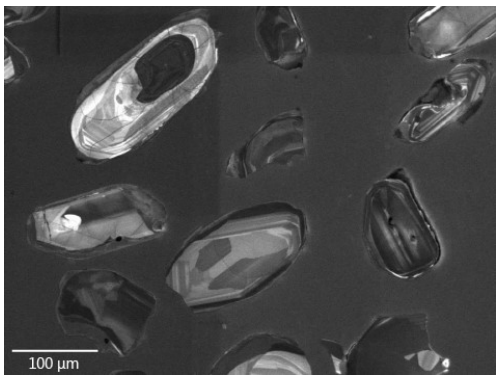

Figure 1: CL image of detrital zircons in sample N09-23A, showing varied growth textures and core-overgrowth structures.

In November 2017, oxygen isotope ratios were measured in these zircons using the CAMECA IMS 1270 at EIMF. Two hundred and thirty measurements were made, targeting different growth domains in both the detrital and metagabbro zircons. In the detrital zircon population of N09-23A, measured $\delta^{18}O$ values range from 3.1 to 7.8 ‰. This range spans from values that are lower than those found in zircon that is in high-temperature equilibrium with the mantle (5.3 ± 0.6 ‰; [17]), to some of the highest values measured in Eoarchaean zircon. The latter are indicative of magma sources that include a significant amount of recycled supracrustal material. The significance of the oxygen isotope data was further revealed by U-Pb isotope analyses at EIMF in May 2018. The targeted grain-domains range in age from 3.8 to 3.0 Ga, providing a new secular record of magmatic evolution spanning from the timings of formation of the earliest cratons to the onset of modern-style plate tectonics [e.g. 1,7]. Excitingly, there are resolvable variations in the oxygen isotope ration measurements through time, which point towards changing magma-sources and tectonic processes. Ten out of twelve analyses from metagabbro zircons, including both cores and sector-zoned overgrowths, fall within the range of mantle zircon. Two further analyses of sector-zoned overgrowths have slightly enriched $\delta^{18}O$ of up to 6.6 ‰. U-Pb data from these grains suggest a metamorphic origin for the differing domains, and provide new constraints on the timing of high-temperature metamorphism of the belt.

Further research

Hafnium isotopes and trace elements are now being measured in the zircons by laser ablation (multi-collector)-inductively-coupled-plasma mass-spectrometry at the University of Portsmouth. These datasets will allow us to further interrogate how the temporal variations in $\delta^{18}O$ values relate to changes in magmatic sources and the tectonic processes of magma generation throughout the Archaean. We

References

[1] Reimink J.R. et al., 2016, Nat. Geosci. Advance. Online Pub.
[2] Kemp A.I.S. et al., 2010, EPSL 296, 45-56
[3] Kemp A.I.S et al., 2015, Precam. Res. 261, 112-26
[4] Harrison T.M., 2009, Annu. Rev. Earth Planet. Sci. 37, 479-505
[5] Wilde S.A. et al. 2001, Nature 409, 175-8
[6] Harrison T.M. et al., 2005, Science 310, 1947-50
[7] Dhuime B. et al., 2012, Science 335, 1334-7
[8] Næraa T. et al, 2012, Nature 485, 627-630
[9] Kinoshita N. et al., 2011, Science 335, 1614–7
[10] O'Neil J. et al., 2008, Science 321, 1828–32
[11] O'Neil J. et al., 2012, Precam. Res. 221, 23–44
[12] Cates N.L. & Mojzsis S.J., 2007, EPSL 255, 9–21
[13] Guitreau M. et al., 2013, EPSL 362, 171–81
[14] Roth A.S.G. et al., 2013; EPSL 361, 50–7
[15] Darling J.R. et al., 2014, Am. J. Sci. 313, 844–76
[16] Gao, Y.-Y. et al, 2015, Scientific Reports 5:16878
[17] Valley, 2005, CMP 150, 561-580

Variations in the volatile contents of primordial and recycled reservoirs in the Galapagos mantle plume

M. Gleeson, S.A. Gibson & M. Stock

Department of Earth Sciences, University of Cambridge, Cambridge, CB2 3EQ, UK

Introduction

The Galapagos Archipelago in the Pacific Ocean represents one of the world's most notable examples of hotspot-derived volcanism. In addition, regional variations in the geochemistry of erupted lavas suggest at least 4 spatially- and isotopically-distinct mantle reservoirs are intrinsic to the Galapagos mantle plume [1] (**Figure 1**). These include a primordial mantle component, with high $^{3}He/^{4}He$ ratios in basalts from the western islands (e.g. Fernandina), and a HIMU-like (extremely radiogenic Pb-isotope) component observed in the southern islands [2] (e.g. Floreana).

Previous studies of volatiles in Galapagos magmas have used analyses of submarine glasses and naturally-quenched melt inclusions to place constraints on the volatile content of high $^{3}He/^{4}He$ basalts from the western island of Fernandina [3,4]. Using additional analyses of volatile- and trace-elements in melt inclusions found in basalts from the southern island of Floreana, we aim to determine whether either of these components represent a major source of volatiles in the Galapagos mantle plume.

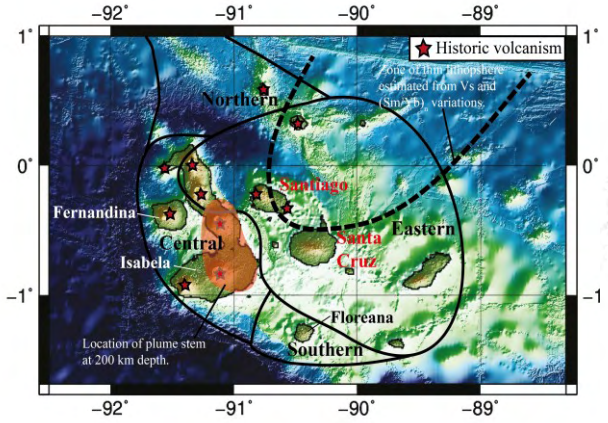

Figure 1. Map showing the spatial variation of the 4 isotopic domains in the Galapagos Archipelago (modified from Hoernle et al. [1]). Samples analysed in this study are from Floreana, located in the far south of the archipelago and appr. 100 km 'downstream' of the centre of plume upwelling (plate motion is west to east). Also shown are the locations of historic eruptions in the archipelago.

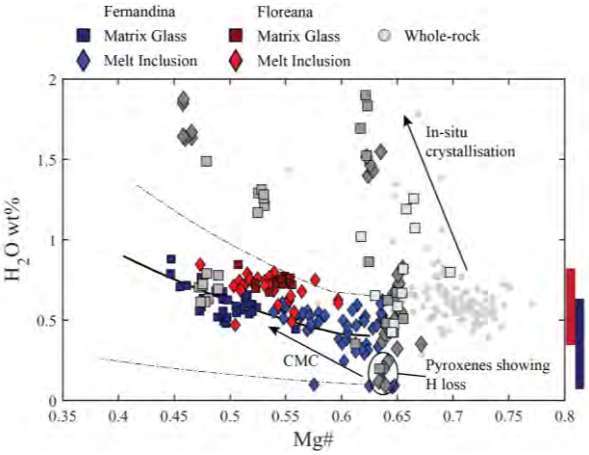

Figure 2. Reconstructed H_2O contents of melt inclusions and matrix glass from Fernandina [3,4] and Floreana. The reconstructed H_2O contents were calculated using a H_2O/La ratio of 410 for Fernandina and 360 for Floreana. Also shown are the H_2O contents in equilibrium with xenocrystic pyroxenes found in Floreana basalts (measured in a previous analytical session).

Methodology

Our investigation focused on naturally quenched olivine-hosted melt inclusions from scoria fragments collected on the island of Floreana (southern Galapagos) in 2017. Trace- and volatile-element analysis of these melt inclusions were undertaken at EIMF in July and August 2018 using the Cameca ims-4f ion microprobe. All analyses were carried out using a $^{16}O^-$ primary ion beam, 15keV net impact energy, 5nA beam current and a ~20 um spot size. Before each analysis, a 3 minute, 50 μm square raster pre-splutter was applied to reduce H^+ background. Background H counts were monitored using a natural olivine crystals at regular intervals. Following SIMS analysis all melt inclusions were analysed by EPMA to determine their major-element composition.

Results and Discussion

Our analyses of olivine-hosted melt inclusions from Floreana allow us to place new constraints on the volatile/incompatible trace-element ratios of the HIMU-like mantle end-member in the Galapagos plume. Reconstruction of the initial concentration of volatiles in the melt inclusions (**Figure 2**) requires careful consideration of secondary processes (e.g. diffusive over-hydration of melt inclusions). On this basis we estimate that the HIMU-like mantle end-member has a H_2O/La of ~360. Similarly, using published analyses of volatile-elements in submarine glass from Fernandina island, and carefully correcting for the influence of hydrothermal brine assimilation, we constrain the H_2O/La ratio of the high $^3He/^4He$ mantle source to be ~410.

We used a simple Monte Carlo simulation, and our new constraints on the H_2O/La, F/Nd, and Cl/K content of the mantle source regions beneath Fernandina and Floreana, to estimate the volatile content of the primordial mantle and the HIMU-like domain in the Galapagos plume (**Figure 3**). These results indicate that the HIMU-like component contains high (and potentially extremely variable) concentrations of F and Cl. Moreover, basalts from Floreana are characterised by slightly higher concentrations of H_2O than those from Fernandina, suggesting that the HIMU-like component contains significantly less H_2O than the primordial mantle component in the Galapagos mantle plume. Paradoxically, our results indicate that the higher H_2O in Floreana basalts results from a lower extent of partial melting in the underlying mantle, rather than from more hydrous mantle source.

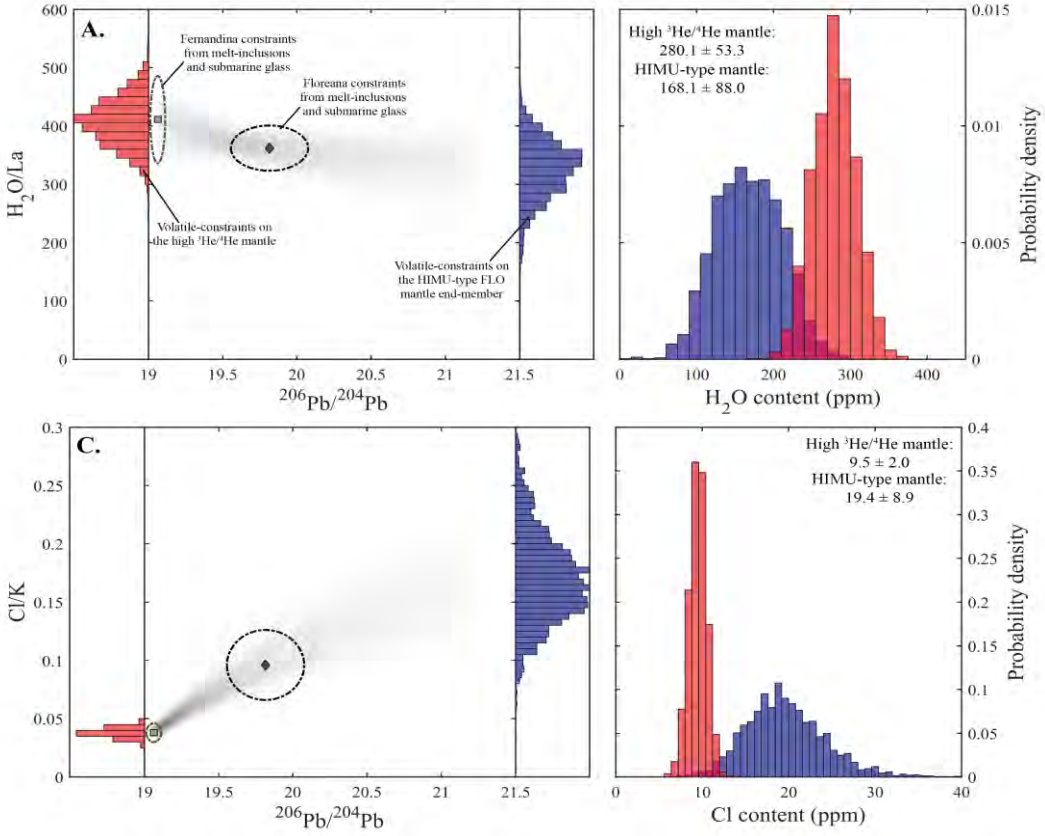

Figure 3. Results of Monte Carlo Simulation to determine the H_2O (**A.**) and Cl (**C.**) content of the two mantle sources expressed in the geochemistry of the Floreana basalts. Source composition for the primordial mantle is taken from Sun and McDonough [5], and the source composition of the HIMU mantle is taken from Weiss et al. [6].

References

[1] K. Hoernle et al. (2000) *Geology*, 28(5), pp. 435-438;
[2] K. Harpp et al. (2014) Galápagos Nat. Lab. Earth Sci. In: AGU Monogr, 204, pp.71-118;
[3] A. Koleszar et al. (2009) *EPSL*, 287(3), pp. 442-452;
[4] M. Peterson et al. (2017) *J. Pet.*, 58(7), pp.1419-1450;
[5] S. Sun and W. McDonough (1989) *Geological Society, London, Special Publications*, *42*(1), pp.313-345;
[6] Y. Weiss et al. (2016) *Nature, 537(7622)*, p. 666.

Forming the first stable continental crust

A.R. Hastie

School of Geography, Earth and Environmental Sciences, University of Birmingham

Scientific reasons for the investigation

The Earth has three central and interlinked distinguishing features: oceans of water, oceanic and continental crust and plate tectonics. Here we examine if the link between these three fundamental features extends back 4 billion years, with the onset of plate tectonics in the presence of early oceans leading to the formation of the first continental crust by the partial melting of primitive oceanic crust in nascent subduction zones.

Background

Hastie et al.[1] recently investigated the petrogenesis of ancient continental-like magmas by generating partial melts in high pressure-temperature (P-T) experiments designed to replicate an Eoarchaean (4.0-3.6 Ga) subduction environment[1]. For a starting composition, a single sample of Mesozoic Ontong Java Oceanic Plateau (OJP) basalt, which is primitive and relatively depleted in incompatible elements (**Kroenke-type basalt: Table 1**), was used as an Eoarchaean oceanic crust analogue. An oceanic plateau starting composition was used because Eoarchaean upper mantle was hotter and less depleted in incompatible elements than the present-day asthenosphere[2,3]. Thus, Eoarchaean spreading centres should have been characterised by larger degrees of partial melting, producing less depleted and thicker oceanic crust (~25-45 km) than today (~7 km)[3-6]. In the absence of preserved Eoarchaean oceanic crust, the closest analogue to oceanic crust formed by melting hot, un-depleted Eoarchaean mantle are the Mesozoic oceanic plateaus that are formed by the partial melting of relatively hot and less incompatible element depleted mantle plume heads[7], are enriched relative to MORB, and are up to 35 km thick[7].

Project Hypothesis

The Kroenke-type high P-T experiments generate tonalites, in equilibrium with plagioclase and garnet-bearing amphibolites that lack rutile (low TiO_2 content prevents rutile stabilising[1]). Most elements from the Kroenke-derived partial melts match early continental rocks (Eoarchaean tonalites and trondhjemites: ETT) compositions; however, the Kroenke-derived tonalites have low K_2O and Ba contents relative to ETT. Furthermore, ETT commonly have pronounced negative Nb-Ta anomalies on multielement diagrams[1] to give (La/Nb)mn (MORB normalised) ratios of 1.3-11.5. The Kroenke-derived tonalites overlap ETT with (La/Nb)mn of 0.7-2.3, but require either enrichment of the light (L)REE and/or residual rutile (partition coefficients for Nb and Ta >>1) in order to increase the (La/Nb)nmn ratio[1]. Hastie et al.[1] present a model where the Kroenke-derived tonalitic melts mix with dehydrated slab fluids from deep within the slab. The modelled Kroenke-melt + slab fluid mixtures have compositions that match a larger portion of, but not all, the ETT because the slab fluid increases the contents of the incompatible elements (K_2O, Ba and LREE) in the mix. However, the question remains: can oceanic plateau starting material that has higher incompatible element contents and higher TiO_2 (to stabilise rutile), undergo fusion to generate melts with ETTG compositions that have higher K_2O and Ba and more pronounced Nb-Ta anomalies to explain the formation of ***all*** ETT without the need for a slab-flux? Our overarching hypothesis is thus:

Partial melting of enriched oceanic plateau starting compositions can generate major and trace element melt compositions similar to all Eoarchaean continental crust (ETT)

Objective

Eight new high P-T experiments have been undertaken using a relatively **enriched** and **less primitive** 'Kwaimbaita-type' oceanic plateau starting composition from the OJP. Major element analyses, determined by electron microprobe, on our new Kwaimbaita-type experimental melts confirm that they are tonalitic in composition and have major element compositions that match ETT. Therefore, with regards to major elements, the new Kwaimbaita-type melts can explain most of the ETT. However, we conducted the SIMS study to confirm that the trace element compositions of the

new melts are similar to **all** ETT to determine if Kwaimbaita-type basalt is a viable Eoarchaean oceanic crust analogue.

Results

Some results are still pending on a final visit to the facility in April 2019. Preliminary analyses of the Kwaimbaita-type melts with the range of ETT compositions are seen in **Fig. 1**. As can be seen, the new melts do have many elemental compositions that match ETT; however, Ba seem to be too low. It is hoped that analyses in April may replicate the results in **Fig. 1** with higher Ba.

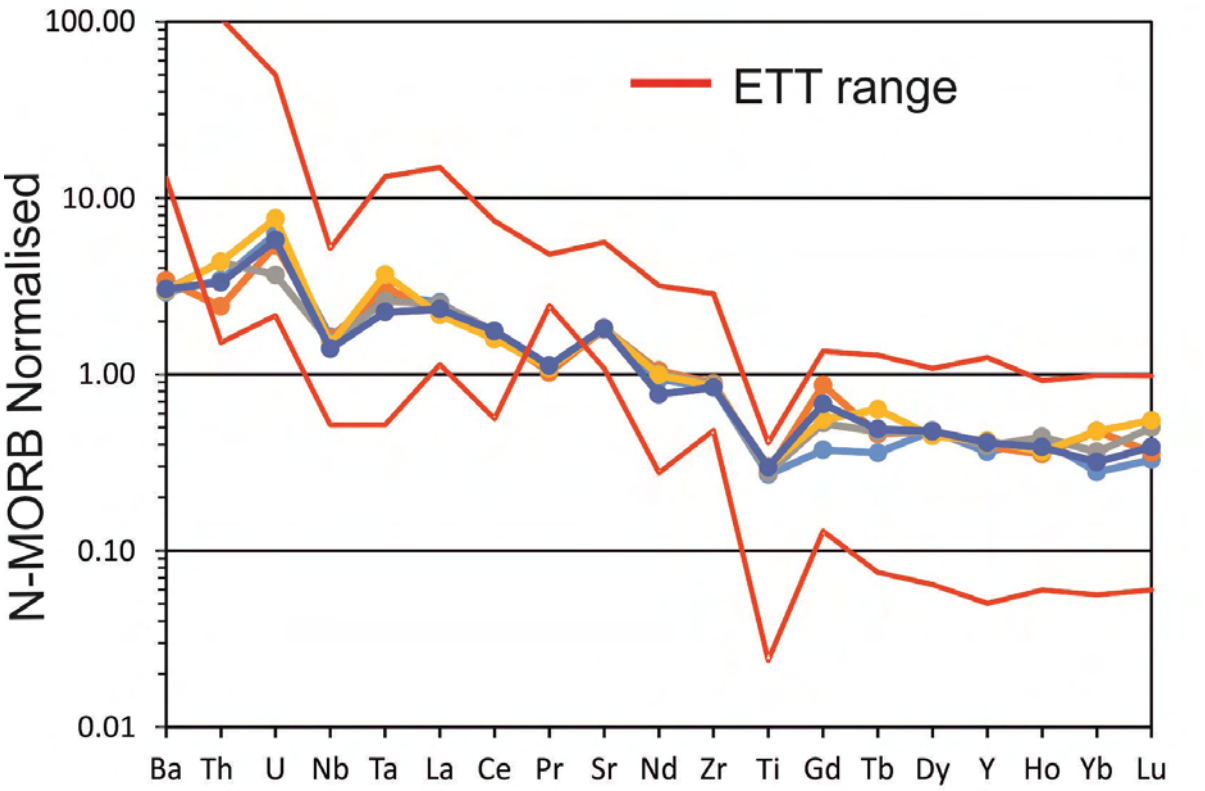

Fig. 1: Analytical results thus far.

References

[1] Hastie A.R., F., J.G., Bromiley, G.D., Butler, I.B. & Odling, N.W.A. (2016) Geology 44, 855-858
[2] Shirey, S. B., Kamber, B.S., Whitehouse, M.J., Mueller, P.A. & Basu, A.R. (2008) The Geological Society of America Special Paper 440, 1-29..
[3] Herzberg, C., Condie, K. & Korenaga, J. (2010) Earth and Planetary Science Letters 292, 79-88..
[4] Abbott, D., Drury, R. & Smith, W.H.F. (1994) Geology 22, 937-940.
[5] Smithies, R. H., Champion, D.C. & Cassidy, K.F. (2003) Precambrian Research 127, 89-101.
[6] Moyen, J.-F. M., H. (2012) Lithos 148, 312-336.
[7] Fitton, J. G. G. M. (2004) Origin and evolution of magmas on the OJP. In: Fitton, J.G., et al (Eds) Geological Society of London Special Publication 229, 151-178

Investigating the potential for brittle star age determination using vertebral ossicles

P. Hollyman[1,3], S. Chenery[2], C. Sands[3], S. Jenkins[1] & C. Suckling[1]

[1] School of Ocean Sciences, College of Natural Sciences, Bangor University, Anglesey
[2] Centre for Environmental Geochemistry, British Geological Survey (BGS), Nottingham
[3] British Antarctic Survey, High Cross, Madingley Road, Cambridge

Background

Marine environments around west Antarctica are thought to be carbon draw down hotspots in certain areas [1,2,3]. This is due to one of the few negative feedbacks on climate change; sea ice loss and primary production increases are resulting in increased carbon sequestration [3]. The benthos in some of these environments has been shown to be a significant sink of carbon especially in calcifying invertebrate species such as bryozoans [1]. One of the more common species groups in this environment are the brittle stars [4]. These species contain a calcium carbonate skeleton [5] and can form dense populations on the seabed [4], potentially representing a significant portion of sequestered carbon. Detailed datasets have been collected regarding abundance and spatial distributions of brittle star species in the Antarctic [4]. Much of this data has been collected using a Shelf Underwater Camera System (SUCS) which allows in-situ analysis of abundance and size distributions of benthic communities [6]. Whilst the carbon content of individuals vs. size can be easily acquired, this data needs a temporal component (i.e. the age of the animals) to allow us to make estimates of the time taken to sequester the carbon present in these individuals. This could be achieved by creating age-at-length keys for brittle star species by ageing a subset of individuals from a population. To do this, a reliable age determination method is required. Skeletal growth lines in brittle stars have been studies previously in both temperate [7], deep sea [8] and Antarctic [9] species. These studies concluded that growth bands present in structures such as vertebral ossicles are likely formed on an annual basis, meaning they can be used for age determination. This ageing method is thought to be more reliable than methods such as length frequency analysis which does not account for the potentially high variability of growth within a slow-growing population [9].

Whilst the reliability of annual growth lines in bio-carbonate structures from temperate environments is well established as a results of annual sea water temperatures [10], this is not always the case for biomineralizing Antarctic species as the annual temperature regime is often minimal. In the case of some Antarctic bivalve species, annual bands have been shown to form due to other environmental factors such as fast ice duration controlling food availability (e.g. Yoldia eightsi; [11]). It is therefore important to understand what is causing the formation of visible lines in the vertebral ossicles of Antarctic brittle stars before relying on them as an age determination tool. No attempts have yet been made to validate the periodicity of brittle star growth lines with chemical analysis which may help to elucidate the reasons for growth line formation. Echinoderm skeletons are composed of high magnesium calcite [5], meaning that they are stable enough to sample with surface analysis techniques such as LA-ICP-MS and SIMS. Using these techniques, elements such as magnesium and strontium can be analysed which may relate to seawater temperature, salinity [12] or potentially growth rate [13, 14].

The aim of this study was to use SIMS to assess changes in trace element concentrations across growth axes from vertebral ossicles of *Ophiacantha antarctica* containing visible growth bands. We hypothesized that clear cycles in Ca:Mg and Ca:Sr will be seen between visible growth rings, relating to annual temperature (Ca:Mg) and salinity (Ca:Sr) cycles, confirming an annual periodicity to the visible growth rings.

Methods

Ossicles from the arms of *Ophiacantha Antarctica* were dissected from several ethanol preserved specimens. Tissue was removed by immersing the specimens in 20% NaOH for 24 hours, the samples were then thoroughly cleaned using deionised water and left to dry in a laminar flow hood at room temperature. Each ossicle was mounted on a separate 1 inch round glass slide in Epothin 2 resin (Buehler) and left to cure for 72 hours. Each resin embedded sample was then ground to expose a

suitable plane for SIMS analysis using sequential grades of silicone carbide wet/dry grinding papers and given a final polish using 3, 1 and 0.5 µm diamond suspension polishing compounds (**Figure 1**). SIMS analysis was undertaken using a CAMECA IMS-4f Ion microprobe along the full growth axis of each ossicle, from the centre towards the outside edge **(Figure 1b**). Samples were pumped to a vacuum of 5× 10−9 Torr, a spot size of 10 µm was used with a step size of 10µm and a beam current of 0.06 nA with a net input energy of 15 keV.

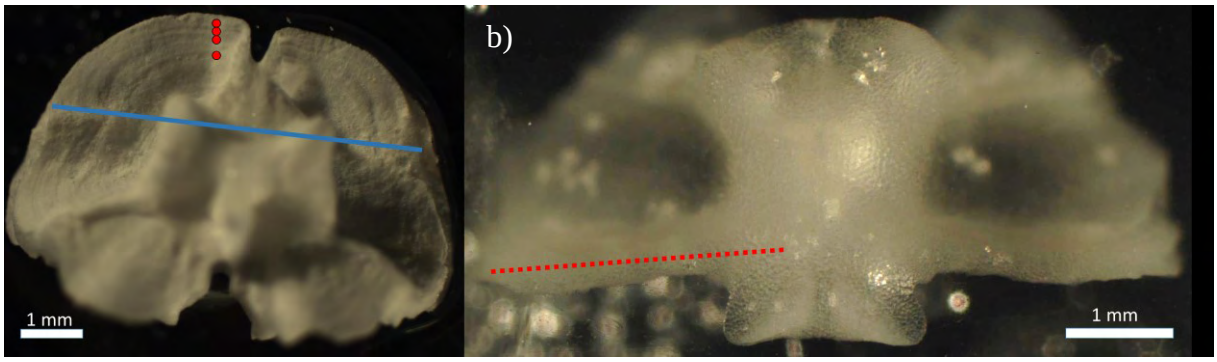

Figure 1. a) lateral view of a vertebral ossicle from *Ophiacantha antarctica*. The blue line indicates the sectioning plane, red dots denote visible growth rings; **b)** dorsal view of a sectioned *O. antarctica* ossicle, imaged using reflected light. Red line indicates the sampling track used for SIMS. The porous nature of the structure is visible.

Results

Due to the unexpectedly porous nature of the internal ossicle structure, the SIMS analysis was undertaken at a resolution too fine to produce representative results, hence, none are presented here. Only two samples were analysed out of a possible 10 as it was agreed that no useable data was being collected. Due to the large amount of resin contained within the structure and the small beam diameter, the beam was regularly passing between carbonate and resin only areas, leading to a noisy dataset that was unsuitable for interpretation. It was decided that any further work on these samples should be undertaken using a surface analysis technique that has a much larger spot size (e.g. LA-ICP-MS) which would be able to spatially average across the carbonate and resin areas, giving a more representative reflection of the actual compositional changes over time.

References

[1] D.K.A. Barnes et al. (2016) Global Change Biology **22**, 1110-1120
[2] D.K.A. Barnes (2015) Current Biology **25**, R789-R790
[3] L.S. Peck et al. (2010) Global Change Biology **16**, 2614-2623
[4] C.J. Sands et al. (2013) Antarctic Science **25(1)** 3–10
[5] J. Weber (1969) American Journal of Science **267,** 537-56
[6] D.K.A. Barnes and C.J. Sands (2017) PLOS one **12(6)**, e0179735
[7] J.D. Gage (1990) Marine Biology **104,** 427-435
[8] J.D. Gage (1990) Journal of the Marine Biological Association of the United Kingdom **70,** 209-224
[9] C. Dahm and T. Brey (1998) Journal of the marine biological association of the UK **78,** 941-951
[10] C.A. Richardson (2001) Oceanography and Marine Biology: an annual review **39,** 103–164
[11] A. Román-González et al. (2017) The Holocene **27(2)**, 271-281
[12] C. Borremans et al. (2009) Geology **37(4)** 351–354
[13] S. Sosdian et al. (2006) Geochemistry Geophysics Geosystems **7,** Q11023
[14] P.R. Hollyman, et al (2017) Chemical Geology, doi.org/10.1016/j.chemgeo.2017.09.034

Calculating the initial H_2O and CO_2 contents of basaltic arc magmas using stable isotope fraction

E. C. Hughes[1], G. Kilgour[2], H. M. Mader[1] & J. Blundy[1]

[1]School of Earth Sciences, University of Bristol, United Kingdom
[2]Wairakei Research Centre, GNS Science, Taupo, New Zealand

Introduction

Volcanoes are a key component of the global C cycle, transferring C from the mantle, subducted slab, and crust to the atmosphere. Additionally, volatiles (of which C is the second most abundant in magmas) have a primary control on eruption dynamics. Quantifying the initial C content of magmas is therefore crucial to our understanding of volatile cycling and eruption triggers. It is difficult to quantify the initial C content because carbon has little effect on the phase relations of magmas and, due to its low solubility, has already begun to degas prior to melt inclusion formation. C isotopically fractionates during degassing, with the melt becoming enriched in ^{12}C compared to the fluid, hence the relationship between the C concentration and isotope ratio of a suite of melt inclusions can be used to infer the initial C concentration and isotope ratio, and style of degassing, of an eruption.

Technique development

We developed a SIMS technique for analysing $\delta^{13}C$ in hydrous basaltic glass at high spatial resolution using the Cameca 1270. Carbon contamination during SIMS analysis was found to be problematic: the level of contamination was found to depend primarily on the vacuum pressure (samples should be left for at least a day in the analysis chamber prior to analysis to obtain useful data; **Figure 1a,b**) and pre-raster area as carbon from the edges of the pre-rastered area was incorporated into the analysis pit (**Figure 1d**) (a pre-raster area of 15×15 μm was sufficient; **Figure 1c**), with a minor effect of pre-raster time (120 s was sufficient with longer times showing no improvement; **Figure 1c**).

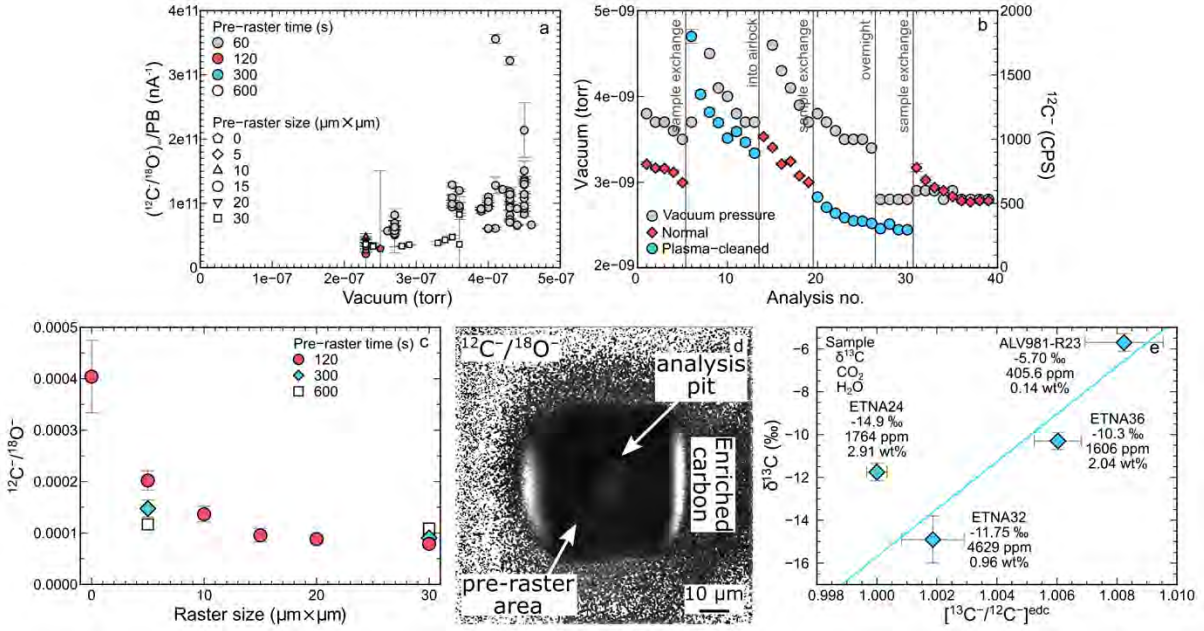

Figure 1. (a)–(c) Olivine analyses to investigate the background: **(a)** $(^{12}C^-/^{18}O^-)_\infty$/PB against vacuum pressure; **(b)** $^{12}C^-$ for consecutive analyses on 'normal' (red diamond) and 'cleaned' (blue circle) olivine; and the vacuum pressure shown in grey circles, where vertical lines show when samples were moved between the airlock and analysis chamber (sample exchange), when samples were loaded into the airlock (into airlock), and when samples were left in the analysis chamber overnight (overnight), and **(c)** $^{12}C^-/^{18}O^-$ against raster size. **(d)** $^{12}C^-/^{18}O^-$ scanning ion microscopy image of SIMS analysis pits. **(e)** Calibration curve.

There may be a matrix effect of H_2O when quantifying $\delta^{13}C$ (**Figure 1e**), but there are currently insufficient standards to investigate this fully. Analysing $^{18}O^-$ helps to align the beam when analysing low carbon samples and also allows the accurate quantification of CO_2 concentration at the same time as $\delta^{13}C$, but adds significant time to the analysis which reduces the precision of the $\delta^{13}C$ measurement.

Experimental glasses

We analysed experimentally produced glasses to constrain the isotopic fractionation factor between carbon dissolved in basaltic melt and exsolved fluid under oxidising conditions at 1250 °C, 1–7 kbar, and 0–6 wt.% H_2O. We used the Cameca IMS 4f to measure CO_2 and H_2O concentrations and the Cameca 1270 for $\delta^{13}C$ and δD. We obtained -0.3 ± 3.4 ‰ for starting batch 5a and +10.2 ± 3.8 ‰ for starting batch 7. These values are very different and there are a few analytical problems which unfortunately compromise these results: CO_2-rich and -poor glasses were analysed during separate sessions; the calibration curve for CO_2-rich glasses contained contaminated analyses; and CO_2-poor analyses are associated with large errors. Hence, further analyses are needed to constrain the fractionation factor from these samples.

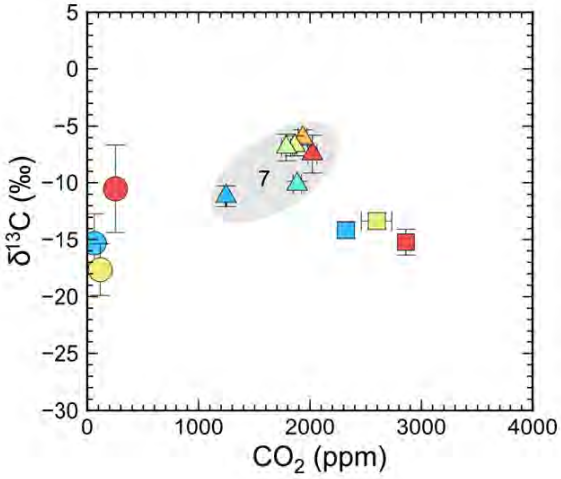

Figure 2. $\delta^{13}C$ and CO_2 of the experimental glasses, where group 7 is labelled and the six data points not labelled belong to group 5a.

Natural melt inclusions

We analysed olivine- and pyroxene-hosted melt inclusions from the 23 November 2013 paroxysmal eruption of Etna, Sicily, for volatile concentrations (CO_2 and H_2O using the Cameca IMS 4f) and isotope ratios ($\delta^{13}C$ and δD using the Cameca 1270). In combination with major and minor elements, and Fe oxidation state, using EPMA we found the eruption was likely triggered by mixing of a more primitive magma from depth containing ~3 wt.% H_2O and up to 1600 ppm CO_2 with a more evolved magma shallowed in the system. The single $\delta^{13}C$ measurement (-5.3 ± 2.4 ‰) is consistent with previous gas measurements at Etna.

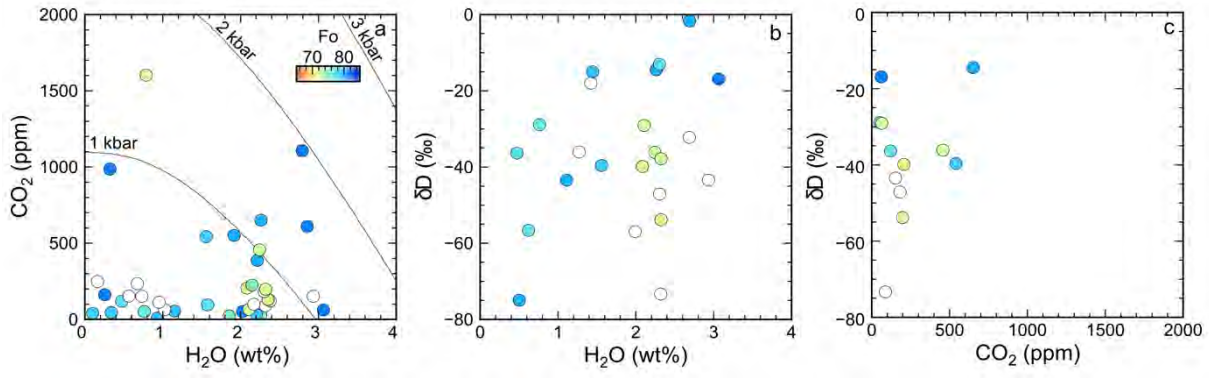

Figure 3. Volatile composition of melt inclusions from the 23 November 2013 paroxysmal eruption of Etna, Sicily: **(a)** CO_2 and H_2O with isobars calculated using VolatileCalc (49 wt% SiO_2 and 1150 °C); **(b)** δD and H_2O; and **(c)** δD and CO_2, where symbols are coloured by forsterite content (Fo) if olivine-hosted or white if pyroxene-hosted. One melt inclusion had -5.3 ± 2.4 ‰ $\delta^{13}C$, 460 ppm CO_2, and 2.24 wt% H_2O.

Evaluating the volatile budget of the Main Ethiopian Rift

F. Iddon & M. Edmonds

Dept. of Earth Sciences, University of Cambridge

Introduction

Magmatic volatiles readily partition between melt, crystals, and exsolved vapour, exerting a strong control over magma properties [1]. The success of constraining shallow crustal magma bodies is dependent on these properties. Geophysical techniques such as magnetotelluric tomography may fail to image volatile poor melts due to higher resistivity [2], observable deformation signals at volcanoes may also be dampened by the presence of a compressible gas phase [3]. Meanwhile, due to the solubility of CO_2 and H_2O within silicate melts being largely pressure dependent, depths of magma storage can be deduced from the volatile contents of melts [4,5].

Constraints on volatile concentrations and systematics in MER magmas are limited [6]. Volcano monitoring in Ethiopia is basic, and geophysical investigations have so far presented complex results. Magnetotelluric surveys have failed to image melt beneath some of the axis central peralkaline calderas (e.g. Aluto [2,7]) despite Holocene volcanic activity and evidence from other techniques (including InSAR observations [8]). Instead likely melt rich features have been imaged beneath basaltic volcanic fields to the West of the MER [2,9] (**Figure 1**). Petrological investigations suggest that magmatic storage might vary across the MER, with melts ascending quickly beneath the rift axis and undergoing protracted fractionation [10,11]. The off-axis melts are thought to be supplied by a more complex system with multiple storage depths, with phase equilibria indicating that they may be more water-rich [11] (**Figure 2**).

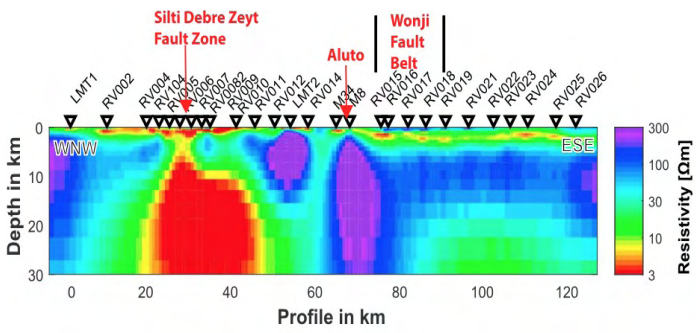

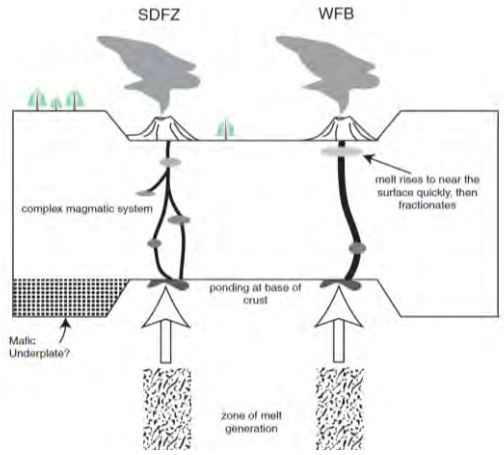

Figure 1 (above) Preferred inversion model of electrical resistivity for the upper 30 km of the MER crust (taken from [2]). **Figure 2 (right)** A cartoon of crustal structure beneath the Silti-Debre Zeyit Fault Zone (SDFZ), where the off axis volcanic fields are located, and Wonjii Fault Belt (WFB), collocated with MER peralkaline calderas (taken from [11]).

Strategy

Phenocrysts of quartz and olivine were picked from crushed fractions of samples from a number of MER calderas, as well as from the off axis Butajira volcanic field. The samples were all scoria or pumice, chosen to minimise the effect of volatile loss from the crystal-hosted melt inclusions. Crystals with melt inclusions were polished then mounted in epoxy for volatile and trace element analysis using Secondary Ion Mass Spectrometry (SIMS) at the University of Edinburgh.

Results and Discussion

Axis central melts are not volatile poor, off axis melts are not notably volatile rich

Magnetotelluric surveys assess Earth subsurface electrical conductivity, a property sensitive to fluid content, allowing the method to identify the presence of partial melt beneath volcanoes [12,13]. However, the electrical conductivity of magmatic reservoirs is dependent on the state of the magma itself, in terms of melt volatile abundance, temperature, composition, and crystal content. It has been hypothesised that the absence of a conductive region beneath some MER calderas may be related to low volatile contents [2] (**Figure 3**).

The quartz hosted melt inclusions from these sites show H_2O enrichment of up to 7 wt.% (**Figure 4b**). Fluorine and Cl contents are also high at up to 0.5 wt.%. Only CO_2 content is low, typically <350 ppm. It has been experimentally determined that H_2O content correlates with silicate melt conductivity [14]. Despite enhanced clinopyroxene fractionation suggesting high melt water content, and the large conductive feature on the magnetotelluric survey, there is no evidence for notably water rich off-axis basalts. They are comparable with basalts believed to be parental to the axis central peralkaline silicic magmas, both showing H_2O contents of up to 1.5 wt% (**Figure 4a**).

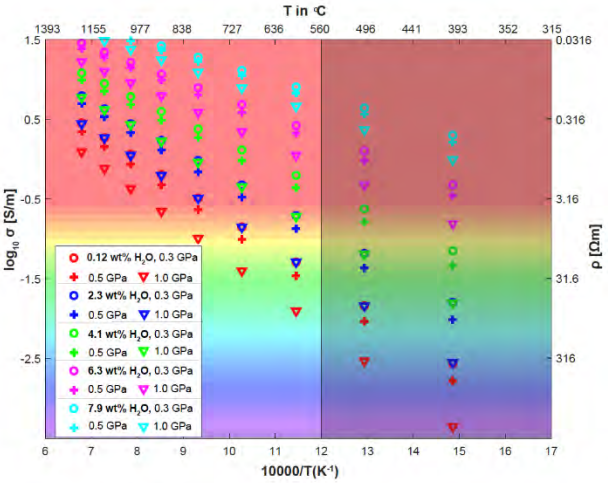

Figure 3. Computed electrical resistivity values for partial melt using the relationship derived by Guo et al., 2016 for peralkaline melts (taken from [2]).

Off axis melts are stored deeper

Whilst melt H_2O contents are similar, CO_2 contents can be much higher in the off-axis basalt samples at up to 5000 ppm (**Figure 4a**). The parental more axis central basalts typically contain <2000 ppm carbon. CO_2 is much more soluble than H_2O, resulting in the rapid loss of CO_2 to a vapour phase at depth, that only becomes enriched in H_2O rich at lower pressures [1]. This suggests that the off-axis basalts are stored at greater depths, which would also the support enhanced clinopyroxene fractionation noted. Geobarometric estimates have been made using the methods of Papale et al. [5] and Newman and Lowenstern [4], constraining basaltic magma storage at up to a depth of 20 km beneath the axis of the MER, but up to a depth of 30 km beneath the off axis volcanic fields to the West of the rift. Silicic peralkaline melts are stored at between 5 and 9 km beneath the axis of the MER, comparable to estimates made using geophysical techniques such as seismics and modelling of InSAR deformation sources (**Figure 4c**).

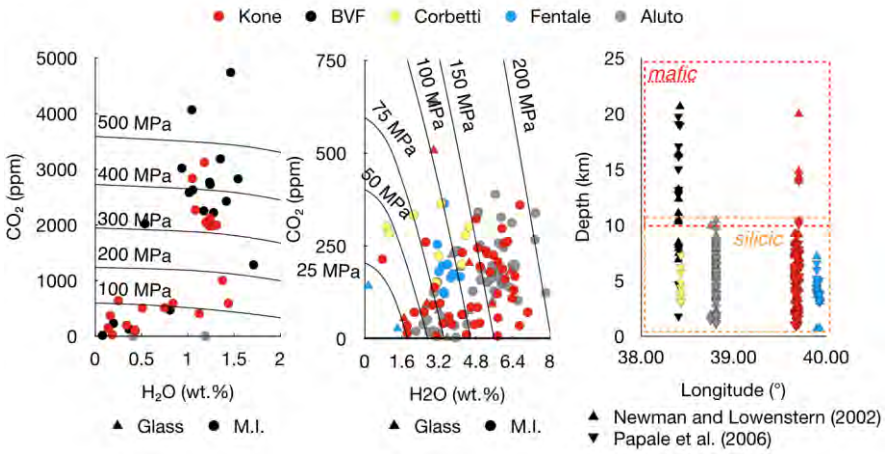

Figure 4 a, b. H_2O against CO_2 plots for MER melt inclusions. Isobars calculated from volatile solubility [4] are plotted on top for a mafic system at 1150°C (**a**) and rhyolite system at 800°C (**b**); **c**) Depth of melt inclusion entrapment calculated using the methods of Papale et al. [4] and Newman and Lowenstern et al. [5].

Forward model construction

Forward models of electrical conductivity/resistivity have been constructed to aid in the interpretation of features observed in recent magnetotelluric surveys across the MER and to test the spatial/temporal restrictions of this geophysical method. The new geochemical data on melt volatile contents has been incorporated with petrological constraints [15] to evaluate the conductivity of a MER magma with varying the crystal content. A grid system (500m x 500m grid squares) was constructed, with pressure, temperature, and melt composition (SiO_2, Na_2O, and H_2O) imposed on each grid square. Experimentally determined relationships were then used to calculate melt conductivity [14,16-18]. Mixing models were

used to incorporate varying amounts of crystals into the system [19] (**Figure 5**). The models highlight the importance of crystal content, suggesting highly crystalline magmatic systems will likely produce a resistive structure in the crust, similar to that observed beneath Aluto volcano. Inversion of the synthetic data also indicated that small melt pockets would be resolved using MT surveys (**Figure 5**).

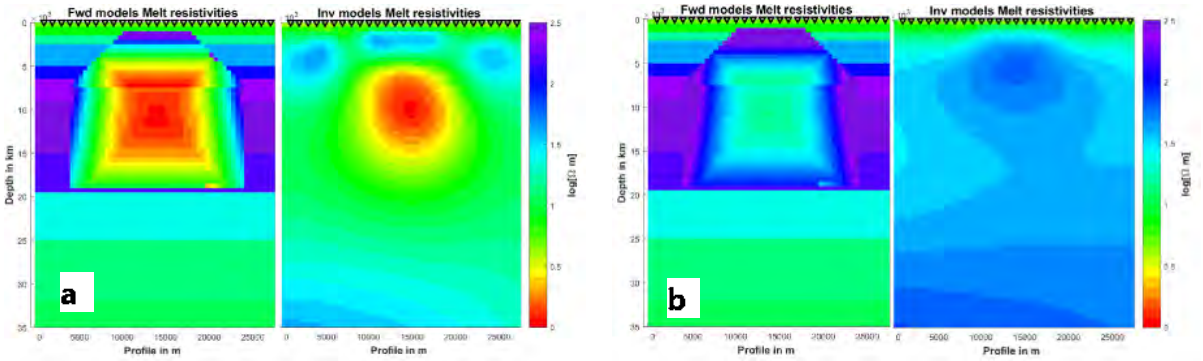

Figure 5. Combined electrical conduc-tivity forward model (left image) and model inversion (right image) for crystal poor (a) and crystal rich systems (b).

References:

[1] Edmonds, M., Wallace, P.J.. 2017. Elements 13, 29–34;
[2] Hübert, J., Whaler, K., Fisseha, S. 2018. Journal of Geophysical Research: Solid Earth 123, 6019–6032;
[3] Biggs, J., Ebmeier, S.K., Aspinall, W.P., et al. 2014.. Nature Communications 5, 3471;
[4] Newman, S., Lowenstern, J.B. 2002. Computers and Geosciences 28, 597–604.;
[5] Papale, P., Moretti, R., Barbato, D. 2006. Chemical Geology 229, 78–95;
[6] Webster, J.D., Taylor, R.P., Bean, C. 1993. Contributions to Mineralogy and Petrology 114, 53–62;
[7] Samrock, F., Kushinov, A., Bakker, J., et al. 2015. Geophysical Journal International 202, 1923–1948;
[8] Hutchinson, W., Biggs, J., Mather, T.A., et al. 2016. Geochemistry, Geophysics, Geosystems 17, 3008–3030;
[9] Whaler, K., Hautot, S. 2006. Geological Society, London, Special Publications 259, 293–305.
[10] Rooney, T., Bastow, I.D., Keir, D. 2010. Journal of Volcanology and Geothermal Research 201, 83–96;
[11] Rooney, T., Furman, T., Bastow, I.D., et al. 2007. Journal of Geophysical Research 112;
[12] Desissa, M., Johnson, N., Whaler, K., et al. 2013. Nature Geoscience 6, 861–865;
[13] Johnson, N., Whaler, K., Hautot, S., et al. 2015. Geological Society, London, Special Publications 420;
[14] Gaillard, F. 2004. Earth and Planetary Science Letters 218, 215–228;
[15] Iddon, F., Jackson, C., Hutchison, W., et al. 2018. Geochemistry, Geophysics, Geosystems;
[16] Guo, X., Zhang, L., Behrens, H., et al. 2016. Earth and Planetary Science Letters 433, 54–62;
[17] Pommier, A. and Le-Trong, E. 2011. Computers & Geosciences, 37(9), pp.1450-1459;
[18] Pommier, A., Gaillard, F., Pichavant, M., et al. 2008. Journal of Geophysical Research: Solid Earth, 113(B5);
[19] Hashin, Z. and Shtrikman, S. 1962. Journal of applied Physics, 33(10), pp.3125-3131;

Fluid-mobile trace elements and $\delta^{11}B$ signatures in Kamchatka melt inclusions

A.A. Iveson[1], M.C.S. Humphreys[1], I. P. Savov[2], J.C.M. de Hoog[3], T.G. Churikova[4] & C.G. Macpherson[1]

[1]Department of Earth Sciences, Science Site, Durham University
[2] School of Earth & Environment, University of Leeds
[3]Grant Institute, School of GeoSciences, University of Edinburgh
[4]Institute of Volcanology and Seismology FED RAS, Petropavlovsk-Kamchatsky, Russia

Introduction & Background

A wealth of recent literature has shown the potential for boron, and its stable isotopic system, to be used as a key proxy for variable fluid addition into the mantle melting region of volcanic arcs[1]. Specifically, the heavier ^{11}B isotope is selectively mobilised during prograde dehydration reactions occurring in the down-going slab, and slab-derived fluids should become progressively isotopically lighter and depleted in total B as subduction continues. Thus, compared to volcanoes located in the forearc region, the most rear arc volcanoes should record the lowest abundances of fluid mobile elements and the lightest $\delta^{11}B$ signatures. This study combines SIMS measurements of volatile (e.g. H_2O, CO_2, Cl) and fluid-mobile trace elements (e.g. B, Sr) with analysis of the $\delta^{11}B$ values preserved in primitive melt inclusions from a transect across nine volcanic centres of the Kamchatka arc (Fig. 1), in order to trace the variable contributions from different hydrous slab inventories between the distinct tectonic locations[2].

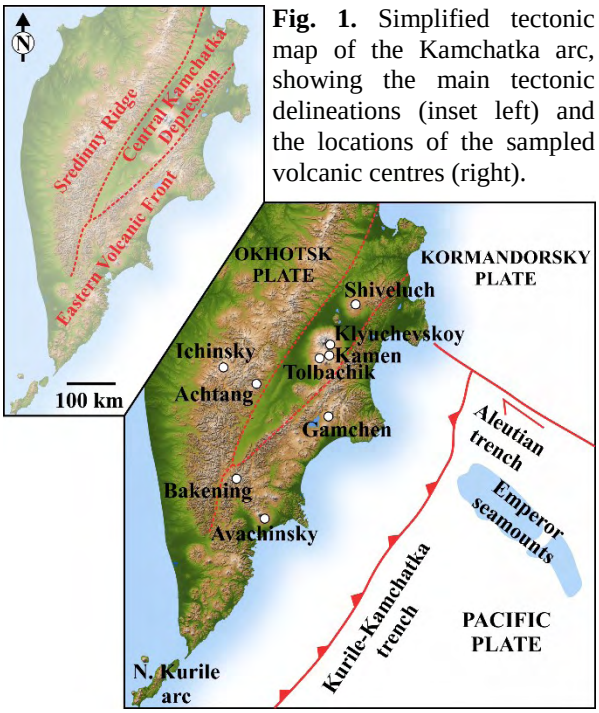

Fig. 1. Simplified tectonic map of the Kamchatka arc, showing the main tectonic delineations (inset left) and the locations of the sampled volcanic centres (right).

Results & Discussion

Around 200 representative melt inclusions hosted in olivine and clinopyroxene phenocrysts have been analysed for volatiles, light trace elements, heavier fluid-mobile and fluid-immobile trace elements, and boron isotopes. Three analytical sessions were completed, using both the Cameca IMS-4f (March 2018 and April 2018), and the Cameca IMS-1270 (May 2018). Similar calibration and standardisation methods used for the analyses in this study are described in recent publications[3].

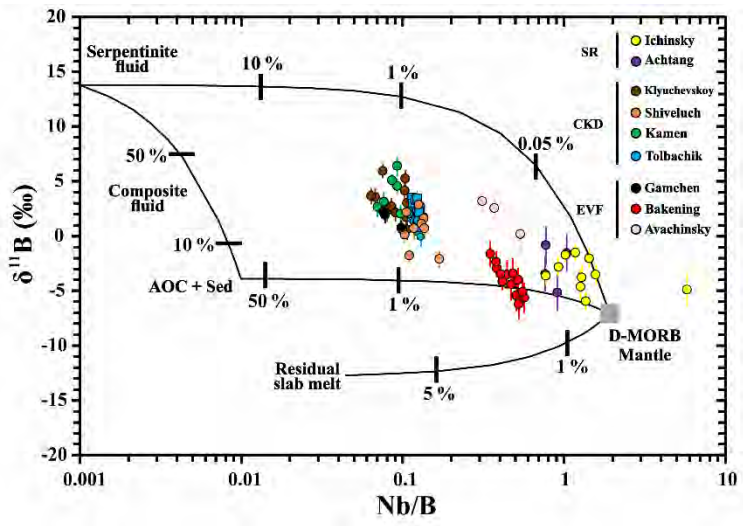

Fig. 2. Plot of $\delta^{11}B$ versus Nb/B for Kamchatka melt inclusions, sampled from Fig. 1. The plot shows mixing calculations between depleted MORB and various fluids released beneath the arc from hypothetical hydrous reservoirs. Modified after [4], with DMM data from [5].

The isotopic compositions and volatile inventories of the melt inclusions reveal significant variability in the geochemistry of the generated magmas, both along-arc and across-arc. The tectonic complexity of the arc is manifested in contributions to the melts from a combination of variably depleted

N-MORB mantle, OIB-type enriched mantle, slab fluids, and potentially slab melts (Fig. 2).
Most interestingly, subsets of the data from tectonically disparate settings show strong and consistent correlations between volatile contents and $\delta^{11}B$ signatures (Fig. 3), which we interpret to illustrate the competing controls on melt inclusion vs. whole-rock trends operating at this subduction zone. The melt inclusions from each volcano preserve large intra-sample ranges in $\delta^{11}B$ values, compared to previous whole-rock data[6], and where the isotopically lightest inclusions are also the most-volatile rich. This apparent contradiction to the current framework whereby heavy ^{11}B should be enriched concurrently with volatiles can be resolved by a model that includes melting of, or mixing/assimilation with, isotopically light hydrous xenolith minerals (e.g. amphibole) known to be present in metasomatised veins in the sub-arc mantle beneath Kamchatka.

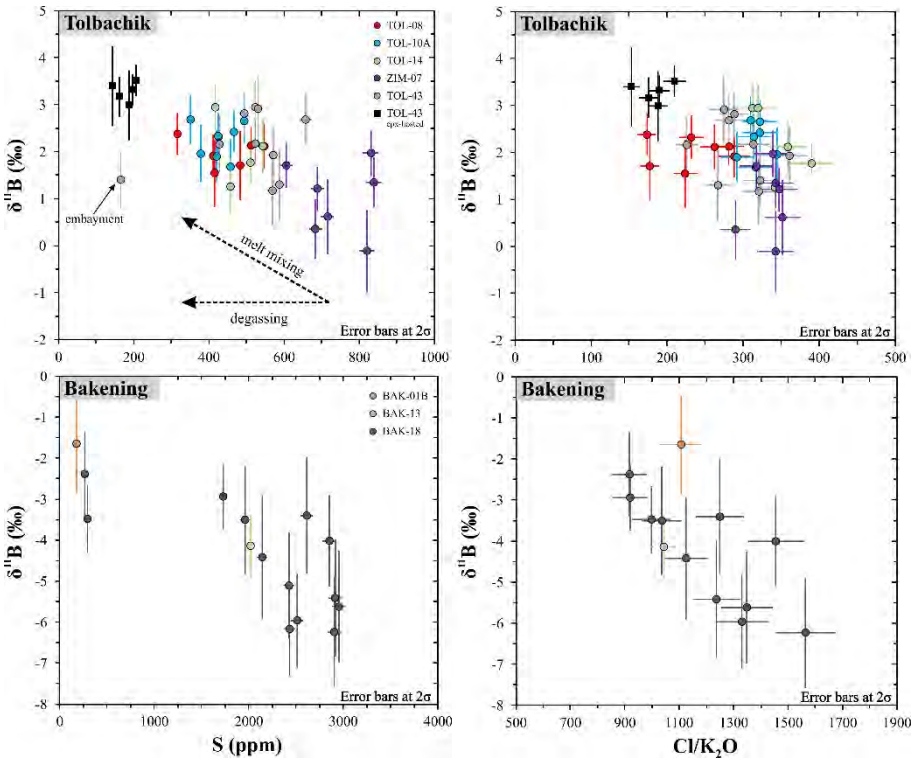

Fig. 3. Correlations between $\delta^{11}B$ and volatile components in melt inclusions from Tolbachik (top) and Bakening (bottom). The two volcanoes are in tectonically distinct settings (Fig. 1) but record large ranges in isotopic composition, and the same trend towards isotopically lighter values that correlate with the most volatile-rich inclusions.

We therefore suggest that while the overall geochemical trend in the Kamchatka arc is consistent with increased fluid addition to the arc front and beneath the Central Kamchatka Depression relative to the back arc (Fig. 2), the $\delta^{11}B$ values of melt inclusions preserve evidence for subduction processes dominated by heterogeneous mixing and assimilation processes in the mantle wedge and lower crust. Furthermore, $\delta^{11}B$ values can also be used to resolve the effects of shallow crustal assembly of different melt batches immediately prior to eruption, since degassing and fractional crystallisation appear to have little impact on the boron isotopic composition of the basaltic melts, thus preserving the original $\delta^{11}B$ inherited from the source region, as evidenced by the Tolbachik samples from individual monogenetic cones (Fig. 3. top panels).

References

[1] De Hoog & Savov (2018). In Marschall and Foster (Eds) Boron Isotopes, Advances in Isotope Geochemistry, Springer, pp. 217-247
[2] Churikova *et al*. (2007) Contributions to Mineralogy & Petrology 154, 217–239
[3] Walowski *et al*. (2019) Earth & Planetary Science Letters 508, 97–108
[4] Tonarini *et al*. (2011) Earth & Planetary Science Letters 301, 275–284
[5] Marschall *et al*. (2017) Geochimica et Cosmochimica Acta 207, 102–138
[6] Ishikawa *et al*. (2001) Geochimica et Cosmochimica Acta 65, 4523-4537

Halogen storage in nominally volatile-free minerals in the sub-cratonic lithospheric mantle

C.G. Jackson & S.A. Gibson

Department of Earth Sciences, University of Cambridge

Background

The sub-cratonic lithospheric mantle potentially represents a significant volatile repository in the solid Earth. Theoretical studies suggest that for billions of years it has been accumulating halogens (F, Cl, Br, I) as well as sulfur, carbon and water via metasomatism linked to the percolation and reaction of fluids associated with subducting slabs or small fraction volatile-rich melts derived from the deep mantle (e.g. McKenzie, 1989). These metasomatised regions are associated with accessory hydrous minerals, such as apatite, amphiboles and mica, that have the potential to accommodate substantial concentrations of halogen; for example, phlogopite can hold up to 5 wt. % F. However, in the past few years it has become clear that the more abundant nominally volatile-free mantle phases (such as, olivine and pyroxene) also have the capacity to store significant volumes of halogens, in fact Grützner et al. (2017) established that the entire fluorine budget of the upper mantle could be stored in nominally volatile-free phases. This is because fluorine's smaller ionic radius makes it only moderately incompatible (compared to Cl) and allows it to substitute for OH^- in hydrous or nominally anhydrous phases (Luth, 2003).

Samples

Our study focuses on the Kaapvaal craton of southern Africa (Figure 1). Eleven samples of peridotite from the Bultfontein kimberlite pipe, South Africa, and 8 samples from the Mothae kimberlite in Lesotho were chosen for SIMS analysis at EIMF. These samples consist of a variety of lithologies (lherzolites and harzburgites) and textures that are representative of sub-cratonic mantle. Furthermore, the xenoliths were selected because PT estimates indicate that they were entrained over a wide depth range in the lithospheric mantle.

Fresh grains of olivine, orthopyroxene and clinopyroxene were separated from coarse crushate and then mounted in indium (Figure 2) and analysed for H, F and Cl by SIMS.

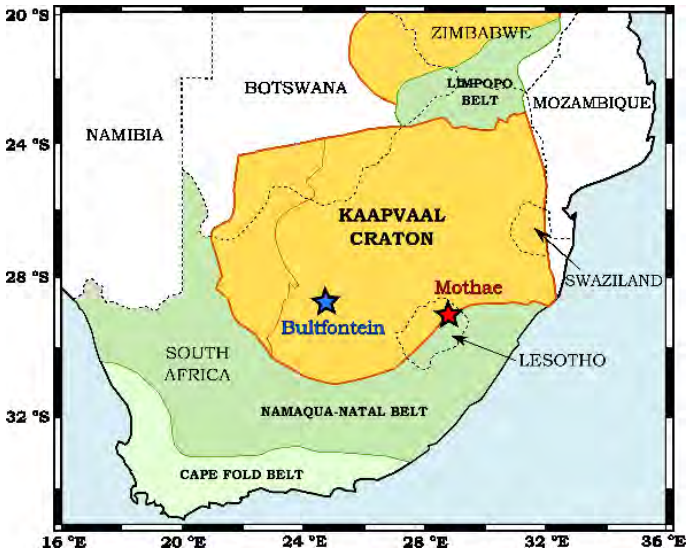

Figure 1: Map of southern Africa, showing the locations of Bultfontein and Mothae on the Kaapvaal craton interior and margin, respectively.

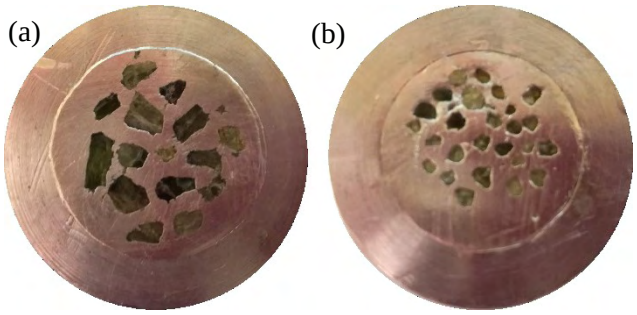

Figure 2: Two examples of the mineral separates mounted in indium: (a) Orthopyroxene; (b) Olivine. Individual crystals were picked, polished and cleaned before being pressed into indium within an aluminium disk.

Results

These new SIMS analyses of mantle xenoliths entrained by the Bultfontein & Mothae kimberlites significantly expand the published dataset for volatiles, especially halogens, in nominally volatile-free minerals from sub-cratonic mantle. The spread of H data in nominally-volatile-free mantle minerals analysed in this study is within the range available for the Kaapvaal and Siberian cratons (Demouchy and Bolfan-Casanova, 2016 and references therein; Peslier et al., 2012, 2010). F contents in ortho- and clinopyroxenes range from 0 to 36 ppm.

On average mantle clinopyroxene and orthopyroxene from Mothae contain lower water and higher fluorine concentrations than those from Bultfontein and suggest that there is spatial variation in the volatile content of the lithospheric mantle beneath the Kaapvaal craton. The partitioning behaviour of water between clinopyroxene and orthopyroxene is consistent with the findings of experiments, but D values are lower than those observed in most natural samples.

Importance of Results

We now have major element (EPMA), minor and trace element (LA-ICP-MS) and H, F and Cl (SIMS) concentrations for each mineral separate from Bultfontein and Mothae. This information together with *PT* estimates will allow us to study incorporation mechanisms of the volatile elements, the partitioning behaviour of volatiles between mantle minerals, the mobilisation of volatiles during metasomatism and more generally the storage of these elements in the sub-cratonic lithospheric mantle. Furthermore, our study of nominally volatile free mantle phases provides the opportunity to compare the storage of volatiles at the relatively undisturbed interior (Bultfontein, South Africa) and margin (Mothae, northern Lesotho) of the Kaapvaal craton.

References

[1] D. McKenzie, (1989) Earth and Planetary Science Letters **95**, 53–72.
[2] T. Grützner et al. **(**2017) Geochimica et Cosmochimica Acta **208**, 160–170.
[3] R.W. Luth (2003) Treatise on geochemistry **2**, 568.
[4] S. Demouchy, S. and N. Bolfan-Casanova (2016) Lithos 240–243, 402–425.
[5] A.H. Peslier et al. (2010) Nature **467**, 78–81.
[6] A.H. Peslier et al. (2012) Geochimica et Cosmochimica Acta **97**, 213–246.

SWEET: Super Warm Early Eocene Temperatures

E. John, C. Lear, P. Staudigel

[1]School of Earth and Ocean Sciences, Cardiff University, Park Place, Cardiff

Introduction

SIMS $\delta^{18}O$ work has identified potentially unaltered domains within diagenetically altered foraminifer shells ('tests'), prompting the exciting suggestion that palaeoclimate data can be extracted from previously rejected material [1][2]. As part of SWEET (Super Warm Early Eocene Temperatures), a major NERC-funded multi-institutional project, we aim to investigate the possibility of using such an approach to greatly expand the spatial resolution of sea surface temperature (SST) datasets for the Late Paleocene and Early Eocene greenhouse. However, there are unresolved issues surrounding the source of a) the reported intra-test variability in foraminifera and b) observed $\delta^{18}O$ offsets between values from gas source mass spectrometry and SIMS methods [3]. To better understand both issues, and thus to validate the potential of using SIMS measurements for SST reconstruction, the influence of cation-derived instrumental mass fractionation (IMF) effects on $\delta^{18}O$ measurements in foraminiferal calcite warrants investigation. As such, we completed a one-day pilot study investigating variability of Mg, Sr, and other trace elements within recrystallised and unaltered foraminifer tests. We also conducted a preliminary investigation into the magnitude of cation-derived IMF using trace element and $\delta^{18}O$ data from various standards, as provided by the Edinburgh ion probe facility.

Methods

Large (>355 µm) specimens of planktonic foraminifera belonging to the 'muricate' genus, *Morozovella*, were picked from Early Eocene samples from four deep-ocean/continental drilling sites with different burial histories (Fig. 1). The specimens from ODP and DSDP sites showed evidence of diagenetic recrystallisation under SEM ('frosty') whereas those from the continental TDP sites displayed original microstructure and were deemed relatively unaltered ('glassy') (Table 1). These foraminifera were mounted and polished for SIMS analysis at the Edinburgh facility. Spot trace element analysis was undertaken using the Cameca IMS 4f across thickened parts of the foraminifera tests.

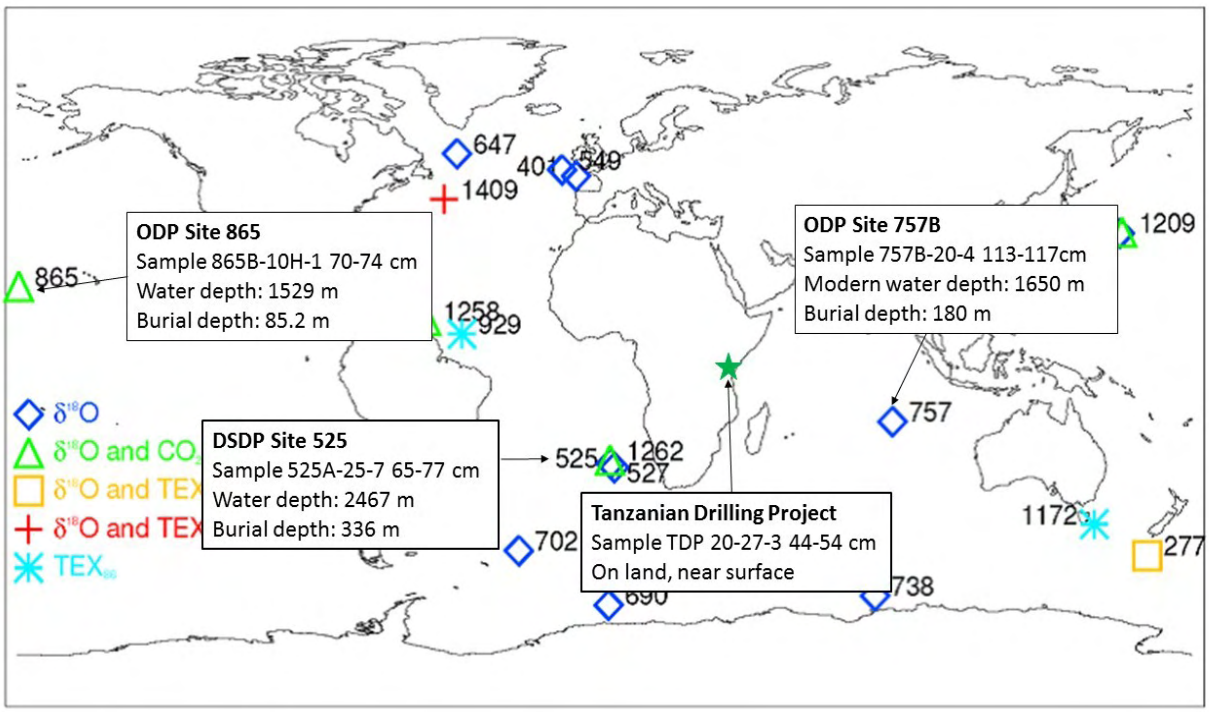

Fig. 1 Location of the four sample sites along with water depth and burial depth information.

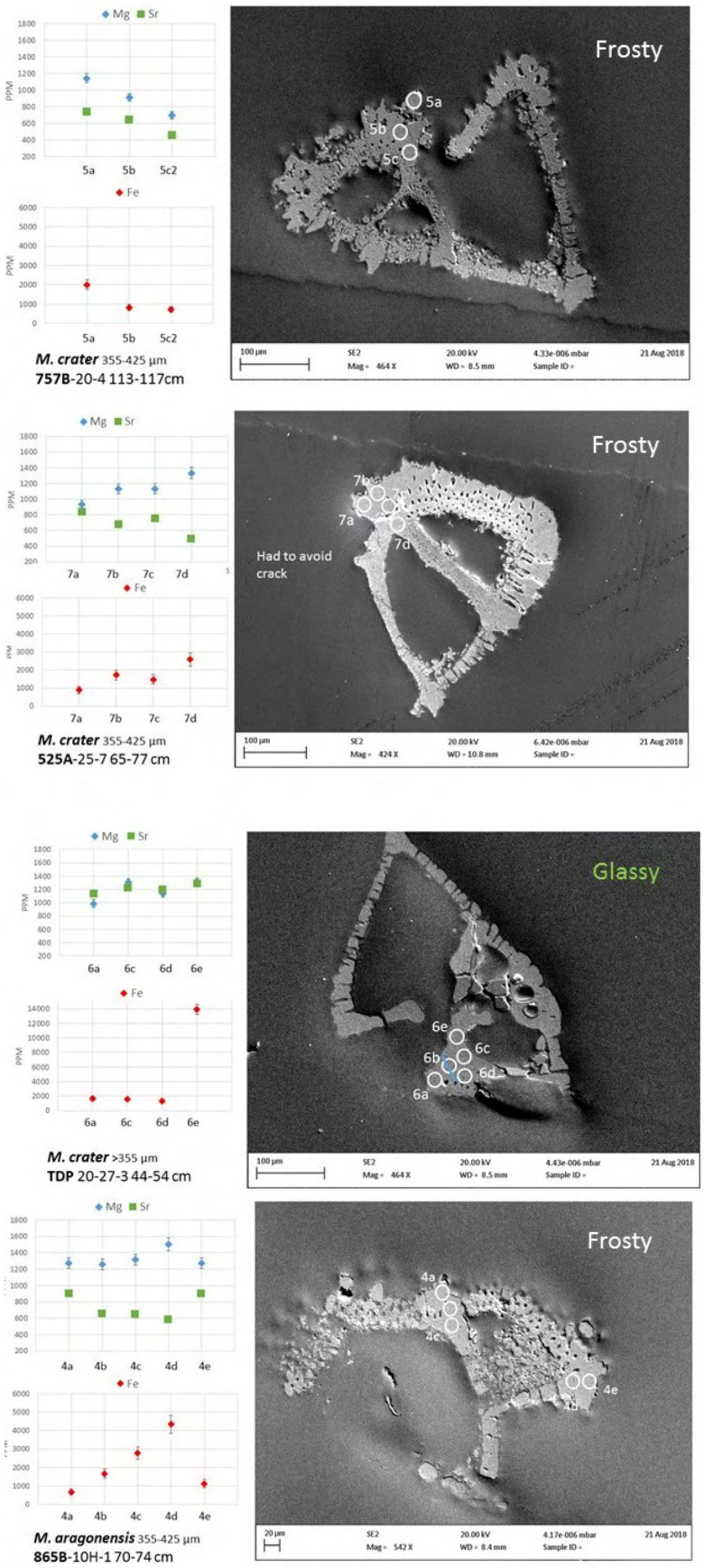

Fig. 2 Mg, Sr, and Fe concentrations for different spots in the foraminiferal cross sections along with SEM images showing the spot locations.

Table 1. List of samples mounted for SIMS analysis during the pilot day study

Sample	Species	Size fraction	Preservation state
TDP 20-27-3 44-54 cm	Morozovella crater	>355 µm	'Glassy'. Original microgranular calcite preserved.
757B-20-4 113-117cm	M. crater	355-425 µm	'Frosty'. Altered microstructure.
865B-10H-1 70-74 cm	M. aragonensis	355-425 µm	'Frosty'. Altered microstructure.
525A-25-7 65-77 cm	M. crater	355-425 µm	'Frosty'. Altered microstructure.

Results

The results from the pilot day are presented in Figure 2. Although these results are preliminary and smaller spot sizes are needed to capture detail, they reveal crude intra-test patterns in Mg, Sr, and Fe concentrations. With the exception of one anomalous Fe datapoint, Mg, Sr, and Fe concentrations in the 'glassy' sample are relatively consistent, as would be expected for unaltered material. However, Mg and Sr concentrations varied by up to 500 ppm and Fe concentrations by several thousand ppm in the frosty samples.

Discussion

Our data and the data in [2] suggest that intra-test $\delta^{18}O$ values vary in the opposite direction to that expected if the variability was solely caused by changes in Mg, Sr, or Fe content. This supports the idea that intra-test variations in $\delta^{18}O$ have a diagenetic origin, with certain domains being more geochemically altered with respect to $\delta^{18}O$ than others. However, it is clear that we need to understand IMF effects better to support any claims to the origin of $\delta^{18}O$ variability.

Determination of cation effect on oxygen isotope fractionation was attempted using a gradient-descent technique [4][5] using the dataset provided by the Edinburgh ion probe facility (Appendix 2). This was a preliminary assessment and there were insufficient materials analysed to account for the necessary number of unknown variables (Si, Mg, Mn, Fe, Sr, Na, and K relative to Ca). Principal component analysis of the trace element compositions reveals that the compositions covaried, with 95% of variance in composition being explained by the first principal component. The SIMS $\delta^{18}O$ data (normalized to known $\delta^{18}O$ values, yielding α_{SIMS} values) were corrected using average daily offsets. The most significant independent variables in governing the alpha value for the measured calcites were Mg, Sr, and Mn abundance, and these are also the most likely to vary within a foraminifer. Thus, the data were fitted using the equation below, which assumes a linear relationship with each trace element abundance relative to calcium. The gradient-descent method optimises an initial guess in values until the model reaches a minimum chi-squared value. The values for each parameter are provided in Table 2, and the model is shown in Figure 3, which compares modeled α_{SIMS} values to measured values. This method can be applied to better effect if more samples of known isotopic and trace element composition are measured, which would allow for better constraint on the ion effects. However, this preliminary data suggest that any correction effect would be very small in the context of achievable SIMS precision for $\delta^{18}O$ measurements and the precision needed for improving $\delta^{18}O$-based temperature reconstructions for global circulation models (~0.5 ‰).

$$\alpha_{SIMS} = \frac{R^{\frac{18}{16}}_{analyzed}}{R^{\frac{18}{16}}_{carboante}} = \alpha_{base} + \frac{Mg}{Ca}K_{Mg/Ca} + \frac{Sr}{Ca}K_{Sr/Ca} + \frac{Mn}{Ca}K_{Mn/Ca}$$

Table 2. Best fit parameters for dataset

	parameter value
α_{base}	0.9869
$K_{Mg/Ca}$	0.295
$K_{Sr/Ca}$	-0.400
$K_{Mn/Ca}$	0.143

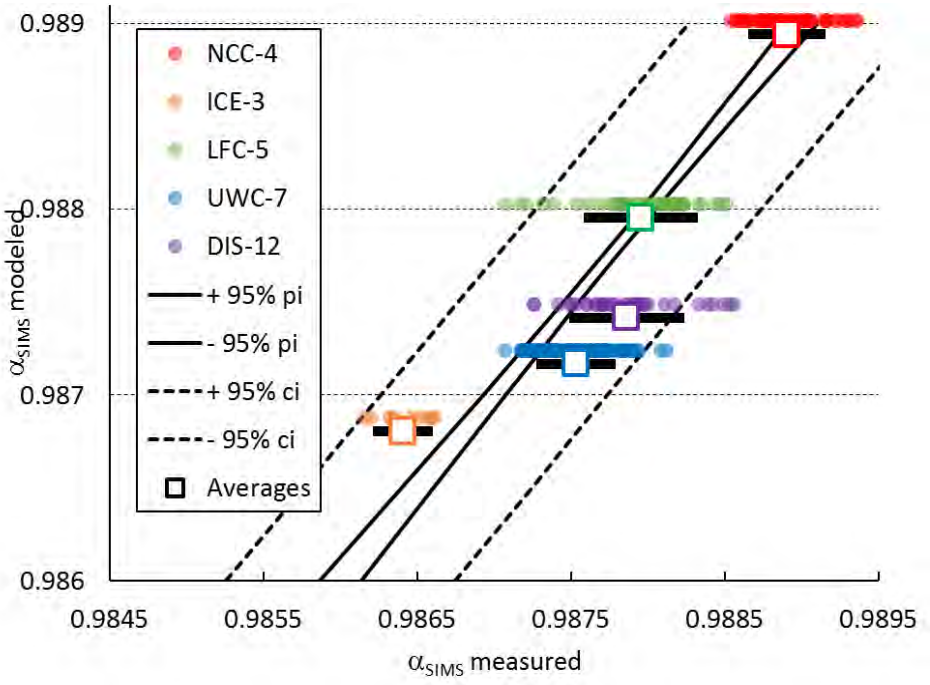

Figure 3. Best-fit alpha values relative to measured alpha values. Measured and modelled α_{SIMS} values for 5 calcite materials, plotted with ±95% predictive interval and confidence intervals. Average values vertically offset to show error bars.

Conclusions

SIMS measurements of the concentrations of trace elements such as Mg, Sr, and Fe, showed little variability in a 'glassy' morozovellid test, whereas greater variability was observed in several 'frosty' tests, supporting a diagenetic origin for intra-test variability. The idea that the reported intra-test variations in fossil foraminiferal $\delta^{18}O$ is caused by cation-derived IMF is not supported here. An initial quantification of cation-derived IMF in calcites suggest that a precise cation correction effect may be determined more accurately if a greater range of standard compositions are analysed, but that any correction will likely remain insignificant relative to the precision needed in the context of SWEET and most other paleoclimate applications.

References:
[1] Kozdon, R., et al. (2011) Paleoceanography **26**, PA3206.
[2] Kozdon, R., et al.. (2013). Paleoceanography **28**, 517–528.
[3] Wycech, J. et al. (2018). Chemical Geology **483**, 119–130.
[4] Levenberg, K. (1944) Quarterly of Applied Mathematics **2**, 164-168.
[5] Marquardt, D.W. (1963) Journal of the Society for Industrial and Applied Mathematics **11**, 431-441.

Volatile (F, Cl, S) availability in mineralised and unmineralised arc magmas of the Lachlan Fold Belt, recorded by apatite inclusions in zircon

L. Kendall-Langley[1], C. Hawkesworth[2], & A. Kemp[1]

[1]School of Earth Sciences, University of Western Australia, Crawley WA, Australia
[2]School of Earth Sciences, University of Bristol, UK

Background

Magmatic volatiles facilitate ore metal transport and concentration into a highly mobile, exsolved volatile phase, and therefore the volatile budgets of arc-related magmas are important to their fertility for ore formation. However, the abundance and behaviour of magmatic volatiles, and whether these vary with the metal endowment of arc-related igneous rocks (e.g., ore grades, Cu/Au ratios), has proven difficult to assess. The common accessory mineral apatite is host to the important magmatic volatiles Cl, F, H_2O (OH), S, and CO_2 in addition to numerous trace elements, making it an ideal recorder of the volatile inventory of melts and hydrothermal fluids. This project employs apatite to assess the volatile inventory of arc magmas that generate porphyry ore deposits, to test whether there is a relationship between volatile content and the size and type of mineralisation hosted by arc-related igneous suites, Samples were acquired from both mineralised Cu-Au porphyry systems and unmineralised, but partly coeval, I-type granitic suites of the Lachlan Fold Belt in eastern Australia. This study targeted apatite crystals encapsulated within nominally anhydrous and resilient zircon, which protects the apatite from chemical modification and allows magmatic volatile data to be tied directly to other established geochemical indicators in zircon, such as trace element profiles and radiogenic (Lu-Hf) and stable (O) isotope variations. Zircon grains of these samples have been characterised microstructurally (CL) and for U-Pb isotopes by a prior SIMS study [1] [2].

Methods and calculations

Back-scattered electron and cathodoluminescence imaging of the mounted zircon samples was carried out to identify zircon growth structures and the presence of inherited cores. Apatite inclusions selected for analysis were those that were deemed to be of primary magmatic origin and in new growth zones of the host zircon, with a lower size limit of 15 µm, to accommodate the interaction volume of SIMS analysis. Volatile (Cl, F, H_2O, S, and CO_2) and trace element measurements were made of 75 apatite inclusions and accompanying matrix apatite samples with the Cameca IMS-4f instrument, over five days. The experimentally derived thermodynamic model of Li and Hermann [3] is applied to the volatile data to estimate the magmatic concentrations of F and Cl. Equations (1) and (2) calibrated with experiments performed with a felsic silicate melt at 900-924°C and 2000 bars [4] is considered the most appropriate for this study.

$$C_{Cl}^{1} = \frac{X_{Cl}^{Ap}}{X_{OH}^{Ap}} \cdot \frac{1}{K_{d\ Cl-OH}^{Ap-melt}} \times 10.79 \qquad K_{d\ Cl-OH}^{Ap-melt} = e^{\left(25.81+17.33\left(X_{Cl}^{Ap}-X_{OH}^{Ap}\right)\right)\times\frac{10^3}{8.314\times T}} \tag{1}$$

$$C_{F}^{1} = \frac{X_{F}^{Ap}}{X_{OH}^{Ap}} \cdot \frac{1}{K_{d\ F-OH}^{Ap-melt}} \times 6.18 \qquad K_{d\ F-OH}^{Ap-melt} = e^{\left(40.33+21.29\left(X_{F}^{Ap}-X_{OH}^{Ap}\right)-3.96\left(X_{Cl}^{Ap}\right)\right)\times\frac{10^3}{8.314\times T}} \tag{2}$$

Magmatic S concentrations are estimated with the partition coefficient following the empirical relationship (3) determined by Peng et al. [5]. The apatite saturation temperature (AST) of each sample is calculated with whole rock SiO_2 and P_2O_5 concentrations, following the experimentally derived formula of Harrison and Watson [6].

$$\ln D = \frac{21130}{AST(K)} - 16.2 \tag{3}$$

$$AST = \frac{[26400 \cdot C_{SiO_2}^{AST} - 4800]}{\left[12.4 \cdot C_{SiO_2}^{\mathrm{AST}} - \ln\left(\frac{C_{P_2O_5}^{\mathrm{AST}}}{1-X/100}\right) - 3.97\right]} \tag{4}$$

Results

Prelimary results of this study have yielded estimates of the magmatic concentrations of F, Cl and S in unmineralised granitic suites of the Lachlan Fold Belt and granitic suites of the Macquarie Arc that are

associated with Cu-Au porphyry deposits. The Jindabyne and Why Worry suites have similar Cl concentrations of 0.01-0.07 wt%, while the Cobargo suite records significantly higher magmatic Cl concentrations of 0.06-0.36 wt%. Macquarie Arc suites have the highest Cl contents ranging 0.07-0.71 wt%. The F concentrations of the Lachlan Fold Belt suites are more constrained, with magmatic F values ranging 0.06-0.13 wt% in the Jindabyne suite, 0.09-0.14 wt% in the Why Worry suite and 0.10-0.19 wt% in the Cobargo suite. The Macquarie Arc suites extend to higher values ranging from 0.09 up to 0.25 wt%. Estimates of magmatic sulfur content are low in the Jindabyne and Why Worry, not exceeding 40 ppm. The Cobargo suite and Macquarie Arc samples record a large range of S concentrations ranging 10-265 ppm and 35-630 ppm, respectively.

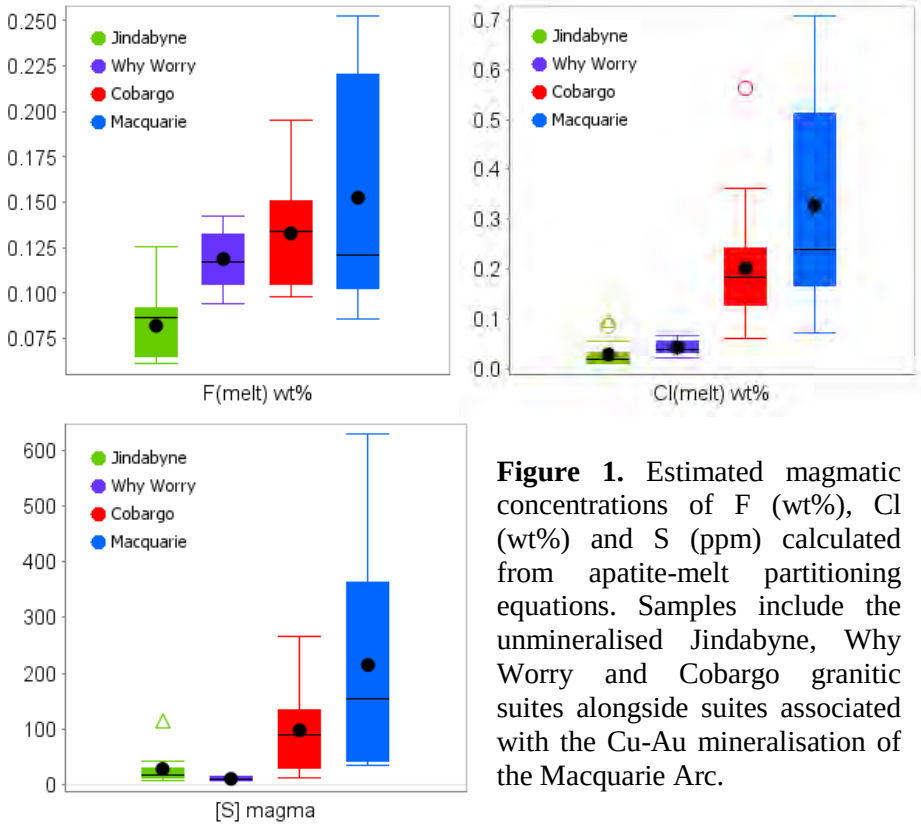

Figure 1. Estimated magmatic concentrations of F (wt%), Cl (wt%) and S (ppm) calculated from apatite-melt partitioning equations. Samples include the unmineralised Jindabyne, Why Worry and Cobargo granitic suites alongside suites associated with the Cu-Au mineralisation of the Macquarie Arc.

Discussion

While the calculated magmatic concentrations of F, Cl and S associated with the Macquarie Arc suites largely overlap those of the unmineralised LFB suites, they are higher on average. The heightened volatile content of these samples suggest that precursor melts to the associated Macquarie Arc Cu-Au porphyries were naturally higher in the volatile components- essential to the concentration and transport of Cu and Au in these deposits. Future work will include a more detailed examination of the volatile content Macquarie Arc suites to investigate the relationship between the abundance of certain volatile species and the characteristics of associated Cu-Au porphyry deposits. The volatile record of the analysed apatite inclusions will also be coupled with Lu-Hf and Oxygen isotope information from the host zircon to investigate the cycling of volatile species in arc settings.

References

[1] A.I.S. Kemp et al. (2005) Contributions to Mineralogy and Petrology **150**, 230-249
[2] A.I.S. Kemp et al. (2007) Science **315**, 980-983
[3] H. Li and J. Hermann (2017) American Mineralogist **102**, 580-594
[4] J.D. Webster et al. (2009) Geochimica et Cosmochimica Acta **73**, 559-581
[5] G.Y. Peng et al. (1997) American Mineralogist **82**, 1210-1224
[6] T.M. Harrison and E.B. Watson (1984) Geochimica et Cosmochimica Acta **48**, 1467-1477

U-Pb dating of zircons from Corsica

C. Lavarini[1], L.Kirstein[1] & M. Attal[1]

[1]School of GeoSciences, University of Edinburgh, Edinburgh EH9 3JW, UK

Introduction

Clastic sediments represent an integrated fingerprint of the erosion, transport and depositional processes that have contributed to their evolutionary history. Pebble abrasion is a key factor controlling the release of minerals into sand. Pebble abrasion is one of many factors that can change the mineralogical composition of sands, which in turn may impact detrital provenance analysis. We were provided with access to the 1270 ion microprobe for 1 day in 2018 to date a number of zircons collected from 3 samples in the Taignano river in Corsica, France. The results generated formed key data for Chapter 4 in the PhD thesis of Chrstiann Lavarini.

Results

The unmixing of U–Pb zircon ages reveals that Hercynian granites, meta–ophiolites and granitoids are the predominant sources in the samples. Although our results fit with the known characteristics of their sources, many uncertainties arise from missing source ages, underrepresented grains, and misfits between predicted source proportions based on exposure area and their real (measured) percentage in the samples.

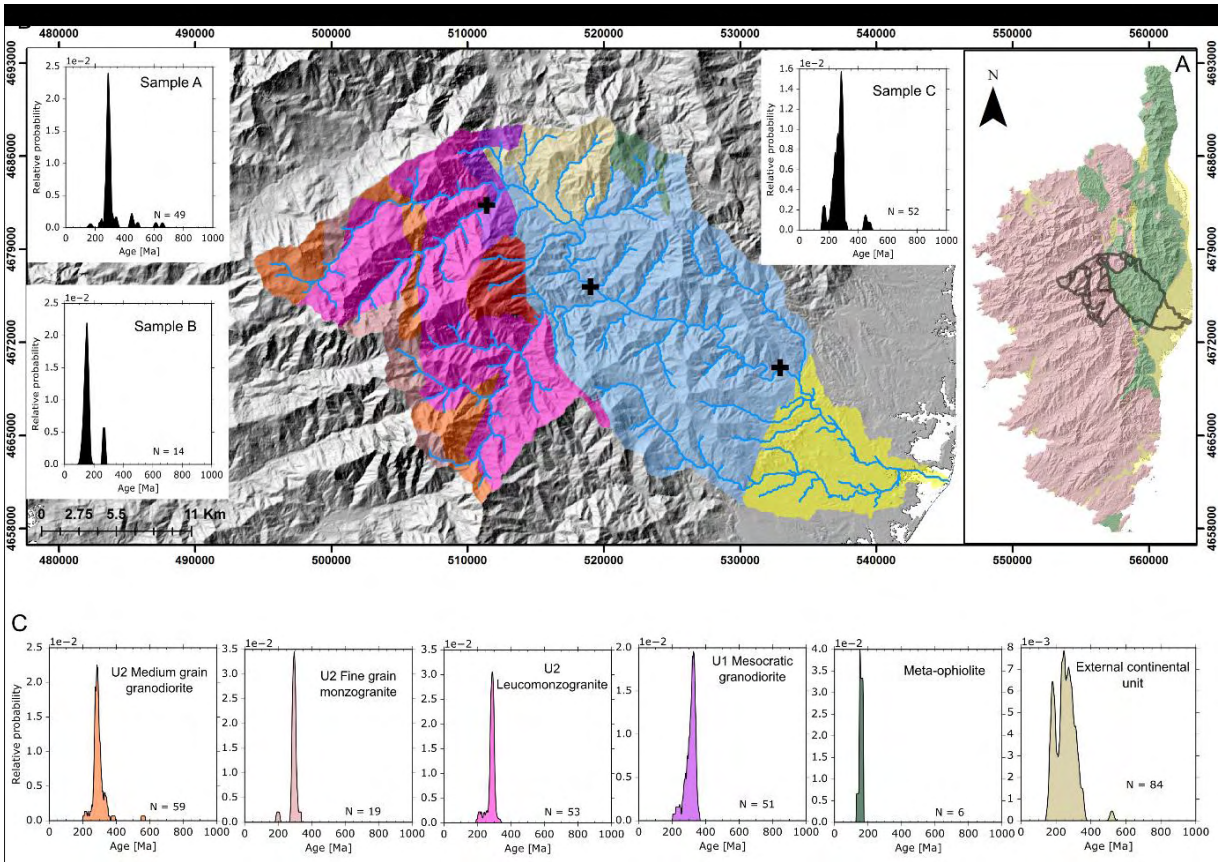

Figure 1. Source rocks and U– Pb zircon ages of the Tavignano watershed. A) Location of the Tavignano watershed in eastern Corsica. Pink rock types are granitoids of Hercynian Corsica, green rock types are from the Schistes Lustrés unit (Alpine Corsica), and yellow rock types are part of the Miocene sedimentary plains (Aleria and Marana). B) Source rocks and U–Pb age distributions of the downstream mixed sand samples in the uppermost (sample A), intermediate (sample B) and lowermost (sample C) sampling sites. C) U– Pb age distributions of the source rocks of the Tavignano watershed. Note that the blue area represents the Schistes Lustrés unit, where no U–Pb age constrains exist. The yellow area represents the Aleria plain, which is not investigated in this work. The colours of the source rocks in panel B are equivalent to those U–Pb ages at panel C. The ages in panel C are from Cocherie et al. (2005), Ohnesnstetter et al. (1981) and Rossi et al. (2015).

Conclusions

Key outcomes from the data when placed in context with work on zircon typologies and numerical modelling include:

(i) Detrital zircons in the Tavignano River have typologies and U–Pb ages that indicate local sources of Hercynian granites, Alpine meta–ophiolites and granitoids.

(ii) Unmixing of U–Pb zircon ages from river samples indicate source contribution proportions that largely differ from their exposure area.

References

[1] A. Coherie et al. (2005) Lithos **82**, 185-219.
[2] M. Ohnenstetter et al. (1981) Earth and Planetary Science Letters **54**, 397-408.
[3] P. Rossi et al. (2015) Bulletin de la Société Géologique de France, **186**, 171– 192

First measurement of intracrystalline H in plagioclase from abyssal gabbros: the role of water in the rheology of the lower ocean crust

C.J. MacLeod

School of Earth & Ocean Sciences, Cardiff University, Cardiff CF10 3AT, UK

Summary

In this project we are reassessing models for the rheology of the (lower) ocean crust by measuring intracrystalline H_2O contents of plagioclase in gabbros from the Atlantis Bank oceanic core complex on the ultraslow-spreading SW Indian Ridge (the 800m-deep IODP Hole U1473A). We are concentrating in particular on examining H_2O contents in relict versus neoblastic plagioclase in plastically-deformed gabbros, which form a substantial part of the plutonic section here, to assess the role of late-magmatic and high-temperature sub-solidus shear zones in contributing to the broader-scale rheology. Current models hold that the lower ocean crust is fundamentally strong, consistent with dry-plagioclase flow laws; instead, we propose it may be fundamentally weak near-axis, much closer to a wet-plagioclase rheology overall. We have tested this premise via the NERC Scientific Services award, using the Edinburgh ion microprobe to measure H-in-plagioclase in U1473A gabbros. We successfully obtained 64 measurements from five gabbros variably deformed at supra- to high-sub-solidus temperatures. Preliminary results show that water levels are indeed elevated (average 330ppm), but as much in relict igneous grains as in recrystallised neoblasts. Initial indications are that the water is most likely to be intrinsic, magmatic- rather than extrinsic, hydrothermal-sourced; and, critically, it is found throughout the 800m-thick drilled section, *not* simply localised in a few thin, late, discrete shear zones as initially speculated. Our preliminary interpretation of the SIMS water-in-plagioclase data is that late-concentrated magmatic water in 'mush' chambers beneath magma-rich slower-spreading mid-ocean ridges contributes to the near-pervasive deformation observed and to a much weaker bulk lower crust than pre-supposed. This very different rheology leads to a previously unrecognised mechanism of exhumation of deep levels of young ocean lithosphere onto the seafloor.

Background

Atlantis Bank is one of a number of oceanic core complexes – the uplifted footwalls of oceanic detachment faults – now recognised as a key feature of slower-spreading mid-ocean ridges. Of those studied so far, long-lived slip and exhumation has been promoted by formation of weak, low-temperature secondary hydrous phases (e.g. talc, serpentinite) localised on the detachment fault plane itself: evidence for early, deep penetration of seawater down the fault [1]. Evidence for high-temperature deformation is generally very limited, and the footwalls are little deformed. Atlantis Bank, on the ultraslow-spreading SW Indian Ridge, is a notable exception: prior ocean drilling investigations (ODP Hole 735B) showed distributed, high-temperature ductile deformation of a thick gabbroic succession [2]. Atlantis Bank has been chosen as the optimal location for a 'slow Mohole': an ultra-deep hole to investigate the nature of the Moho at slower spreading rates. IODP Hole U1473A was accordingly initiated as the first part of this broader project, with the aim of it being extended ultimately to a Moho target at ~5km below seafloor. Currently at a depth of 800m, all in gabbro, Hole U1473A has penetrated gabbroic rocks similar overall to those in 735B, but marked by even more intense crystal-plastic deformation observed near-pervasively throughout the hole, some of it associated with late-stage evolved melt [3]. These relationships demonstrate a very different 'hot' mechanism of detachment faulting to the 'cold' mechanisms found elsewhere, much more closely tied to the magmatic accretion than to subsequent hydrous fluid-fault interaction. Previous work has concluded that away from localised shear zones the bulk strength of lower ocean crust is very high and follows dry plagioclase flow laws, with a rheology similar to that of dry upper mantle [4,5]; however, this does not accord with the qualitative observations from U1473A for wholesale weakness nor with the widespread involvement of late melt in the deformation. Is a dry plagioclase rheology appropriate for the lower ocean crust? This has never been tested directly, hence the justification for the current project. The concentration and distribution of intracrystalline H is known to be fundamental in controlling the strength of plagioclase, the most abundant mineral in the lower ocean crust. In particular, experiments have shown that the rheology of plagioclase-bearing rocks is reduced by orders of magnitude by only trace (but poorly quantified) contents of water in the plagioclase lattice [6,7].

Sample selection and data acquisition. We analysed five samples of variably deformed mid-ocean ridge gabbro (IODP Hole U1473A, Expedition 360). One was an undeformed olivine gabbro (84R4B),

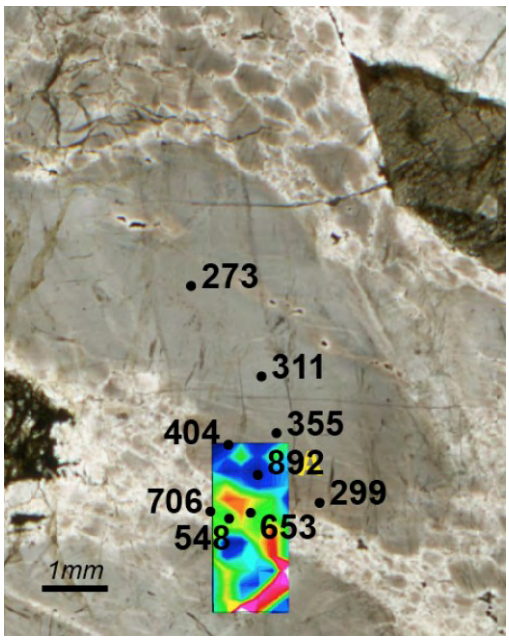

Figure 1. Water contents in neoblastic plag in slightly deformed olivine gabbro 13R1B (H_2O in ppm)

albeit containing a cryptic melt channel, to establish a baseline igneous plagioclase water content. We chose two samples with discrete crystal-plastic shear zones in little-deformed olivine gabbro (30R5B, 79R4B) and two samples with penetrative deformation and extensive plagioclase neoblast formation: one incipient (13R1B) and one protomylonitic (11R3B). Over a 5-day period in October 2018, with the close, continual and invaluable assistance of a very tolerant Dr Cristina Talavera Rodriguez, we successfully employed the Edinburgh Cameca ims 4f ion micro-probe to acquire 64 analyses of H in plagioclase from the five samples; also of Li, B, F, Mg and Al, and Si for cross-calibration. Because we had omitted to request the latter volatile elements in our original proposal we wrote and had approved an auxiliary application for an additional day of machine time to allow us to measure and quantify them. The Li, B and F data thus obtained will be important in allowing us to assess the origin of the water we have measured in the plagioclase crystals. Following acquisition of H and other volatile elements in Edinburgh, Si contents and anorthite ratios of all points were subsequently measured using the Zeiss Sigma FEG HD analytical scanning electron microscope (ASEM) in Cardiff. All SIMS data are now externally calibrated with reference to Si. All samples have additionally been mapped using the Quantitative Assessment of Compositional Distribution (QACD) method developed in Cardiff [8], which utilises the ultra-high count rates of the Cardiff system (up to 1M cps) to generate quantitative element maps of whole thin sections, and up to 800K mineral analyses per thin section.

Some results, and preliminary interpretations

Water contents in neoblastic plag in slightly deformed olivine gabbro 13R1B (**Figure 1**) are systematically higher than in relict igneous plag (or cracks in plag) and correlate with An content, consistent with the simplistic concept of wetter, weaker plag in shear zones. This is mirrored by the FTIR results, though the correlation is inexact because of the much greater volume of investigation of the FTIR. The relationship is however less pronounced in other samples (e.g. the shear zone in 79R4B, **Figure 2**). QACD element mapping reveals complex zoning and reactions associated with late melts in a ductile shear zone (N.B. abundance of Fe-Ti oxides and apatite, and lower An plag [lighter cyan]). The breakdown of correlation of H_2O in plag appears to relate to the presence of syn-tectonic amphibole in recrystallised Fe-rich cpx, suggesting a complex control on H_2O distribution.

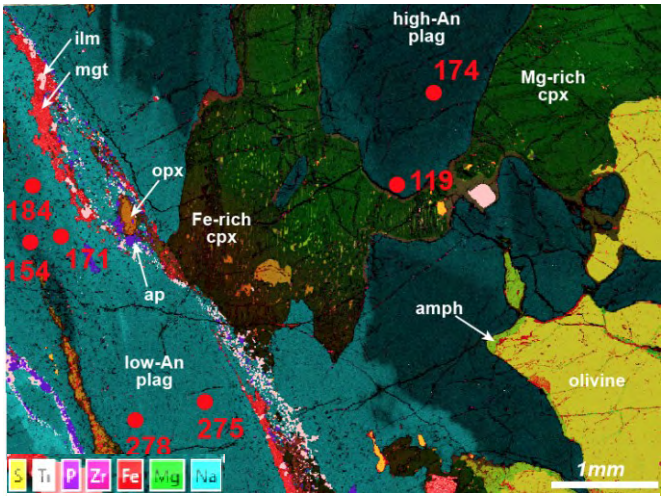

Figure 2. Water contents in the shear zone in sample 79R4B (H_2O in ppm)

References

[1] MacLeod CJ et al., 2002. *Geology* 30, 879–882. [2] Dick HJB et al., 2000. *EPSL* 179, 31-51. [3] MacLeod CJ, Dick HJB, Blum P et al., 2017. *Proc IODP Vol.360* 10.14379/iodp.proc.360.102.2017. [4] Mehl L & Hirth G 2008. *JGR* 113, B05202. [5] Hansen LN, Cheadle MJ, John BE, Swapp SM, Dick HJB, Tucholke BE & Tivey MA 2013.. *G3* 14(8), 10.1002/ggge.20184. [6] Dimanov A, Xiao X, Dresen G & Wirth R 1999. *JGR* 104, 10483–10497. [7] Rybacki E. & Dresen G, 2000. *JGR* 105(B11), 26017–26036. [8] Loocke MP, Lissenberg CJ & MacLeod CJ 2017*Eos*, 2017 Fall Meeting, V43C-0544.

The nature of the deep nitrogen cycle

E. R. Mare[1], J.C.M. de Hoog[2] and S. Mikhail[1]

[1]School of Earth and Environmental Sciences, University of St. Andrews, St. Andrews KY16 9AL, UK
[2]School of GeoSciences, University of Edinburgh, Edinburgh EH9 3JW, UK

Introduction

Interactions between the Earth's atmosphere and interior have helped maintain habitable conditions for nearly 4 billion years. In the atmosphere, nitrogen is a major component and an essential element for life, but how nitrogen has cycled between the atmosphere and mantle is poorly understood. We aim to unravel this by understanding the chemical behaviour of nitrogen in silicate mineral–melt–fluid systems. To do this we require the ability to measure nitrogen at low concentrations in silicate minerals and glasses with high spatial resolution. In this pilot study, we aimed to establish analytical protocols for such measurements – in particular, matrix effects between different nitrogen-bearing silicate minerals and glasses.

Methods and Results

For this one-day pilot study we measured nitrogen in several reference materials using an $^{16}O^-$ beam (measuring $^{14}N^+$) on the Cameca IMS 4f in high resolution ($\Delta M/M$ ~1200) to avoid $^{28}Si^{2+}$ and $^{12}CH_2^+$ interferences. We compared a calibration based on six rhyolitic glasses (**Figure 1**) [1] to a calibration based on a single measurement of a phengite standard [2].

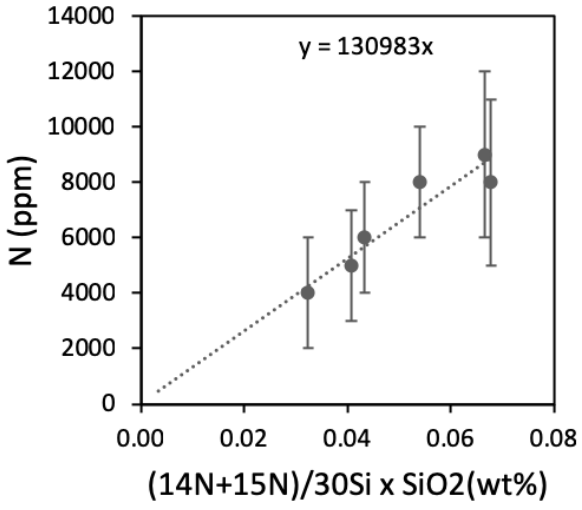

Figure 1. Nitrogen calibration based on rhyolitic glasses [1].

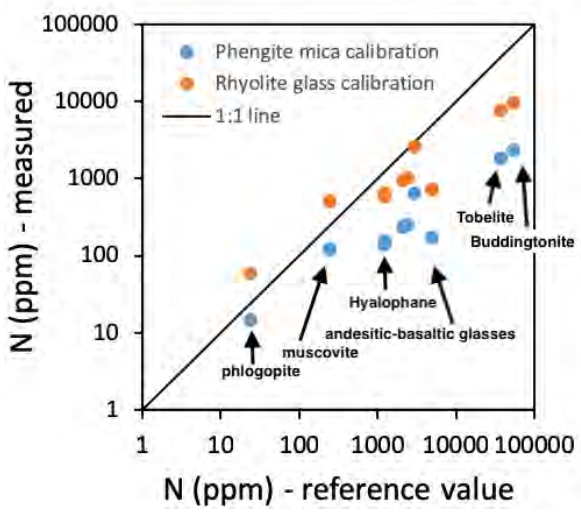

Figure 2. Nitrogen contents (ppm) of various reference materials using two calibrations.

We found significant matrix effects – e.g. a factor of two between rhyolitic and basaltic glasses. Tobelite (NH_4-mica), buddingtonite (NH_4-feldspar) and hyalophane (Ba-rich feldspar) appear to lie on a single calibration line. These results indicate that future SIMS work for nitrogen will require closely matrix-matched standards.

References

[1] A. Mallik et al. (2018) Earth and Planetary Science Letters **482,** 556–566.
[2] V. Busigny et al. (2003) Chemical Geology **198**, 21-31

Halogen volatility from silicate melts

A. K. Matzen & B. J. Wood

Department of Earth Sciences, University of Oxford

Introduction

The silicate Earth is depleted in volatile elements [e.g., 1]. The extents of these depletions is shown in **Figure 1** where the concentrations of elements in the bulk silicate Earth, relative to CI chondrite meteorite—the primitive proto-planet material—are plotted against the temperature at which 50% of the element is predicted to condense from the solar nebula [2]. Apart from the highly-siderophile elements (e.g., Au, Pt, Re), the normalized ratios for the refractory lithophile elements (e.g., Mg, Ca, Ti, Al) are all ~1. With decreasing condensation temperature, however, the lithophile elements show a general decrease in abundance indicating that the Earth is relatively depleted in volatile elements. Although the trend for the volatile lithophile elements is robust, there are some pronounced anomalies. For example, In is enriched and Cl is depleted compared to elements with similar volatilities and proclivities for segregating into the core. This raises a series of fundamental problems, the most general being the cause of the volatile element depletion observed on Earth. The Moon-forming impact, and others late in Earth's accretion, were probably energetic enough to melt significant fractions of the proto-Earth. For this reason, we have been investigating an alternative explanation for the depletion of volatiles observed in **Figure 1**: degassing from a high-temperature melt.

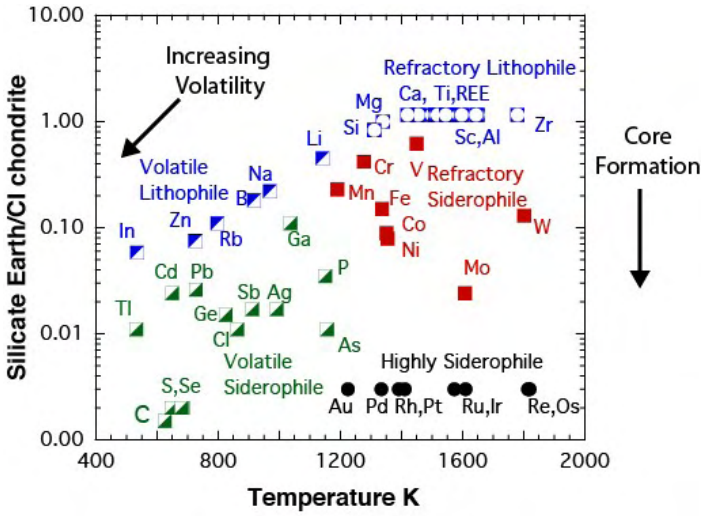

Figure 1. Abundance in silicate Earth, normalized to CI chondrite, versus 50% condensation temperature

To do this we have been performing experiments, under a controlled atmosphere, in a furnace where a crucible of melt is constantly stirred. At the end of the experiment the crucible of melt is rapidly removed from the furnace and plunged into water where the melt cools to form a glass. This glass is then recovered and its composition analysed. To quantify element loss we define a volatility factor as the ratio of the post-experiment to the pre-experiment glass concentration was then calculated. A volatility factor of ~1 indicates that an element was not appreciably lost from a silicate melt, and a volatility factor of ~0 indicates that all of the element in question was lost from the silicate melt over the course of the experiment. All experiments were performed at 1300°C, using flowing CO and CO_2 to control the log of oxygen fugacity between −7 and −13. Experiments were run for different lengths of time, allowing us to examine the time-dependent loss of elements, and in crucibles comprised of two different materials: pure Ni metal and Al_2O_3. In an ideal world the crucible will not interact with the sample at all, and the measured volatility should be independent of crucible material.

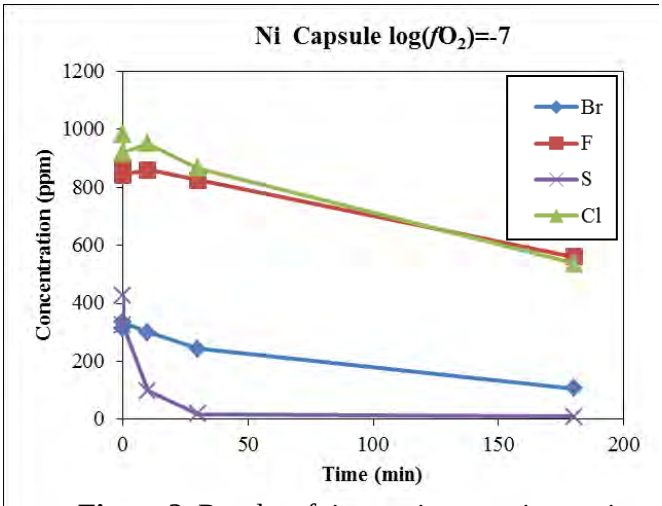

Figure 2. Results of time series experiments in nickel capsules

Results and discussion

Here, we present SIMS measurements on F, Cl, Br, and S measured using the Cameca 1270 at the NERC Ion Microprobe facility at the University of Edinburgh. **Figure 2** shows the concentration data for a series of experiments done in at a $\log_{10} fO_2$ of −7 in Ni crucibles. The results from the series in Ni crucibles show a gradual decrease in concentration with time. For example, Cl and F concentrations go from ~1000 ppm at time zero to ~600 ppm after two hours. S and Br show similar systematics, although the loss rate of S seems to be the highest, with essentially all S leaving the sample after 30 minutes. The data from these experiments show the type of behaviour we would expect: decreasing concentrations as a function of time. In **Figure 3** we show the data from a similar series of experiments where an Al_2O_3 crucible was used to hold the melt. In these experiments the concentration of all elements, except S, seemingly increase during the first 30 minutes of the experiment, after which the concentration decreases.

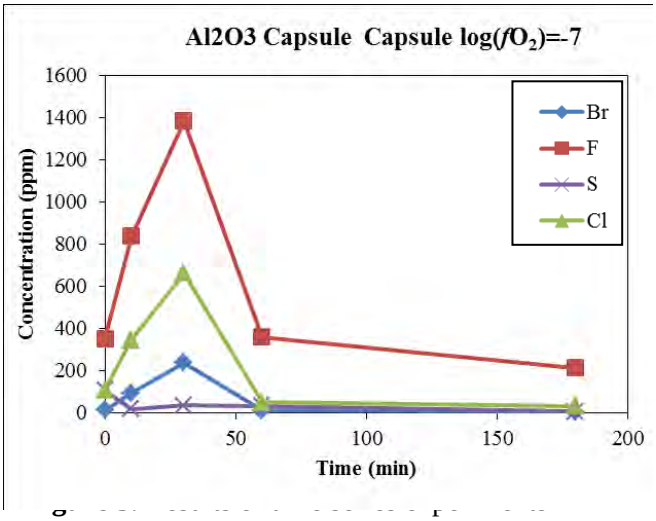

alumina capsules

Another source of disagreement between the experiments run in Ni and Al_2O_3 crucibles is the measured concentrations of the zero time experiments. For example, in the Ni-crucible experiments run for a very short time our measurements suggest that both F and Cl are present at, approximately, 900 ppm.

Contrast this to the experiments run in Al_2O_3 crucibles, which used the same starting composition, our measurements of F and Cl suggest starting concentrations of ~400 and 100 ppm, respectively. The differences of the time-dependencies and apparent starting compositions led us to closely examine the experiments run in Al_2O_3 crucibles. Imaging with a FEG-SEM at the University of Oxford revealed the presence of needle-like crystals of thenardite–arcanite (Na_2SO_4–K_2SO_4, respectively). **Figure 4** shows a backscattered electron image for the zero time experiment plotted in **Figure 3**. In this image the light-grey background is silicate glass and the lighter needles, approximately 200 microns long and 2 microns wide, are the thenardite–arcanites. We hypothesize that the presence of these sulphates is what causes the unexpected time dependence shown in **Figure 3**: at zero time the concentrations of Cl, Br, S and F in the silicate glass are depressed because these elements are sequestered in the sulphate phase. As time progresses, and S is volatilized from the sample, the mass of the sulphate phase decreases which causes the apparent concentrations of Br, F and Cl in the silicate glass to rise.

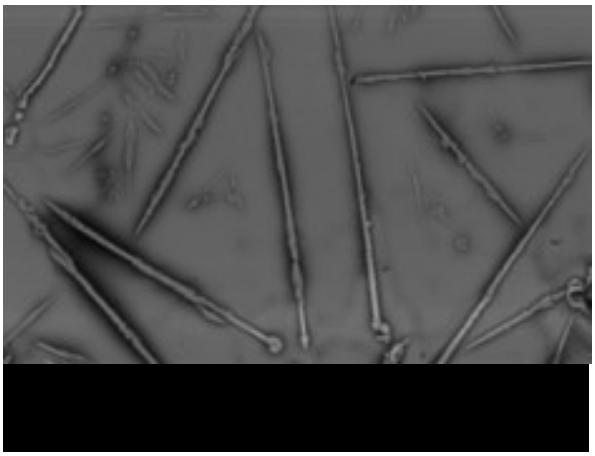

Figure 4. Backscatter electron image of a zero time experiment run in an Al_2O_3 crucible at a $\log_{10}(fO_2)=-7$

It not known why the samples held in Ni crucibles do not show the same systematics as those from Al_2O_3 crucibles. Our working hypothesis is that the presence of the Ni crucible limits the mass of thenardite than can form, either because it buffers the fO_2 (to below the nickel-nickel oxide buffer), or because S is soluble in the metal crucible.

References

[1] W.F. McDonough and S.-s. Sun (1995) Chemical Geology **120**, 223-253.
[2] K. Lodders (2003) The Astrophysical Journal **591**, 1220-1247.

CO_2 partitioning between plagioclase and melt

A. McCarthy & J. Blundy

School of Earth Sciences, University of Bristol

Introduction

Volatiles, such as H_2O, CO_2, in arc magmas play fundamental roles in governing crystallization, eruption dynamics, and hydrothermal mineralisation **[1]**. Moreover, CO_2 fluxing during degassing of deep-seated magmas might affect overlying magmatic reservoirs with consequences for eruption dynamics. Melt inclusions are conventionally used to infer pre-eruptive volatile contents of arc magmas. However, inclusions only form after significant crystallisation of the host magma has taken place. Consequently, the initial magmatic volatile budget may not be reliably captured by melt inclusion analysis if some degassing precedes the onset of major crystallisation. This situation is commonly the case for volatile-bearing arc magmas, notably for CO_2, which is significantly less soluble and less abundant than H_2O. In that case, using melt inclusions to estimate original magmatic CO_2 can lead to significant underestimates of the original concentration, with profound implications for subduction zone CO_2 budgets.

Aims

To assess whether CO_2 can be accurately measured in plagioclase using the SIMS facility at Edinburgh, we targeted experimentally-grown plagioclase crystals from five, high-pressure (15 kbar) carbonate-bearing crystallization experiments. By selecting plagioclase from such carbonate-rich systems we expect dissolved CO_2 abundances to be maximised, providing a valuable test as to whether CO_2 can be incorporated significantly into plagioclase. Additionally, plagioclase-bearing marbles (anorthite + calcite assemblage) and granulites collected from the Swiss-Italian Alps, as well as gabbroic rocks from high-pressure to mid-upper crustal pressure of arcs (Chelan Clomplex and Ivrea Zone, and St-Kitts, respectively) were targeted in order to look at the natural variation in CO_2 in plagioclase.

Results

Our one-day Pilot proposal showed that significant variations in CO_2 on the order of several 100s of ppm at the grain scale are recorded in plagioclase from high-pressure lithologies, but remain heterogeneously distributed within individual grains. However, experimental plagioclase grown in high-pressure and CO_2-rich conditions showed low (background levels) CO_2 abundances. This proposal allowed to show that high-resolution and high-precision analysis of CO_2 in plagioclase can be obtained using current SIMS technology. However, due to a lack of further time to investigate the mechanism of incorporation of CO_2 in plagioclase, the mechanism(s) allowing for the heterogeneous distribution of CO_2 in plagioclase remains open.

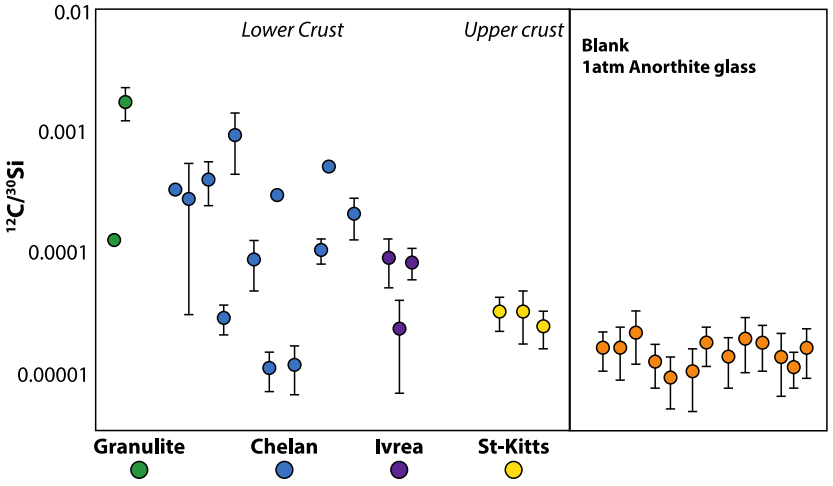

Figure 1: Variations in $^{13}C/^{30}Si$ in natural plagioclase and analysed blank (1atm anorthite glass). Note the sharp variations in analysed CO_2 in high-pressure plagioclase (Green, blue, purple circles) and low CO_2 abundances in shallow (yellow circles) mid-upper crustal conditison.

References

[1] J. Blundy et al., (2010) Earth and Planetary Science Letters, **290**, 289-301

Plagioclase glomerocrysts: short timescale of H_2O-CO_2 fluctuations in subvolcanic reservoirs

A. McCarthy & J. Blundy

School of Earth Sciences, University of Bristol

Introduction

Erupted volcanic products, such as plagioclase aggregates (glomerocrysts) **(Figure 1)** and large (cm-size) plagioclase phenocrysts provide important information about the timescales and dynamics of volcanic eruptions, melt reservoirs and fluctuations in magmatic conditions. Unique plagioclase-glomerocrysts and plagioclase phenocrysts are formed in erupted products from Tolbachik Volcano, Kamchatka, and are the focus of this Pilot-project. This Pilot-proposal is related to the NERC-funded project **[1]** which targeted trace element variations in zoned plagioclase as well as compositional variations within melt inclusions to quantify fluctuations in magmatic conditions in subvolcanic reservoirs prior to eruptions, kinetics of plagioclase growth and residence timescales of plagioclase-glomerocrysts in subvolcanic reservoirs. This previous proposal revealed the homogenous composition of glass inclusions, which is surprising considering i) the crystallization of cm-long plagioclase crystals, ii) significant variations in plagioclase compositions (An53-An71), and iii) cyclical resorption patterns of plagioclase. Melt inclusions however show significant variations in H_2O abundances (0.2-0.9wt %) with no consistent core to rim variations. Our aim was therefore to measure CO_2 and H_2O in individual melt inclusions to constrain whether CO_2 can cause rapid shifts in P_{H2O} as a result of CO_2-fluxing of melt reservoirs [2]. However, prior to the analytical session, it was noted that the variation in CO_2 required to shift the P_{H2O} would be at- or below- the detection limit of the available SIMS using routine CO_2 analysis. It was therefore deemed more constructive to use this analytical session to target H_2O abundances only in these glass inclusions, in order to get a better spatial resolution of the H_2O variation in these glomerocrysts.

Results

During this one-day pilot proposal, we were able to confirm the variation in H_2O abundances at constant glass composition of our previous report and were able to measure a H_2O profile along a plagioclase embayement, which will enable us to model decompression timescales of these orbicules, thereby complimenting the residence timescales of plagioclase and olivine. This modeling is currently taking place at the University of Bristol.

Although we were not able to analyse CO_2 abundances at the SIMS facility in Edinburgh, our one-day pilot project allowed us to characterise in high-detail these plagioclase glomerocrysts, and is enabling us to currently map out variations in CO_2 using the SIMS at Caltech in collaboration with Ed Stolper.

Figure 1: SEM image (*Field-Emission Gun Tescan Mira LMU, University of Lausanne, Switzerland*) of a 3 cm wide plagioclase glomerocryst showing comb-textured plagioclase growing from a centre towards the exterior, forming a micro-orbicule

References

[1] J. Blundy et al., (2017) NERC Proposal, Plagioclase glomerocrysts: eruption timescales of Tolbachik volcano
[2] J. Blundy et al., (2010) Earth and Planetary Science Letters, **290**, 289-301

Plagioclase glomerocrysts: eruption timescales of Tolbachik volcano

A. McCarthy, J. Blundy &, K. Cashman

School of Earth Sciences, University of Bristol

Introduction

Plagioclase-aggregates (or glomerocrysts) found in volcanic products are key to understanding eruption dynamics and timescales. These features might represent remobilized crystal-mush or small volcanic orbicules formed in subvolcanic conduits. Tolbachik volcano (Kamchatka) erupted unique glomerocrysts formed of cm-long, oscillatory-zoned plagioclase **(Figure 1)**, containing olivine- and melt inclusions. Such volcanic glomerocrysts and large plagioclase phenocrysts (macrocrysts) provide important information about the dynamics of volcanic eruptions, including the timescales of melt reservoirs and fluctuations in magmatic conditions. For example, zoning patterns in plagioclase, in particular oscillatory zoning patterns, might be driven both by open-system processes involving replenishment of reservoirs by new melt batches, or by local processes of rapid crystal growth, including i) heating through latent heat of crystallization, ii) formation of a compositionally depleted/enriched boundary layer, iii) interfacial process of solute trapping of an enriched boundary layer trapped by the rapid growth of the crystal lattice. We therefore aimed to study i) μm-scale oscillatory-zoning and resorption textures, ii) the composition of melt inclusions and iii) melt embayments in these unique plagioclase-glomerocrysts and plagioclase phenocrysts from Tolbachik Volcano, Kamchatka in order to decipher i) decompression-rates of explosive volcanic eruptions; ii) fluctuations in magmatic conditions in subvolcanic reservoirs prior to eruptions; iii) kinetics of plagioclase growth and residence timescales of plagioclase-glomerocrysts.

Results

Our Analytical session at the SIMS Facility at Edinburgh has allowed to constrain the formation of such plagioclase glomerocrysts to shallow subvolcanic systems. Analysis of major- and trace element composition of glass inclusions reveals near-homogenous melt composition from the core to the rims of individual plagioclase crystals **(Figure 2)**, indicating a lack of melt differentiation upon crystallization of these phenocrysts. This implies that the crystallization of such plagioclase occurred in a dynamic melt-dominated environment. Though the glass composition remains homogenous through time, the analysis of H_2O abundances in these glass inclusions indicates fluctuations in H_2O between 0.1-0.9wt % throughout individual crystals, without any core-rim consistency. As H_2O abundances play a fundamental role on the composition and stability of plagioclase [1], this implies that the control of mineral growth, oscillatory zoning and resorption patterns is driven by variations in PH_2O in a subvolcanic system on very short timescales. Moreover, such low H_2O abundances imply crystallization pressures <1 kbar in volatile saturated basaltic melts, indicating that the crystallization of these glomerocrysts occurred at shallow level, likely within subvolcanic conduits.

Figure 1: SEM image (*Field-Emission Gun Tescan Mira LMU, University of Lausanne, Switzerland*) of a 3 cm wide plagioclase glomerocryst showing comb-textured plagioclase growing from a centre towards the exterior, forming a micro-orbicule

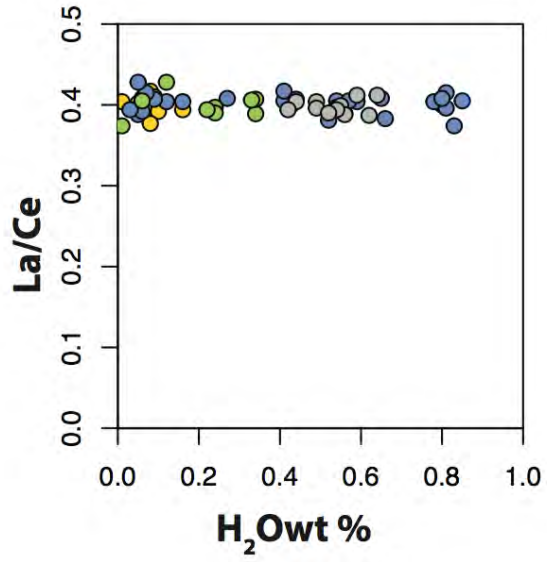

Figure 2: La/Ce vs H_2Owt % of glass inclusions. The La/Ce ratio, affected by crystal fractionation, is constant even though H_2O abundances vary between 0-0.9wt %. **Blue circles**: glass inclusions in plagioclase, **green circles**: glass inclusions in olivine; **Yellow circles**: interstitial glass; **Grey circles:** embayment in plagioclase.

Moreover, high resolution 50µm long Sr-Mg-Ba-Ti profiles crosscutting plagioclase zonations and resorption textures were done in order to determine residence timescales of these plagioclase and to constrain whether they are consistent with the short timescales of associated olivine obtained by NanoSIMS. Overall, Sr concentrations remain near-constant as Anorthite abundances change **(Figure 3)**, implying a lack of diffusive-reequilibriation. The modelling is currently being undertaken at the University of Bristol and final residence timescales should be obtained shortly using Sr +/- Mg diffusion profiles.

Conclusions

As a result of the use of the analytical capabilities of the NERC facility at Edinburgh, were are able to show that cm-sized, oscillatory-zoned plagioclase crystals record variations in P_{H2O} within subvolcanic reservoirs on the timescales of volcanic eruptions. Oscillatory-zoned plagioclase therefore do not necessarily record changes in magmatic input and melt replenishment, but dynamic changes in volatile content of subvolcanic reservoirs during volcanic eruptions.

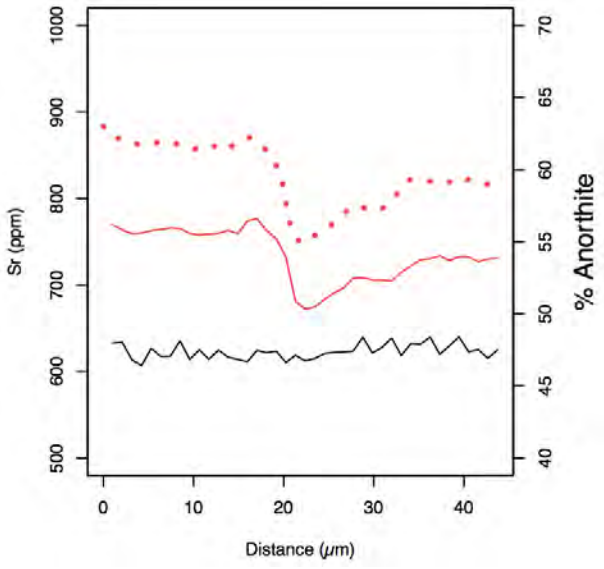

Figure 3: Plagioclase Anorthite Profile (red dots) and measured Sr abundances (grey line) compared to initial Sr abundances (red line) as a function of Anorthite content.

References

[1] T.B. Housh and J.F. Luhr (1991) American Mineralogy 76 (3-4), 477-492

A combined geochronological approach to investigating long lived granite magmatism

A.J. Miles[1], N.H. Woodcock[2]

[1]School of Geography, Geology and the Environment, University of Leicester
[2]Department of Earth Sciences, University of Cambridge

Summary

Zircon provides a robust and time-sequential record of granitic magma evolution. However, it is increasingly apparent that most zircon dates show older emplacement ages than other dating methods. It is therefore uncertain where the majority of zircon crystallises within complex systems that are often trans-crustal in scale. Furthermore, crystals within individual samples commonly record a range of different ages and compositions that reflect a propensity to survive crystal recycling between different magma batches. This one day pilot study provided a valuable opportunity to supplement a previous U-Pb SIMS study of zircons from the Caledonian Shap granite. The results demonstrate that the majority of zircons are antecrysts (crystals formed from earlier magmas) as opposed to autocrysts (crystals in the host magma) and that zircon provides a valuable opportunity to investigate protracted episodes of magma evolution within deeper regions of trans-crustal systems.

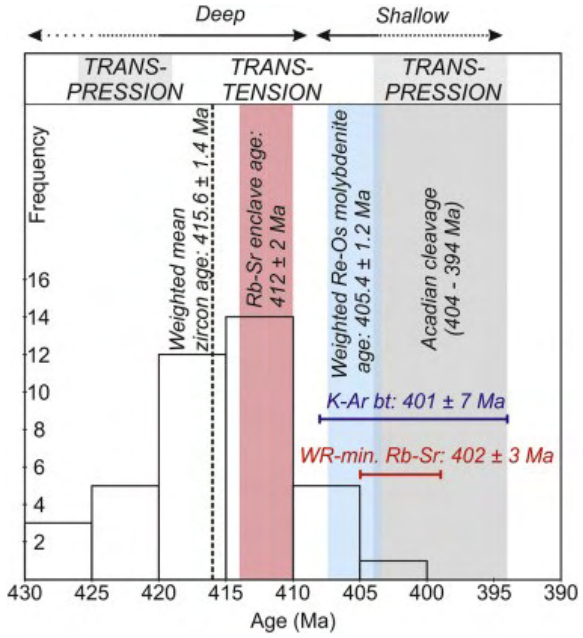

Figure 1. A compilation of age data from the Shap granite, UK. Zircon ages are plotted as a histogram. The mean weighted age of all zircons is shown with a vertical dashed line.

Main study

Metamorphic minerals within the thermal aureole of the Shap granite overgrow the regional Acadian cleavage, dated at 394 - 404 Ma[1]. Re-Os dating of molybdenite mineralisation associated with magmatic fluids also overlaps within error with Acadian deformation[2]. By contrast, zircon U-Pb dates give an older weighted mean age of 415.6 ± 1.4 Ma (2σ). Xenocrysts are absent in the Shap granite and the majority of magmatic zircons appear to have grown prior to final emplacement by about 10 Ma. Mafic enclaves contain a similar population of zircons that are likely to have been scavenged from the host granite and have been independently dated at 412 Ma[1,3]. Gravity data[4] suggests that the small, cylindrical Shap granite roots into a larger, 1500 km^2 batholith in the mid crust. It is likely that the majority of zircons and mafic enclaves record a protracted and episodic history of magma evolution within this mid-crustal batholith. Final emplacement appears to have coincided with the onset of regional transpression and transport of a mobile crystal mush to shallower crustal depths. This study emphasises the importance of integrating different dating methods in understanding the evolution of plutonic systems and that final granite emplacement is most reliably recorded by the youngest zircon crystals. Zircon antecrysts are a useful target for investigating magmatic and ore-forming processes that operate within deeper regions of trans-crustal magmatic systems.

References

[1] A.J. Miles et al. (2016) Gondwana Research **39**, 250-260
[2] D. Selby et al. (2008) Applied Earth Sciences 117, 11-28
[3] J. Davidson et al (2005) Geology **33**, 29-32
[4] M.K. Lee (1986) Journal of the Geological Society **143**, 425-435

Tracing geodynamic changes in Palaeoproterozoic rocks from SE Brazil

H. Moreira[1], C. Storey[1], J. Darling[1], M. Fowler[1] and L. Seixas[2]

[1]School of Earth and Environmental Sciences, University of Portsmouth, UK
[2]Departamento de Geologia, Escola de Minas, Universidade Federal de Ouro Preto, Brazil

Background

Evolution of the continental crust has been studied intensely over the past few decades. The use of *in-situ* U-Pb and Lu-Hf isotopic systems in zircons has greatly improved our understanding of the source(s) of magmas that built the continental crust. Oxygen isotopes have more recently also been used as a filter for Hf model ages, distinguishing "mantle-like" zircons from "hybrid" ones with significant upper crustal components. This approach enables distinction of real juvenile additions to the crust from reworked pre-existing crust, which then permits better constraints on crustal growth rates [1, 2].

Aims and objectives

This project aims to resolve geodynamic processes during the Palaeoproterozoic, a critical time period in the transition to modern tectonic processes, by applying U-Pb, Lu-Hf and O isotope systematics to zircons from Palaeoproterozoic igneous rocks within the Mineiro Belt, an orogenic belt that bounds the Archaean southern São Francisco craton, Brazil. These igneous rocks represent the largest occurrence of plutonic trondhjemite-tonalite-granodiorite (TTG) magmatism intruded during the so-called "global magmatic shutdown" at 2.45 to 2.2 Ga [3], proposed due to the paucity of evolved igneous rocks with ages within this interval, and more recently re-defined as a "magmatic lull" between 2.3 to 2.2 Ga [4]. The belt contains a large juvenile magmatic arc, with an age of ca. 2.1 Ga, which is geochemically similar to Late Archaean mantle-derived sanukitoids [5]. Contemporaneous 2.1 Ga high Ba-Sr granitoids comprise another suite, distinguished from the sanukitoids by the depletion in compatible elements [6]. This age relationship of TTG followed by sanukitoid magmatism provides evidence of geodynamic changes, which has been associated with the onset of modern-style subduction-driven plate tectonics and the opening up of mantle wedges above steepened subduction zones [7]. However, elsewhere on Earth the transition from TTG to sanukitoid magmatism occurred at around 2.9-2.7 Ga. Hence, this area records a much younger transition during a time period widely believed to have generated very little evolved new crust. The belt also contains ca. 2.18 Ga old tonalites that are less evolved than the 2.13 Ga high Ba-Sr magmas and have a different geochemical evolution marked by assimilation of older mafic xenoliths. The plutonic rocks are surrounded by sedimentary sequences that are sourced from this basement and contain abundant detrital zircons. Our study will give significant insights into an important and poorly understood interval of time in terms of evolved magma generation, building of new crust and the implications for the onset and evolution of subduction-driven plate tectonics.

Sample preparation and analytical details

Zircon grains were hand-picked and positioned in square shape on parcel tape, in which sides are smaller than 5 mm (diagonals < 7 mm). A 25 mm diameter round mount was then centred on top of the grains, where epoxy resin was poured and dried in vacuum. Reference materials were arranged at the middle and corners of the square (**Figure 1**). The grains show minimal polishing relief that is indistinguishable from the epoxy surface. Combined with the high sensitivity of the Cameca IMS-1270 from 15 μm spots, the oxygen secondary ion yielded on average 3 x 10^9 cps and 6 x 10^6 cps for masses ^{16}O and ^{18}O, respectively, and most of the $\delta^{18}O$ values have a precision better than 0.25‰ (2SD).

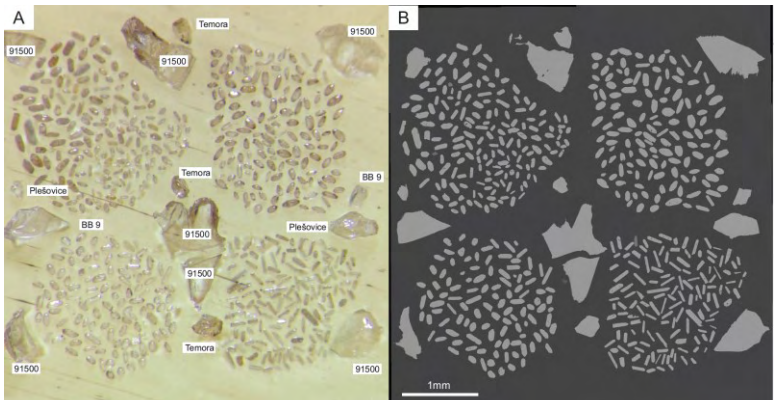

Figure 1. A) Zircon grains and reference materials on parcel tape. B) Backscatter image of one of the mounts produced in this study.

Results

During 5 days in January 2018, some 400 zircon grains from granitoids and metasedimentary rocks from the Mineiro Belt were analysed for oxygen isotopes. Zircons from the early 2.35 Ga TTG magmas have a narrow range of values consistent with a depleted mantle source to lower mafic ocean crust. In progressively younger rocks, some crustal contamination is identified by a broader spectrum towards $\delta^{18}O$ above mantle values (Fig.2). The oldest rocks (c.2.350 Ga) are TTG in composition and have $\delta^{18}O$ between 4.2 and 5.0 ‰. The youngest suite of rocks (c. 2.13 Ga) are sanukitoids and have $\delta^{18}O$ values between 5.5 and 6.7 ‰, reflecting a crustal contribution, possibly from subducted sediments in a metasomatised mantle source. The suite of c.2.13 Ga rocks (high Ba-Sr granitoids) have a broader $\delta^{18}O$ composition, ranging from 2.8 to 7.5 ‰. The lowest values are likely due to U-Pb discordance (yet to be confirmed), but the highest values are consistent with crustal assimilation. The suite of c.2.18 Ga rocks (tonalites) have an average $\delta^{18}O$ composition of 5.5 ‰, indicating derivation from an uncontaminated mantle derived source. An extensive passive margin is inferred for the early stages of the Mineiro Belt tectonic setting, whereas underplating melt and/or contamination of the mantle wedge from a subduction zone explains the isotopic and geochemical signature of the younger magmas. U-Pb and Lu-Hf analyses will further validate the range of $\delta^{18}O$ values found in the zircons and contribute to the debate about mantle derived contributions and continental crust growth rates in the Palaeoproterozoic.

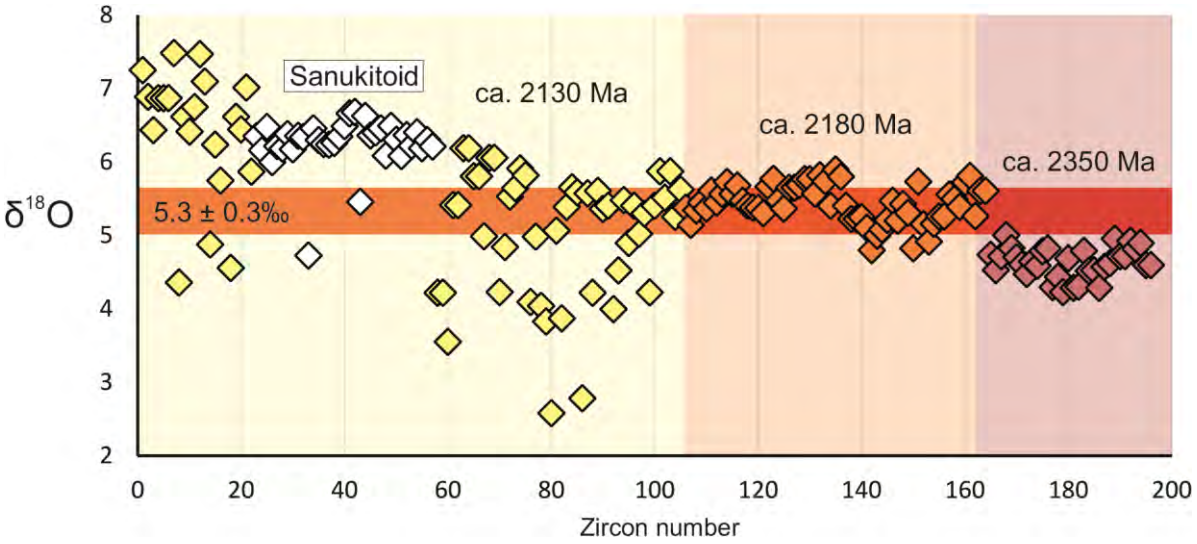

Figure 2. Oxygen analyses from zircon grains of igneous rocks. 5.5 ± 0.3 ‰ (1SD) is the $\delta^{18}O$ value of zircons in equilibrium with mantle melts [8].

References

[1] Hawkesworth, C.J., Kemp, A.I.S., 2006. Chem. Geol. 226, 144–162
[2] Dhuime, B., Hawkesworth, C.J., Cawood, P.A., Storey, C.D., 2012. Science 335, 1334–1336
[3] Condie, K.C., O'Neill, C., Aster, R.C., 2009. EPSL 282, 294–298
[4] Spencer, C.J., Murphy, J.B., Kirkland, C.L., Liu, Y. and Mitchell, R.N., 2018. Nature Geo. 11, 97-101
[5] Seixas, L.A.R., Bardintzeff, J-M., Stevenson, R., Bonin, B., 2013. Prec. Res. 238, 18–41
[6] Moreira, H., Seixas, L., Storey, C., Fowler, M., Lasalle, S., Stevenson, R. and Lana, C., 2018. Geos. Front.
[7] Martin, H., Moyen, J.-F., Rapp, R., 2010. Transactions of the Royal Society of Edinburgh-Earth Sciences. 100, 15–33
[8] Valley, 2005, CMP 150, 561-580

Improving the Fe/Si proxy in diatom frustules with the microprobe

L.Pichevin[1] & S. Akse[2]

[1]School of GeoSciences, University of Edinburgh, , UK
[2] Vening Meineszgebouw, Utrecht University, The Netherlands

Rationale

In 2014, Pichevin et al. [1] proposed the use of Fe/Si in diatom frustules as a proxy for past iron availability by applying this to a glacial-interglacial record from the Eastern-Pacific. Despite the great potential of this technique some reservations were raised concerning the role of diagenesis in dictating the Fe/Si of the frustules. The authors applied established mechanical and chemical cleaning techniques as well as the microprobe technique in an attempt to remove the influence of contamination in determining the Fe/Si of the frustule. Nonetheless, some samples exhibited high Al counts, which suggested that contamination or diagenesis might still be an issue.

In an attempt to test and resolve these issues, the Nanometer Secondary Ion Mass Spectrometer (nanoSIMS) facilities at Utrecht University was used to map changes in diatom chemistry on a frustule-level. The resulting data revealed the main sources of contamination and allowed for correction. These measurements also revealed that the influence of contamination was significantly greater for the exterior of the diatom frustule compared to the interior, suggesting that the inside of the frustule is better protected from outside influences. The corrected data significantly improved the correlation of the Fe/Si with other existing proxies measured in that core affirming the strong potential of this proxy.

In this pilot study (1 day) we re-analysed four (4) samples previously studied by both SIMS (Grant IMF396/0510) and nanoSIMS (Utrecht) techniques. However this time the samples were subjected to an additional chemical leaching step that aims to dissolve the outer part of the frustules and leave the inner matrix exposed hence reducing the possibility of contamination by terrigenous or authigenic Fe.

Results

We measured Na, Mg, Al, Si, K, Fe and Ba in cleaned individual diatom frustules. Concentration of Na and Ba remained similar between both sets of measurements indicating that the further cleaning did not alter the Na and Ba concentration in the diatom frustules. Al, Mg, Fe and K concentrations decrease drastically with the new cleaning process by a factor of about 7 for both Al and Fe. The overall The $Fe:SiO_2$ ratio in the newly cleaned samples is lower than the ratio obtained by nanoSIMS indicating that the additional cleaning process removes more contamination than could be corrected by removing the high Al "spots" identified by nanoSIMS. Overall, $Fe:SiO_2$ ratios in the 4 samples studied with both techniques and cleaning methods conserve the same trend (highest in #2, lowest in #3).

These results demonstrate the effectiveness of the new cleaning method for SIMS analyses and reaffirm the potential of the $Fe:SiO_2$ proxy as a tracer for Fe availability.

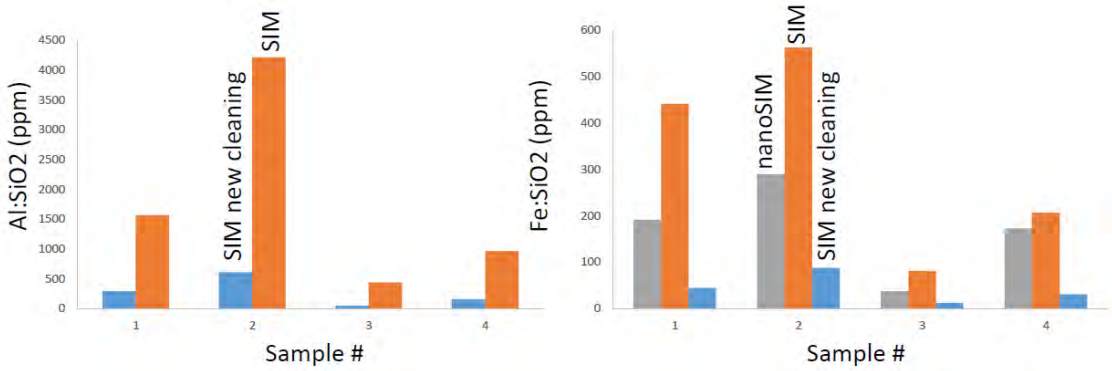

Figure 1. Al and Fe concentration in diatom frustules analysed with SIMS (2 cleaning methods) and nanoSIMS (original cleaning method).

References

[1] Pichevin, L. E., Ganeshram, R. S., Geibert, W., Thunell, R. & Hinton, R. (2014) Nature Geoscience **7**, 541-546, doi:10.1038/ngeo2181.

Chlorine isotope fractionation during degassing of lunar magmas

N.J. Potts & G.D. Bromiley

School of GeoSciences, University of Edinburgh, Edinburgh EH9 3JW, UK

Rationale

It is generally believed that the Moon formed following collision of a Mars-sized planetessimal with the early Earth. As such, the Earth and Moon share a common history; constraining the nature of the Moon-forming event is key to understanding the nature and evolution of the Earth. Any model for formation of the Earth-Moon system must account for the remarkably similar isotopic compositions of both bodies. Similarities in the isotopic signatures of calcium, chromium, iron, potassium, stable strontium isotopes, silicon, titanium, and zirconium [1] are all consistent with a model where the Moon is formed by reconsolidation of material largely derived from the proto-Earth's mantle, or with a high-temperature equilibration process between the two bodies. In contrast, differences in copper, hydrogen, and zinc isotopes between the silicate Earth and lunar samples have been explained by isotope fractionation as a consequence of volcanic degassing, and are not thought to reflect primary differences between the Earth and Moon [1]. An additional isotopic system which varies considerably between the Earth and the Moon is chlorine [2], suggesting that substantial fractionation of Cl isotopes occurred during and/or after the formation of the Moon. This is of particular interest as the bulk Cl abundance of the Earth is thought to be depleted compared to carbonaceous chondrites (F/Cl ratio = 0.99), which is anomalous compared to its 50 % condensation temperature. The Moon shows an even greater Cl depletion (F/Cl ratio = 30). Cl depletion of Earth has been used to hint at high temperature processes occurring during planet formation [2], although the mechanisms behind this are poorly constrained. Understanding the processes that contributed to fractionation of Cl isotopes in lunar magmas and rocks could provide new insight into the history and evolution of volatiles (including Cl, F, H_2O) in the Moon and Earth and the Moon-forming event.

$\delta^{37}Cl$ [i.e. the $^{37}Cl/^{35}Cl$ ratio relative to standard mean ocean chloride (SMOC)] for lunar samples [3] ranges from ~ -4 to +40 ‰, much higher than terrestrial mantle values of ~ 0 ± 1 ‰. Two competing mechanisms can explain high temperature Cl isotope fractionation [3,4]: lighter ^{35}Cl should be preferentially vapourised during degassing, while heavier ^{37}Cl, with a higher bond strength, should preferentially form gaseous HCl in H-rich systems. Absence of strong fractionation of Cl in terrestrial systems indicates that these two mechanisms cancel each out. Sharp et al. [3] suggested that, in contrast, the inherently low H in lunar basalts promoted Cl degassing as metal chlorides (e.g., NaCl, $FeCl_2$, etc.), preferential loss of ^{35}Cl during degassing and a heavy Cl isotopic signature. In contrast, Boyce et al. [5] observed that lunar samples with the heaviest Cl isotopes signatures were also the most Cl-rich. They also observed strong fractionation of Cl in modelled melt compositions containing higher H contents, and failed to observe a correlation between Cl and H/D isotopic signatures. These observations all appear to preclude the possibility that high $\delta^{37}Cl$ values in lunar samples result from magmatic degassing of Cl. Instead, Boyce et al. [6] attributed large-scale Cl isotope fractionation to processes occurring during formation and cooling of the lunar magma ocean (as opposed to a later fractionation processes during lunar magmatism). However, it remains unclear why degassing of a terrestrial magma ocean would not have resulted in fractionation of Cl isotopes to a similar or greater extent. Possible explanations for this discrepancy might be the effect of more reducing conditions in the lunar magma ocean, which could fundamentally alter Cl speciation/complexing, or a greater degree of degassing from the smaller Moon.

All models for Cl isotopic fractionation are reliant on degassing mechanisms which are theorised but experimentally unconstrained. Therefore, we performed short duration, high-temperature degassing experiments in model lunar and terrestrial systems, under correspondingly reducing conditions, to experimentally constrain the extent of, and mechanisms for, chlorine degassing. Experiments were performed in both H-free, H-bearing and Zn-bearing systems. Following experiments, major element chemistry of all samples was verified by electron microprobe, and Cl isotopic composition determined by SIMS using the Cameca 1270 ion microprobe. Basaltic and silicic glass standards were kindly donated to this project by Magali Bonifacie and Jamie Barnes. These glasses span a range of Cl

abundance and isotopic composition, while also allowing for major composition matrix effects to be addressed.

Results and Discussion

The figure below shows results from the analysis of one time series of experiments. Under the high temperature run conditions used (1500°C), rapid Cl degassing occurred, and a characteristic systematic change in Cl isotopic signature: progressive loss of total Cl in all compositions (shown in the figure as CPS, counts per second, an uncalibrated measure of Cl content) results in enrichment of melt in ^{37}Cl. However, the extent of Cl loss and isotope fractionation is greatest in Zn-bearing melt and lowest in H- and Zn-free melt, contrary to expectations. Thus, we find that (1) presence of H increases Cl degassing from magmas, although kinetic isotopic fractionation of Cl dominates, and HCl complexing does not result in enrichment in ^{35}Cl in magmas as expected; instead, degassing of H-rich magmas results in isotopic enrichment of ^{37}Cl. (2) As proposed [3], presence of Zn results in preferential degassing of ^{35}Cl due to formation of metal chlorides (or kinetic fractionation dominates), and isotopically heavy magma. However, this also occurs in H-bearing systems, implying that either H loss occurs rapidly at high temperature and that presence of Zn promotes additional Cl loss, or that complexing of Zn with Cl in the vapour phase dominates or is independent of H-Cl complexing. (3) high temperature degassing under all conditions results in preferential ^{35}Cl loss and isotopically heavy magma, contrary to the observations that isotopically heavy lunar basalts are Cl-enriched.

We have successfully demonstrate a protocol for in-situ analysis of Cl isotope signatures in experimental run products, and first results which allow high temperature processes for Cl isotopic fractionation to be determined. Based on these results, we are planning a larger experimental study to provide new insight into Cl isotope fractionation during Moon formation and lunar magmatism aimed at determining causes for the moons unique Cl isotopic signature. Initial results suggest that the lunar Cl isotopic signature might provide useful insight into the Moon forming process and nature of the early Earth-Moon system.

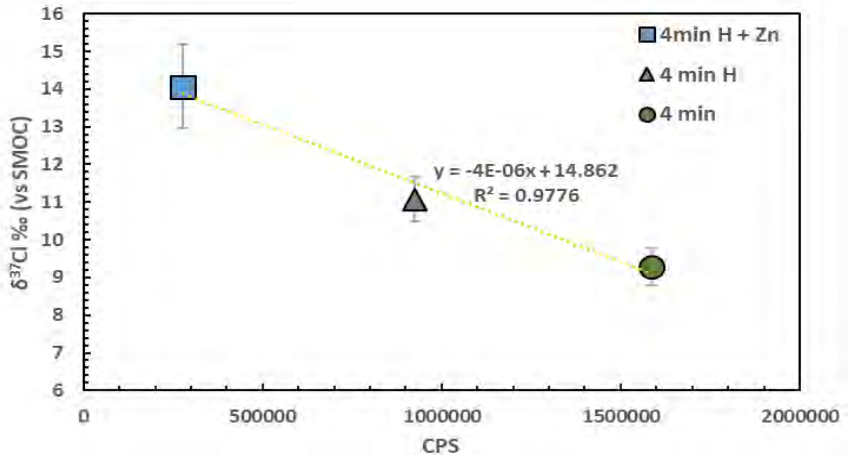

References

[1] Hauri, E.H., et al. Water in the Moon's interior: Truth and consequences. EPSL, 409: 252-264.
[2] Sharp, Z.D., Draper, D.S. The chlorine abundance of Earth: Implications for a habitable planet. EPSL, 369-370; 71-77.
[3] Sharp, Z.D., et al. The chlorine isotope composition of the Moon and the implications for an anhydrous mantle. Science, 329: 1050-1053.
[4] Bonifacie, M., et al. The chlorine isotope composition of Earth's mantle. Science, 319: 1518-152.
[5] J.W. Boyce, S.A. Kanee, F.M. McCubbin, J.J. Barnes, H. Bricker, A.H. Treiman (2018) Early loss, fractionation, and redistribution of chlorine in the Moon as revealed by the low-Ti lunar mare basalt suite. Earth and Planetary Science Letters 500, 205-214.
[6] J.W. Boyce, A.H. Treiman, Y. Guan, C. Ma, J.M. Eiler, J. Gross, J.P. Greenwood, E.M. Stolper (2015) The chlorine isotope fingerprint of the lunar magma ocean. Science Advances 1 (8) e1500380

Fluorine and Cl partitioning between olivine and silicate melt under lunar conditions

N.J. Potts& G.D. Bromiley

School of GeoSciences, University of Edinburgh, Edinburgh EH9 3JW, UK

Rationale

Isotopic similarities between the Earth and Moon have led to the canonical giant impact hypothesis. This states that the Moon formed following collision of a Mars-sized projector with the newly-formed Earth. Subsequently, Earth has been progressively modified by melting and plate tectonics, while the Moon has remained relatively unchanged over the past 4.5 billion years, preserving a much better record of the early Earth-Moon system and, by extension, of the early inner solar system. Of particular importance is the Moon's ability to provide insight into the role of volatiles during planetary formation and early evolution. For example, comparable volatile contents between the Earth and the Moon are consistent with a common origin for a terrestrial volatile element budget which predates the Moon-forming event, or volatile contents set by equilibration during this event. However, considerably lower F and Cl contents of the lunar compared to terrestrial interior suggest volatile delivery to the Earth-Moon system by the addition of a late veneer.

Lunar volcanic glasses and Mare basalts contain significant quantities of volatiles [1,2] (F, Cl, S, H_2O), implying that at least part of the lunar mantle is volatile-rich. Overlapping water contents between Mare basalts and terrestrial mid-oceanic basalts have been used to imply that the water contents of the lunar mantle might be similar to that of Earth's mantle [3]. In contrast, low modelled F and Cl contents in the lunar mantle have been used to suggest the Moon is depleted in volatiles compared to the Earth. Direct comparison of volatile contents with modern terrestrial magmas, however, may be misleading, as lunar magmas formed under more reducing conditions. Existing estimates of the lunar mantle volatile contents are based on values of H, F, Cl, S partitioning between minerals and melt under the more oxidising conditions relevant to Earth's modern upper mantle. Under these conditions, volatiles are known to be highly incompatible and readily incorporated in magmas, with only small amounts (ppm level) remaining in residual minerals as structural defects. All current data on H, F, Cl, S partitioning are based on experiments conducted under oxidised conditions, and estimates of lunar mantle contents are based on these values. The inherent assumption of existing studies, therefore, is that fO_2 has no influence on volatile partitioning.

In order to accurately assess the volatile content of the lunar interior, we conducted a series of experiments in a model H, F and Cl-bearing model lunar system. Two contrasting capsule assemblies were used to maintain reducing conditions. Experiments were performed to synthesise mantle phases (olivine, orthopyroxene, clinopyroxene) in equilibrium with silicate melt (quenched to glass) at high pressures and temperatures, but reducing conditions. H, F and Cl contents of mineral phases and glass were determined by Secondary ion mass spectrometry (SIMS). Major element compositions were determine by electron microprobe. Raman and IR spectroscopy (conducted at the University of Bristol in collaboration with Richard Brooker) was conducted to provide additional information on speciation/incorporation mechanisms for volatile elements.

Results and discussion

Despite evidence of a change in H speciation at low fO_2, we see no discernible effect of fO_2 on mineral-melt H or F partitioning (top and middle graphs). However, fO_2 has a strong influence on Cl partitioning; Cl could not be detected in any mineral phases analysed, although was present in large concentrations within the melt. Under reduced conditions, there is also a negative correlation between H and F olivine-melt partitioning. This is in contrast to oxidised, terrestrial conditions and is consistent with a marked change in defect chemistry.

Partition coefficients determined here imply that terrestrial H and F partitioning data can be used to model volatile content of the lunar interior, implying a variously hydrated lunar interior. Chlorine partitioning is fundamentally different in the reduced lunar interior, consistent with highly anomalous F/Cl ratios determined in lunar samples. Contrary to previous suggestions, the Moon's low Cl content could reflect the contrasting behaviour of Cl during lunar magma ocean crystallisation, rather than Cl loss during the Moon forming event [4].

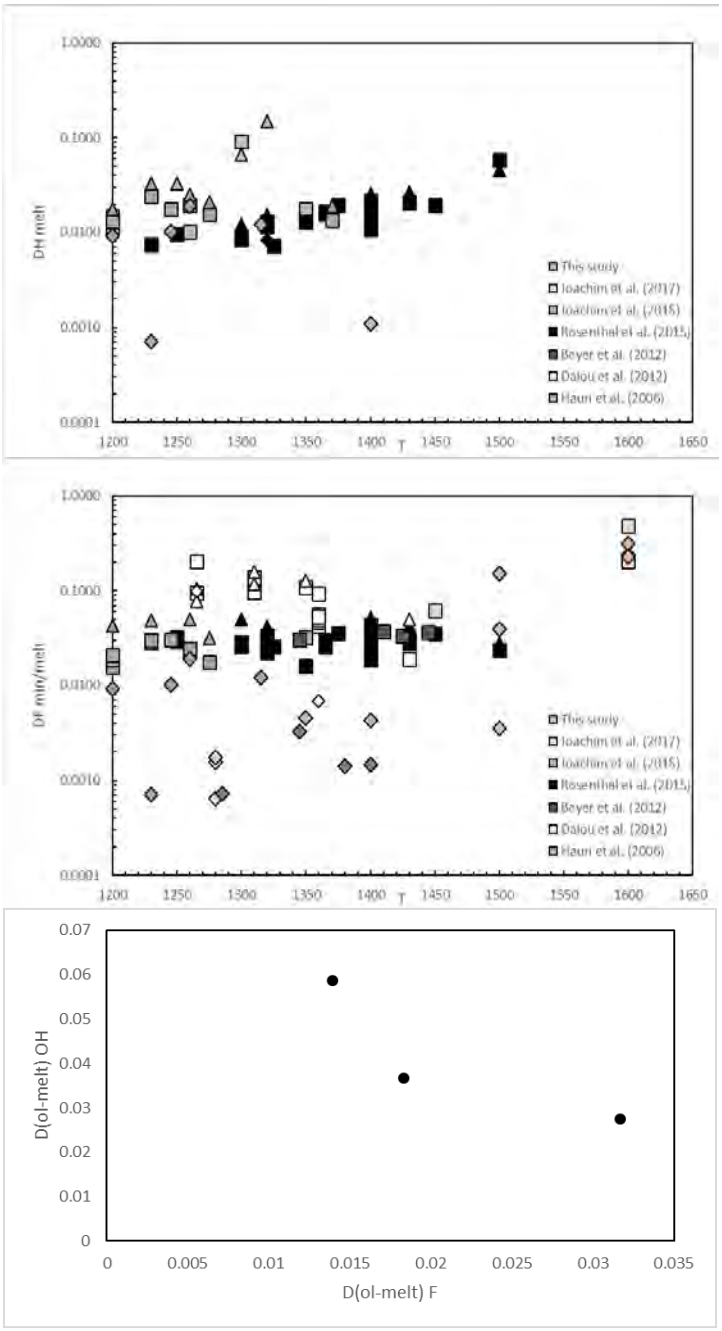

Contrasting behaviour of Cl and H also implies that Cl content of Mare basalt provides little useful insight into the 'water' content of the lunar interior, in contrast to a number of recent studies. F and OH partitioning data, furthermore, suggest that halogen and H incorporation mechanisms are fundamentally different under lunar and terrestrial conditions. As such, low F and Cl contents of the lunar interior do not necessarily imply that the Moon is less hydrous than the Earth. This supports the assertion that volatiles were delivered to the early Earth before the Moon-forming event.

References

[1] McCubbin F. M. *et al.* Magmatic volatiles in the lunar mantle, crust, and regolith: Abundances, distributions, processes, and reservoirs. *Am. Min.*, **100**, 1668-1707 (2015).

[2] Saal A. *et al.* Volatile content of lunar volcanic glasses and the presence of water in the Moon's interior. *Nature* **454**, 192-196 (2008)

[3] Hauri E. H. *et al.* High Pre-Eruptive Water Contents Preserved in Lunar Melt Inclusions. *Science* **333**, 213-215, (2011).

[4] Sharp Z.D. & Draper D.S. The chlorine abundance of Earth: Implications for a habitable planet. EPSL, 369-370; 71-77.

Tracking the evolution of slab fluids at the Izu-Bonin arc with B isotopes

I.P. Savov [1] & J.C.M. De Hoog[2]

[1]School of Earth & Environment, University of Leeds
[2]School of GeoSciences, University of Edinburgh

During one day of reconnaissance study and three days of follow up SIMS work we have successfully measured the B and $\delta^{11}B$ isotope ratios in 42 melt inclusions (MI) trapped in pyroxene grains extracted from various core depths of Site U1348, drilled during IODP Expedition 351 to the Amami Basin in the Izu-Bonin-Mariana (IBM) region [1]. Site U1438 core is unique in that it penetrated the 49 M.yrs old basement representing very depleted tholeiitic basalts erupted just prior to the subduction (arc) initiation [1,3,4]. Together with the pre-arc basement we also recovered >1300m of exceptional volcaniclastic sediment cover, preserving a record of the entire proto-IBM arc development and subsequent destruction. The goal of our study was to see if there are trends in the B and $\delta^{11}B$ with the recorded increases in magma production rates with depth/time [4].

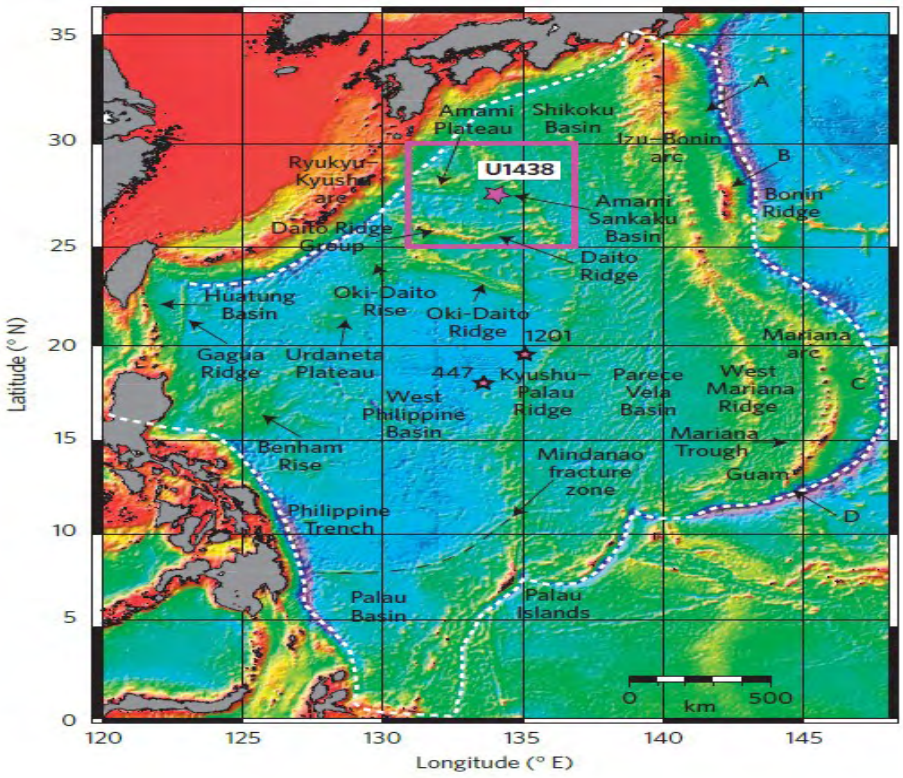

Figure 1. General setting and bathymetry (blue deep, red shallow) of the bounding trenches, basins and ridges comprising the Izu-Bonin-Mariana region in the Western Pacific. Locations of IODP drill site U1438, ODP Site 1201, and DSDP Site 447 are shown by pink stars (from [1])

The $\delta^{11}B$ ratios in the melt inclusions vary from -1.6 to +9.2 ‰ and the B concentrations vary from 4 to 65 ppm. Interestingly, and although boron is considered fluid mobile element, the melt inclusion B and $\delta^{11}B$ do not show statistically significant correlations with any major or trace element fluid tracer, including Cl, F and H_2O itself. However, B and $\delta^{11}B$ show remarkable correlations with core depth i.e. depositional ages (see Figure 2, 3). Interestingly, the melt inclusions we studied also show excellent positive correlation between B and $\delta^{11}B$. This relationship seems to be independent of any other melt inclusion chemical parameter. Our results resemble the overall heavy $\delta^{11}B$ measured in tephras from the Miocene-to-modern Izu volcanic arc (Straub & Layne, 2001). We interpret the combined MORB-normalized high B and heavy $\delta^{11}B$ dataset as highlighting the extreme fluid mobile nature of boron. The latter seems to be added to the arc magmas immediately after the subduction begins and thus most

probably from forearc-modified serpentinite fluids (with high $\delta^{11}B$). This heavy $\delta^{11}B$ is added irrespectively of variations in the slab fluid volumes and chemistry and the resulting variations in the degree and style of melting (Mg#, crystallization order).

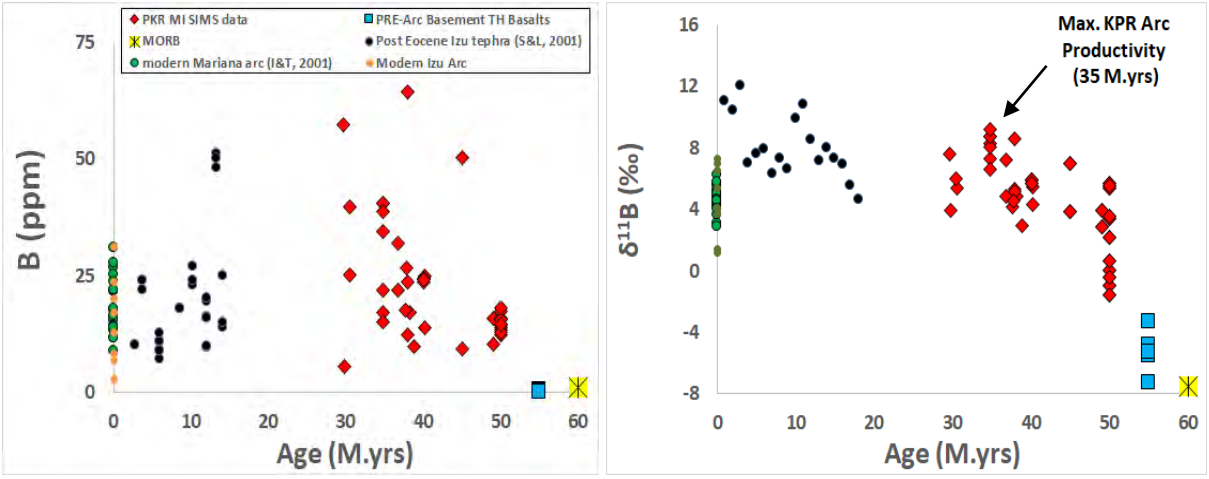

Figure 2 (left). Age versus B concentrations in melt inclusions from IODP Site U1438. Also shown for comparison are the values from background MORB [5], as well as those for the arc initiation (or pre-arc) tholeiitic basement (Savov & Agostini, *unpublished*), as well as for the modern Mariana arc and post Eocene Izu arc [2, 6]. It is clear that since the inception of the Palau-Kyushu (Proto-IBM) arc at ~52 M.yrs the B concentrations are increasing in diversity and reach a peak at the same time as the peak of arc magma production (melt outfluxes) as evidenced from the sedimentology and the overall early arc petrology and geochemistry [3,4 and references therein]. **Figure 3 (right).** Age versus $\delta^{11}B$ ratios in melt inclusions from IODP Site U1438. Also shown for comparison are the values for background MORB, as well as those for the arc initiation (or pre-arc) tholeiitic basement (Savov & Agostini, *unpublished*), as well as for the modern Mariana arc and post-Eocene Izu arc [2, 6]. Symbols and data sources are the same as those used in figure 1. The error bars on both graphs are comparable to the size of the symbols.It is clear that since the arc initiation the $\delta^{11}B$ ratios have been steadily rising, most probably reflecting the increasing influence of forearc-modified (serpentinite) inputs to the arc magma sources.

Future work:

We will proceed to explore the lack of correlations with any other geochemical tracers of slab fluids, especially in the bottom core samples (earliest arc). We will also aim to link the new B and $\delta^{11}B$ dataset with current geodynamic models of subduction initiation and arc geometry [1, 3]. Pinpointing the source of the early $\delta^{11}B$ enrichments in volcanic arcs may uniquely decipher the role (if any) that modern slab fluids (dehydrated sediments and oceanic crust) may play in the arc magma generation.

References

[1] Arculus et al. (2015) Nature Geosci. 8, 728-733.
[2] Straub SM, Layne GD (2002) Earth Planet Sci Lett 198, 25–39.
[3] Ishizuka, O., Hickey-Vargas R., Arculus, R., Yogodzinski G., Savov, I.P., Kusano,Y., et al. (2018) Earth Planet Sci. Lett.481, 80-90.
[4] Brandl., P., Hamada, M.; Arculus, R., Johnson; K., Marsaglia, K., Savov, I.P., Ishizuka, O., (2017) Earth Planet Sci. Lett. 461, 73-84.
[5] Marschall, H.R., Wanless, V.D., Shimizu, N., Pogge von Strandmann, P.A.E., Elliot, T., Monteleone, B.D., (2017) Geochim. Cosmochim. Acta 207, 102-138.
[6] Ishikawa, T. and Tera, F. (1999) Geology 27, 83–86.

The role of fO_2 on apatite-melt partitioning: developing tools to probe the oxidation state of the early Earth

T. Stokes, G. Bromiley, K. Saunders & N. Potts

School of GeoSciences, University of Edinburgh, Edinburgh EH9 3JW, UK

Rationale

Apatite [nominally $Ca_5(PO_4)_3(F,Cl,OH)$] is a common mineral in sedimentary, igneous and metamorphic rocks. Nearly half the known elements can substitute into apatite, which makes it an important mineral in studying the trace element budget of magmas and investigating processes associated with magmatic plumbing. Apatite occurs in lunar and Martian rocks, and detrital apatites are some of the oldest know minerals in terrestrial rocks. As such, apatite can provide insight into conditions in the newly-formed planets of the inner solar system. The three end member apatite compositions (fluoro-, chloro- and hydroxyapatite) highlight that this mineral is also important for an understanding of the volatile contents of terrestrial magmas and gives insights to the volatile budgets of extraterrestrial magmas.

Oxygen fugacity (fO_2) is an important parameter in understanding igneous systems due to the role it plays in controlling species in volcanic gases, its influence on mineral stabilities, and the need for it to be quantified for modelling geophysical processes in the mantle. [1] hypothesised that the Mn content of igneous apatite could be used to calculate the fO_2 of parental melts. Any such oxybarometer would be of considerable use in determining fO_2 in igneous bodies, and by inference, in planetary interiors through time. Manganese is a redox sensitive element which can exist as Mn^{2+}, Mn^{3+}, Mn^{4+} and Mn^{5+} in geological systems. Based on observed trends in apatite geochemistry, [1] inferred that the size and charge of Mn^{2+} meant that it would be preferentially incorporated into apatite over Mn^{3+}, replacing Ca^{2+}. Therefore, under low fO_2 conditions apatite would contain higher amounts of Mn than apatite which formed under more oxidising conditions.

We set out to experimentally test the hypothesis of [1] by synthesising Mn bearing apatite in equilibrium with silicate melts over a range of fO_2 conditions comparable to those found in terrestrial magmas. A second series of experiments were performed to synthesise apatite in equilibrium with silicate melts in a bulk composition doped with Ce and Eu. Both these elements are also redox sensitive, existing in Ce^{3+}/Ce^{4+} and Eu^{2+}/Eu^{3+} oxidations states respectively, and may also be of use for determining the fO_2 of magmas based on their concentration/oxidation state in apatite. Both Ce and Eu are commonly found as trace elements in apatite and are already used to calculate fO_2 based on their oxidation state in other minerals.

For the two sets of experiments we synthesised apatite at 1 GPa and at 1250-1400 °C in the piston cylinder apparatus. Metal-metal oxide powders were used to buffer fO_2 in these experiments using the double capsule procedure. This experimental approach necessitates the presence of water in both the experimental melt and surrounding buffer, and water activity controls the absolute fO_2 value of the melt. Water can be incorporated into apatite as OH in the apatite X site. The usual approach to determine OH content is to work out the content based on stoichiometry from EPMA measurements; however, F can be difficult to accurately analyse using EPMA. Secondary ion mass spectrometry (SIMS) was, therefore, necessary to accurately determine apatite compositions. SIMS measurements also allow us to constrain any structural role the X site has on Mn partitioning into apatite, as well as providing a check on how successfully the metal-metal oxides buffered fO_2.

Results and discussion

Measured melt water contents for buffered experimental runs show that water is present in all samples. Whilst most experiments are not fully saturated in water, this enables each experiment to be ranked in order of relative fO_2. Results showed that the Mn content of apatite is not strongly influenced by fO_2 (Fig. 1) but is instead controlled by the degree of melt polymerisation (NBO/T – number of bridging oxygen to tetrahedral). Manganese is not the only element in apatite whose concentration depends on melt polymerisation (Fig. 2), with Cl apatite-melt partitioning also appearing to be dependent on melt polymerisation, whereas, F apatite-melt partitioning appears to be independent of melt structure.

The carbon content of apatite between runs is variable, likely the result of infiltration from the graphite furnace rather than carbon present in the preliminary starting material. The carbon content of apatite that crystallised in basaltic melts is consistently higher than runs carried out in more silicic

compositions. Further work is needed to determine C contents in appropriate melt composition standards to determine if higher C contents in basaltic apatite reflect an increased compatibility of C in basaltic melts compared to more silicic melts.

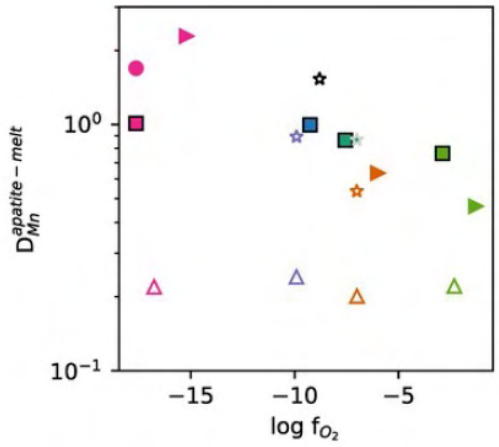

Figure 1: $D_{Mnl}^{Ap\text{-}m}$ against melt fO_2 for basaltic starting compositions (triangles), and four more silicic compositions (stars, triangles, squares and circles)

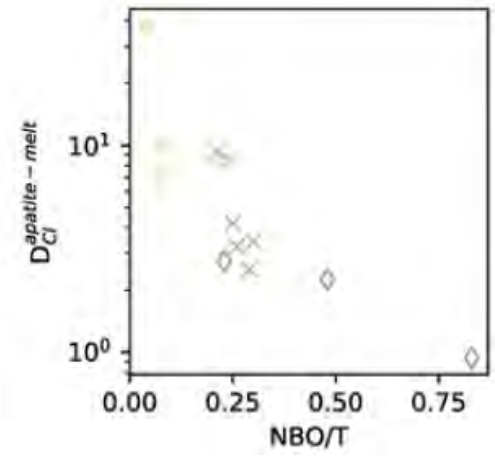

Figure 2: $D_{Cl}^{Ap\text{-}m}$ against melt NBO/T for our study (crosses) and literature data ([2] – stars, [3] – diamonds.).

This study also collected data on volatile content in Ce and Eu bearing melt compositions in equilibrium with apatite. These again confirmed the presence of water in the silicate melt phase for all runs. This suggests that these experiments again have a relative difference in fO_2. Unlike Mn, D_{Ce} and D_{Eu} (apatite-melt) appear to be strongly affected by fO_2, which may suggest the suitability of apatite as a Ce or Eu oxy-geobarometer. Further work is currently being conducted to calibrate the influence of fO_2 on the relative partitioning of Ce and Eu compared to other Rare Earth Elements. Results will be used to develop an alternative apatite-based oxybarometer.

References

[1] A.J. Miles et al. (2014) Geochimica et Cosmochimica Acta 132, 101-119
[2] A. L. Doherty et al. (2014), Chemical Geology 384, 94–109.
[3] Prowatke and Klemme (2006), Geochimica et Cosmochimica Acta 70, 4513-4527

Volatile element fluxes from a subducted, hydrated fracture zone

L. Tomanikova[1], I. Savov[1] & J. Harvey[1]

[1]School of Earth and Environment, University of Leeds, Leeds LS2 9JT, UK

Project rationale

Fluids metasomatizing the sub-arc mantle are generally thought to be released during dehydration of the altered-oceanic crust (AOC), sediment and, in most subduction zones, fore arc serpentinite. Subducting fracture zones extensively hydrated by seawater, however, may also introduce vast amounts of fluids into the sub-arc mantle [1,2]. For example, the Aleutian transform fault, subducting underneath the Shiveluch volcano in Kamchatka, is thought to have a major effect on the distribution of volatiles and FME due to extensive serpentinization of large portions of the oceanic crust and exposed oceanic lithospheric mantle [1]. Here, we report halogen compositions of hydrous vein minerals in Shiveluch mantle xenoliths and employ our halogen data to infer the nature and origin of the fluids and melts in equilibrium with crystallized vein minerals.

Background

Halogens (e.g., Cl and F) serve as tracers of slab-derived fluids and melts percolating through the sub-arc mantle because of their contrasting partitioning behaviour between hydrous silicates, fluids and melts. Chlorine can be used as a proxy for fluid-induced metasomatism of the sub-arc mantle because of its fluid-mobile character [3] whereas F can be used as a proxy for melt-induced metasomatism [4]. Furthermore, we can employ halogens to investigate slab fluid and melt sources as serpentinite dehydration will produce Cl-rich fluid [5] and the AOC melting will produce F-rich melt [6].

Results and discussion

Halogen contents (Cl and F) of Shiveluch vein amphibole and phlogopite were measured on Cameca ims 4f. Amphibole and phlogopite Cl contents range from 70 to 340 µg g^{-1} and from 168 to 934 µg g^{-1}, respectively and their F contents range from 465 to 1580 µg g^{-1} and from 435 to 2090 µg g^{-1}, respectively (**Figure 1**). Shiveluch vein minerals are depleted in Cl relative to olivine-hosted melt inclusions from Kamchatka arc volcanic rocks [6,7], except for phlogopite grains in SHIV-16-12-06. All the other vein minerals are preferentially enriched in F indicating percolation of AOC-derived melts through the veins. Most of Shiveluch vein minerals are enriched in Cl relative to Avachinsky vein amphiboles [8] (**Figure 1**) indicating higher slab fluid influx underneath the Shiveluch than Avachinsky. We have not found convincing evidence for significant slab mantle serpentinite dehydration, to the contrary to the recent Kamchatka subduction zone model [1].

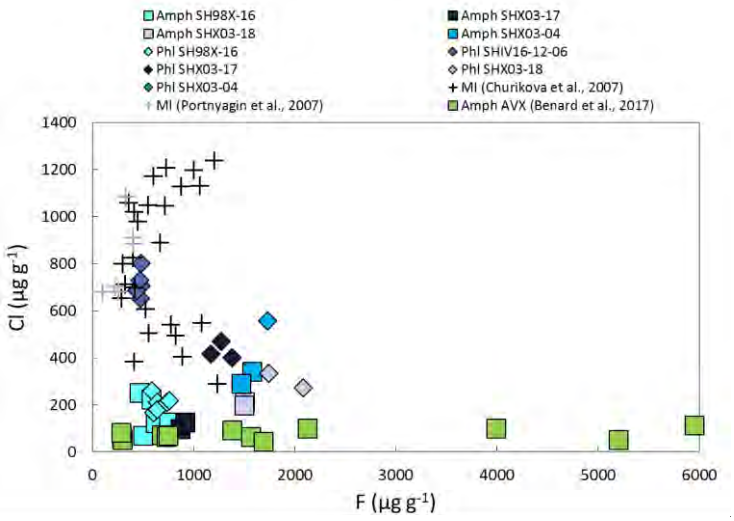

Figure 1. Cl and F contents of Shiveluch vein amphibole and phlogopite compared to olivine-hosted melt inclusions from Kamchatka arc volcanic rocks [6,7] and Avachinsky vein amphibole [8].

References

[1] M. Konrad-Schmolke and R. Halama (2014) Lithos, **208-209**, 393-414. [2] V.C. Manea et al. (2014) Nature Comm. **5**. [3] A. Fabbrizio et al. (2013) Contrib. Mineral. Petrol. **166**, 639-653. [4] J. Wu and K.T. Koga (2013). Geochim. et Cosmochim. Acta **119**, 77-92.[5] J. Kodolanyi and T. Pettke (2011). Chem. Geology **284**, 351-362. [6] M. Portnyagin et al. (2007). EPSL **255**, 53-69. [7] T. Churikova et al. (2007) Contrib. Mineral. Petrol. **154**, 217-239. [8] A. Benard et al., (2017) Geochim. et Cosmochim. Acta **199**, 324-350.

Coupled C and O isotope geochemistry of calcite in calc-silicate crustal xenoliths from Merapi volcano, Indonesia

S. Whitley, R. Gertisser & R. Halama

School of Geography, Geology and the Environment, Keele University

Introduction

Crustal magma-carbonate interaction has been suggested as a process that may dominate the CO_2 output in several volcanic arcs [1], influencing eruptive dynamics [2], modifying magmatic differentiation trends [3], and as a possible source of magmatic carbonate melts [4]. Direct evidence for this process has often remained elusive, but the occurrences of calc-silicate (skarn) xenoliths in the eruptive products of some active volcanoes provide a unique opportunity to study high temperature magma-carbonate interaction and the subsequent effects on the host magmatic system.

Carbon and oxygen isotopes are powerful tracers of magma-carbonate interaction processes, where calc-silicate skarn rocks are formed. Sedimentary carbonates are isotopically distinct from mantle-derived igneous rocks, allowing the quantification of chemical exchange during magma-carbonate interaction. Individual processes, including decarbonation and magmatic fluid interaction, can be readily distinguished, using these two stable isotope systems [5].

At Merapi volcano (Indonesia), calc-silicate xenoliths are ubiquitous throughout the volcanic succession. Some of these xenoliths contain texturally distinct types of calcite, which provide an exceptional opportunity to gain novel insights into magma-crust interaction processes. We used the Cameca ims-1270 ion microprobe to make seventy paired carbon and oxygen isotope analyses in calcite across six calc-silicate xenolith samples. Analyses were made on microdrilled cores, retaining the calcites' unique textural characteristics.

Calcite Textures

We distinguish five textural types of calcite across two Merapi crustal xenolith groupings – magmatic skarns and exoskarns (**Figure 1**). Each textural type represents a specific process, or a combination of processes, operating during magma-carbonate interaction, which C-O isotopes provide a means to quantify.

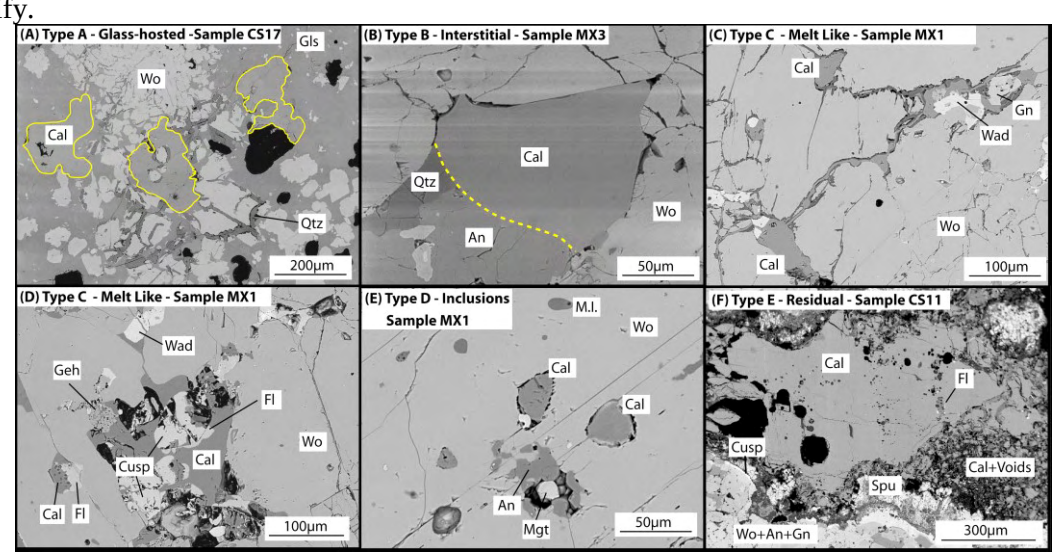

Figure 1. Calcite textures: A) Calcites within Ca-enriched glass. B) Calcites interstitial to wollastonite. C-D) Melt-like calcite and associated volatile-rich mineral phases. E) Calcite inclusions within wollastonite. F) Large residual calcites with volatile-rich reaction rims. Abbreviations: An - anorthite, Cal - calcite, Cusp - cuspidine, Fl - fluorite, Geh - gehlenite, Gls - glass, Mgt - magnetite, M.I. - melt inclusion, Qtz - quartz, Spu - spurrite, Wad - wadalite-like phase, Wo - wollastonite.

Type A calcites consist of rounded globular calcite grains within the glass-rich xenolith textural zone (**Figure 1A**). Type B calcites occur as subhedral crystals (50-100 µm in size) that are found interstitial to wollastonite, and as fractured crystals at vesicle borders within wollastonite-dominant cores (**Figure 1B**). Type C calcites are anhedral interstitial crystals (50-100 µm in size) exhibiting a melt-like, infil-

trative texture between wollastonite crystals. They are found as thin interconnected veins with a rim of quartz at the wollastonite contact (**Figure 1C,D**). These veins form rare ~50 µm pools of calcite, with occasional fluorite crystals nucleating at the edges and around calcite-hosted vesicles. Type D calcites occur as rounded inclusions (< 50 µm) in wollastonite and garnet (**Figure 1E**). Type E calcites occur as millimetre-sized crystals with vesiculated reaction rims containing spurrite and sulphur and fluorine-enriched phases (**Figure 1F**).

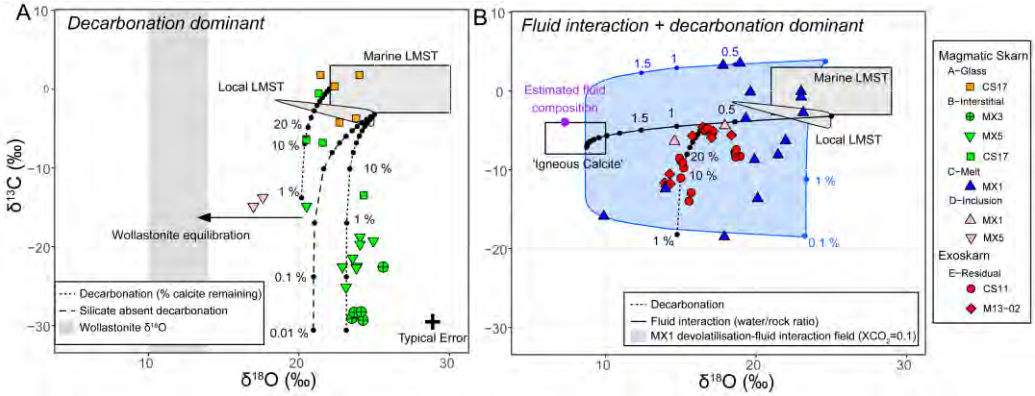

Figure 2. $\delta^{13}C$ (‰ PDB) vs $\delta^{18}O$ (‰ SMOW) isotope diagrams of calcite in calc-silicate xenoliths. A) Calcite types showing influence dominantly by decarbonation processes with model curves for decarbonation. B) Calcite types showing a mixture of magmatic fluid interaction and decarbonation with fluid-rock interaction modelling.

C-O isotope geochemistry

The calcite types span a large range in C-O compositional space (**Figure 2A-B**). Individual calcite types can be distinguished by compositional grouping. The highest $\delta^{13}C$-$\delta^{18}O$ calcites are type A glass-hosted calcites, forming a compositionally tight cluster with $\delta^{13}C$ between -4.2 and +1.8 ‰, and $\delta^{18}O$ ranging from +21.4 to +24 ‰. Type B interstitial calcites have the largest $\delta^{13}C$ variation, but a restricted $\delta^{18}O$ range ($\delta^{13}C$ -29.3 to -0.6 ‰, $\delta^{18}O$ +20.5 to +25.6 ‰). Type C melt-like calcites have the widest $\delta^{18}O$ variation, between +9.9 and +23.1 ‰, and a large $\delta^{13}C$ variation, ranging from -18.5 to +3.5 ‰. Data for Type D calcite inclusions within wollastonite are few, but show a similar compositional range of $\delta^{13}C$ (-14.9 to -4.4 ‰), and $\delta^{18}O$ (+14.6 to +17.9 ‰) to the type E calcites. Type E-residual calcites in the exoskarn xenoliths define a tight compositional cluster between $\delta^{13}C$ of -14 to -4.6 ‰ and $\delta^{18}O$ of +13.9 to +19 ‰.

Discussion

Type A calcites represent the closest to unmodified calcites, and three trends can be observed and modelled from these data: (1) a trend towards pure decarbonation, (2) inclusion re-equilibration, and (3) magmatic fluid mixing combined with decarbonation (**Figure 2**). Calcites demonstrating pure decarbonation isotopic character (Type B, Fig. 2A) represent the last < 1% of calcite remaining, showing extremely efficient decarbonation in the xenoliths. Type C and E calcites (Fig. 2B) show a combination of mixing with magmatic fluids and decarbonation. In type C, F-rich magmatic-derived fluids facilitated calcite melting. Type D inclusion calcites show isotopic exchange with their wollastonite hosts.

Using our calcite data, published mantle $\delta^{13}C$ values for Indonesia, and current Merapi fumarole $\delta^{13}C$ compositions, we show that 24-56% of CO_2 emitted during periods of quiescence at Merapi is crustal derived. Decarbonation from a contact aureole around an estimated Merapi magmatic intrusion occurs on timescales of only hundreds to thousands of years. Decarbonation globally of arc volcanoes hosted on carbonate substrate has the potential to influence global climate.

References

[1] E. Mason et al. (2017) Science **357**, 290-294; [2] V. Troll et al. (2012) Geophysical Research Letters **39**, L11302; [3] G. Iacono-Marziano et al. (2008) Contributions to Mineralogy and Petrology **155**, 719-738; [4] P. Fulignati et al. (2001) Geology **29**, 1043-1046; [5] J. Valley (1986) Reviews in Mineralogy and Geochemistry **16**, 445-490.

Speleothem records of acid sulphate deposition and organic carbon mobilisation

P.M. Wynn[1], R. Bartlett[2], I.J. Fairchild[2], J. Baldini[3] & C. Bourdin[2]

[1]Lancaster Environment Centre, University of Lancaster
[2]Geography earth and Environmental Sciences, University of Birmingham
[3]Department of Earth Sciences, University of Durham

Background to the investigation

Dramatic increases in measured surface water DOC across the UK, western Europe and parts of N. America have been widely accepted as a consequence of changing environmental conditions and destabilisation of long-term soil carbon pools. However, identifying the drivers of DOC change is complex. Two of the suggested key drivers for DOC mobilisation are rising temperatures and acid sulphate deposition [e.g., 1]. Rising temperatures enhance the metabolic drivers of soil carbon degradation and DOC export [2]. Acid sulphate deposition provides a chemical suppressant to DOC mobilisation. Declining acid sulphate emissions may have therefore enhanced fluxes of DOC into river systems [3]. However, whilst both drivers of DOC dynamics are plausible, they are difficult to test due to the restricted nature of the available records of riverine DOC flux (1978 to present), and the limited availability of SO_2 emissions inventory data at the regional scale. Speleothems are known to offer long term reocrds of both sulphur and carbon which stretch beyond the 1970s and into the pre-industrial era. These records are therefore currently being investigated to decipher the relative importance of sulphur acidification and temperature as drivers of changing DOC flux.

Due to the large dynamic range in sulphur isotopic values from end member sources (marine aerosol ~ +21 ‰ to continental biogenic emissions ~-30 ‰) and limited environmental fractionation under oxidising conditions, sulphur isotopes form an ideal tracer of industrial pollution and environmental acidification in the speleothem palaeo-record. New techniques to extract sulphur concentrations and isotopes from speleothem calcite have enabled archives of pollution history and environmental acidification to be reconstructed both in the UK [4] and the Italian/Austrian Alps [5]. The overall aim of this facility application was therefore to analyse sulphur isotopes and concentrations in speleothem calcite from the modern-acidifying site of Heshang cave, China, forming a complimentary record to those already in existence which are all sourced from previously-acidified locations. Coupling these data to the carbon record should therefore allow assessment of acidification as a mechanistic control on carbon solubility and export.

Results and discussion: Speleothem calcite from the top 120 years of sample HS4 (collected from Heshang Cave, Hubei province, China) was meticulously prepared as four separate sections and impregnated using low sulphur resin. Each section was cut into strips and mounted

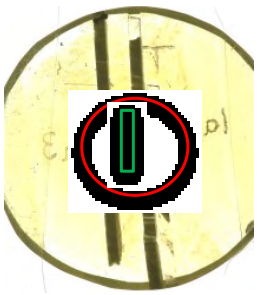

Figure 1. Dissected sample mounted as offset stripe to enable continuous timeseries analysis within the red circle demarking analytical area.

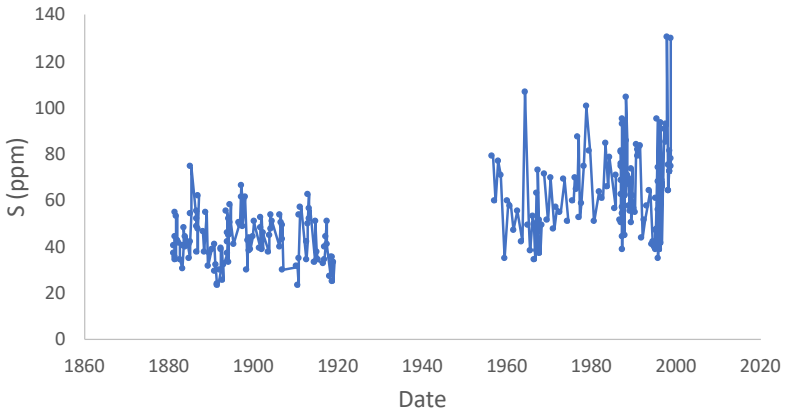

Figure 2. Sulphur concentrations in speleothem calcite (HS4) between 1880 and 2000.

in an offset fashion to enable the full length of each section to be analysed on one mount (**Figure 1**). Sections 1 and 3-4 were analysed over two separate weeks to obtain a high-resolution sulphur traverse starting in the pre-industrial era (pre-1950) and moving throughout the period of environmental acidification (1950 to present). The expected pattern of change was confirmed as one of increasing speleothem sulphur concentration throughout the era of industrialisation, likely associated with increasing emissions of SO_2 into the atmosphere from coal burning and other combustion-related activities (**Figure 2**).

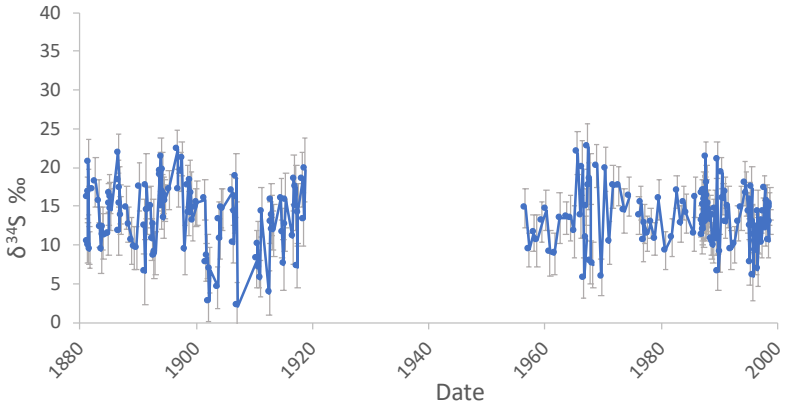

Figure 3. Sulphur isotopic values in speleothem calcite (HS4) between 1880 and 2000. Errors based on poisson counting statistics.

Throughout the sulphur isotopic record, signatures demonstrated an unusually broad range in values (+2 to +22 ‰) although average values were similar to those measured using bulk wet chemistry techniques. The sulphur isotopic composition of speleothem calcite was expected to link the source of sulphur to industrial activity by demonstrating an inverse relationship with concentration. Increasing sulphur concentrations sourced from industrial emissions of SO_2 were therefore expected to be associated with progressively lighter isotopic values. However, this inverse trend between sulphur isotopic composition and concentration was only weakly apparent post 1970, with much fluctuation in the record prior to this where concentrations are low and consequently errors based on counting statistics are high (**Figure 3**). Emissions modelling has demonstrated a post 1950's rise in atmospheric sulphur loading in China, with peak emissions status being reached in 2005 [6]. This weak relationship between isotopes and concentration data post 1970 therefore suggests there must be significant retention of sulphur within the biogeochemical cycle, such that the main period of acidification was not incorporated into the speleothem prior to collection. This suggests a retention of sulphur within the biogeochemical cycle and karst aquifer of approx. 20-30 years.

Conclusions: The relative significance of temperature driven changes in DOC production, and acid sulphate suppression of DOC solubility is difficult to determine in this particular speleothem record due to the long retention of sulphur in the biogeochemical cycle. The extensive (approx. 20-30 year) lag in sulphur transfer through the biogeochemical cycle and karst aquifer is likely to drive significant temporal offset from other trace elements contained within the speleothem record, as well as from atmospheric drivers of change. This particular speleothem record therefore needs to be supplemented with calcite growth which has occurred over the past 20 years in order to capture the main period of environmental acidification and assess the significance of sulphur acidification as a control on carbon release mechanisms from the soil.

[1] Worrall F & Burt TP 2007 Global Biogeochem. Cycl. 21: GB1013
[2] Freeman et al. 2001 Nature 412: 785
[3] Evans CD et al. 2006 Global Change Biol. 12: 2044–2053
[4] Wynn PM, Fairchild IJ, Baldini JUL et al. 2008 Geochim. Cosmochim. Acta, 72, 2465-2477
[5] Wynn PM, Fairchild IJ et al. 2010 Chem. Geol. 271, 101-107
[6] Smith, S.J., et al. 2011 Atmospheric Chemistry and Physics, **11**, 1101-1116